# ANOMALOUS THERMAL RELAXATION AND THE MPEMBA EFFECT IN OVERDAMPED LANGEVIN SYSTEMS AND MARKOV JUMP PROCESSES.

Matthew Robert Walker

Yorktown, Virginia

Bachelor of Science, University of Virginia, 2018

A Dissertation submitted to the Graduate Faculty
of the University of Virginia in Candidacy for the Degree of
Doctor of Philosophy

Department of Physics

University of Virginia

May 2025

Advisor:
Marija Vucelja, Chair

Committee Members:
Marija Vucelja
Eugene Kolomeisky
Gia-Wei Chern
Leo Petrov

# Anomalous Thermal Relaxation and the Mpemba Effect in Overdamped Langevin Systems and Markov Jump Processes.

Matthew Robert Walker

(ABSTRACT)

*The Mpemba effect* is an example of anomalous thermal relaxation. It occurs when a physical system cools down faster, starting from a hot temperature, than starting from a warm temperature when coupled to the same cold bath. There's also an interesting counterpart in the heating process, often dubbed the *Inverse Mpemba effect*. The two effects have been observed in a variety of systems, including water, clathrate hydrates, polymers, magnetic alloys, quantum dots, quantum circuits, and colloidal systems. This work concerns our efforts in understanding the Mpemba effect, guided by the recent colloidal experiments, and it's applications in Markov jump processes. Below, you will find a summary of our findings.

In particular, we will focus more on the *Strong Mpemba effect* – a more pronounced version of the Mpemba effect, characterized by a jump in the relaxation time, which yields an exponentially faster approach to equilibrium. Sometimes, the "regular" Mpemba effect is referred to as the *Weak Mpemba effect* to delineate between the two. In an attempt to gain intuition with the occurrence of the Mpemba effect, we model an overdamped Brownian particle diffusing on a potential energy landscape. We solve the Fokker-Planck equation for a piecewise constant potential for two wells separated by a barrier. Using this simple model that can be solved exactly, we explore the phase space and note that we can observe the Mpemba effect in systems that lack a notion of metastability. This challenged the previous intuition that the

Mpemba effect requires metastability. In the considered physical system, the borders of the areas where the effect happens correspond to either eigenvector changes of direction or to phase transitions. Finally, we discuss the topological aspects of the strong Mpemba effect and propose using topology to search for the Mpemba effect in a physical system. Later, colloidal experiments conducted measured the inverse Mpemba effect for a system without metastability [1].

Next, we now consider a continuous and smooth potential energy landscape like the one used by [2]. We derive the condition for the Mpemba effect in the small-diffusion limit of overdamped Langevin dynamics on a double-well potential. Our results show the strong Mpemba effect occurs when the probability of being in a well at initial and bath temperature match, which agrees with experiments. We also, for the very first time, derive the conditions for the weak Mpemba effect and express the conditions for the effects in terms of mean first passage times. We confirm our theoretical findings by simulating the dynamics using Monte Carlo simulations.

In the next two chapters, we study the Mpemba effect in Markov jump processes on linear reaction networks as a function of the relaxation dynamics. The dynamics are characterized by the so-called load factor, which is introduced to control the transition rates in a manner that ensures the system still relaxes to the same thermal equilibrium (i.e., detailed balance holds). We find a surprising connections between optimal transport and the Mpemba effect. Optimal transport is a resource-efficient way to transport the source distribution to a target distribution in a finite time. By "a resource-efficient way," what is often meant, and what we will consider, is with the least amount of entropy production. Our paradigm for a continuum system is a particle diffusing on a potential landscape, while for a discrete system, we use a three- and four-state Markov jump process. The Mpemba effect is generically associated with high entropy production in the continuous case. At large yet finite times,

the system evolution toward the target is not optimal in this respect. However, in the discrete case, we show that for specific dynamics, the optimal transport and the strong variant of the Mpemba effect can occur for the same relaxation protocol.

In our last example, we provide analytical results and insights on when the Mpemba effect happens in the unimolecular reactions of three and four species as a function of the dynamics. We derive that in the unimolecular reactions of three species, the regions of the Strong Mpemba effect in cooling and heating are non-overlapping and that there is, at most, a single initial temperature leading to the Strong Mpemba effect. Next, we apply our results for the Markov jump processes on a Maxwell demon setup. Maxwell demon setups first appeared as thought experiments that explored the connection between information processing and thermodynamics. The first one to introduce such concepts was James Clerk Maxwell. We show that one can utilize the Strong Mpemba effect to have shorter cycles of the Maxwell demon device, leading to increased power output. We find a region of parameters where the device has increased power output and stable operation without sacrificing efficiency.

# Acknowledgments

To my family, who have supported me every step of the way and encouraged me to pursue my dreams with unwavering love and belief in my abilities. Thank you for being my rock and my constant source of inspiration. This dissertation is dedicated to you.

To my advisor, Marija Vucelja, whose guidance and expertise have been invaluable in shaping my research and helping me navigate the complexities of academia. Thank you for pushing me to think critically and pushing me to reach my fullest potential. This work is dedicated to you.

To my colleagues and friends, who have stood by me through the long hours of research, writing, and editing. Your encouragement and support have meant the world to me, and I am grateful for the camaraderie and friendship we have shared. This dissertation is dedicated to you. To Samantha, whose support was the most integral in my pursuit as a physicist. To John and Mary Seymour, whose kindness knows no bounds. To LeAnne, for believing in me and for your support. To my brother Eric, whom I spent the last two and a half years traveling the whole world with.

To all those who have played a part, big or small, in my academic journey, thank you. Your presence in my life has made a significant impact, and I am grateful for the lessons learned and the memories shared. This work is dedicated to each and every one of you.

Finally, to myself. Through the challenges and triumphs, the setbacks and successes, I have persevered and grown in ways I never thought possible. This dissertation is a testament to my hard work, dedication, and passion for knowledge. I dedicate

this work to the person I have become and the person I strive to be.

# Contents

# Chapter 1

# Introduction

## 1.1 Motivation

The Mpemba Effect, first observed in 1969 by Tanzanian student Erasto Mpemba and Dennis G. Osborne in 1969 [3], is a phenomenon where a hot system reaches thermal equilibrium faster than an identical cold system under certain conditions. This counterintuitive phenomenon has puzzled scientists for decades and continues to spark debate and intrigue in the scientific community. The Mpemba Effect challenges our understanding of the physics of freezing and thermal dynamics, as it goes against the conventional belief that colder temperatures lead to faster cooling times. The exact mechanism behind the Mpemba Effect remains a subject of ongoing research and investigation.

Systems where the Mpemba effect has been observed include: water [4, 3], clathrate hydrates [5], magnetic systems [6], polymers [7], colloidal particle systems [2], and qubits [8]. Numerically it has been seen in spin-glasses [9], systems without equipartition [10], driven granular gasses [11, 12, 13, 14, 15, 16, 17, 18], cold gasses [19], quantum systems [20, 21, 22], molecular gases [23, 24], and antiferromagnets [25, 26, 27, 28, 29]. The copious observations imply that the effect is general. It was studied in several theoretical works [25, 26, 30, 31, 32, 33, 34]. The prevalence of the effect suggests that in understanding such "shortcuts" to thermalization, we might gain in-

sight into a general aspect of nonequilibrium statistical mechanics. On the practical level, the Mpemba effect is closely tied to optimal heating and cooling protocols and efficient sampling of phase spaces. It is thus of broad interest to industry and science to characterize this effect.

In this doctoral dissertation, we aim to explore the Mpemba Effect in depth, examining the various factors that may contribute to this phenomenon, both using theoretical models and by directly modeling the experimental conditions that demonstrated the existence of the strong Mpemba effect in a colloidal setting.

Additionally, this dissertation will consider the potential applications of the Mpemba effect in various situations, such as optimal transport, and engine performance. By shedding light on this mysterious phenomenon, we hope to contribute to the growing body of knowledge surrounding the Mpemba Effect and its broader implications for scientific understanding.

## 1.2 Outline

The subject of this dissertation is out-of-equilibrium dynamics in stochastic systems studying the existence of the Mpebma effect. There are two distinct parts of this work. In the first half, we will consider overdamped Langevin dynamics and search for intuition by examining when you see the Mpemba effect and what might be the reason for its existence. In the second half, we consider discrete Markov jump processes and look to introduce the Mpemba effect in order to take advantage of faster relaxation, or more optimal transport protocols.

### 1.2.1 Anomalous thermal relaxation of Langevin particles in a piecewise constant potential

Our intuition tells us that we would expect a cold system to reach thermal equilibrium than an identical warm system when both are in contact with an even colder bath. The Mpemba effect is when the opposite is observed. Originally it was believe that metastability might be required for the Mpemba effect to be present in a system. In chapter 2 we model a system of overdamped Langevin particles diffusing in a double well system separated by a barrier. We use a piecewise constant bistable potential that is analytically solvable, and this allows us to solve the spectrum of the corresponding Fokker-Planck equation in closed form. By controlling the width and height of the barrier, we can explore the systems phase space and note the existence of the strong Mpemba effect. In particular, we find the existence of the strong Mpemba even when there is no notion of metastability in the system. We show that the regions where the strong Mpemba effect is present have borders where either eigenvector changes of direction or there is a phase transition. We also explore the mismatch in the cumulative probability for each of the wells as a function of the barrier width and height. This will become an important point of interest that we will revisit in chapter 3.

### 1.2.2 Mpemba effect in terms of mean first passage times

The colloidal experiment conducted by [2] was the first time the strong Mpemba effect was experimentally measured. In chapter 3. we seek to model their experiment by following a similar approach like the model introduced in chapter 2. However, this time we will consider a smooth continuous double well potential very similar to the

one used by [2]. We will analytically derive the conditions for both the strong and weak Mpemba effects in terms of mean first passage times. We get good agreement with the experimental findings, and for the first time, derive conditions for the weak effect. We also compare our analytical findings to numerical Monte Carlo simulations of overdamped Langevin particles diffusing down the potential energy landscape. We condlude by making some remarks on how general the Mpemba effect is for overdamped Langevin systems.

### 1.2.3 Optimal transport and anomalous thermal relaxations

Optimal transport deals with finding the most resource-efficient way to transport one distribution to another. It has applications in diverse fields, including economics, image processing, and machine learning. In chapter 4. we explore a surprising connection between optimal transport and the Mpemba effect. In this chapter we will no longer fix the dynamics and optimize the initial conditions, instead we fix the initial and finial conditions and vary the dynamics. We begin with our bread and butter example of an overdamped particle diffusing on a potential energy landscape. In this case we find an intriguing result that there seems to be an "antipodal" relation between optimal transport and fast relaxation for continuous energy landscapes. However, in certain discrete cases, we observe that the trajectory for fastest relaxation is also the one that exhibits minimal cost, indicating optimal transport. This unexpected relationship challenges our conventional understanding of the Mpemba effect and highlights the complex nature of the underlying dynamics.

### 1.2.4 Effect of dynamics on anomalous thermal relaxations and information exchange

In chapter 5. we continue in the spirit of chapter 4. by systematically varying the dynamics of the system and investigate how it influences the occurrence and characteristics of the Mpemba effect. This approach allows us to explore the regions of the parameter space where the Mpemba effect is enhanced or suppressed in the context of discrete Markov jump processes. This methodology provides valuable insights into the underlying mechanisms. Furthermore, we extend our investigation to the interplay between dynamics and information exchange in anomalous thermal relaxations. We study a three-level Markov jump process that interacts with a thermal reservoir and an information-carrying tape kept at a finite temperature. This setup resembles a Maxwell's demon, a thought experiment that explores the connection between information processing and thermodynamics. The main objective in this chapter is to understand how the dynamics of a system can be harnessed to enhance the performance of thermodynamic devices. By carefully designing the dynamics protocol, we aim to achieve a strong variant of the Mpemba effect, which can stabilize and increase the power output of a Maxwell demon setup without compromising efficiency.

# Chapter 2

# Anomalous thermal relaxation of Langevin particles in a piecewise constant potential

## 2.1 Introduction

Simple models that are exactly solvable serve as a foundation of condensed matter physics. These straightforward cases often yield significant insights and illuminate the intricate phenomena present in the natural universe. A representative instance is the quantum particle confined within a square well, an essential topic any undergraduate physics student studying quantum mechanics encounters. Utilizing this fundamental model allows for the exploration and explanation of numerous physical phenomenon seen in the laboratory. For example, George Gamow famously employed the square well to explain alpha decay [35].

We will begin our analysis with an infinite square well separated by a barrier to represent a double well potential energy landscape. The Fokker-Planck equation will be introduced, which we can transform into a Schrödinger equation using specific techniques. This transformation allows the resolution of the problem in closed form,

where we can manipulate the width of the barrier separating the two wells. Our findings will demonstrate that the Mpemba Effect can occur even in systems that lack metastability—a claim that was validated experimentally shortly after publishing our results [1, 30].

Furthermore, in chapter 3. we will extend our consideration from a piecewise constant double well potential to a continuous model, which will enhance our understanding of the Mpemba Effect.

Driven by our desire to deepen our understanding of the Mpemba effect, we explore this phenomenon in the context of a Langevin particle diffusing and advecting across a potential energy landscape, specifically in the overdamped regime. Our investigation into the Mpemba effect—characterized by non-monotonic thermal relaxation—focuses on how various parameters of the potential landscape influence this behavior. It's worth mentioning that Kumar and Bechhoefer conducted an experimental study of a similar system, utilizing optical tweezers to establish a double-well potential [2]. They observed how a colloidal particle submerged in water responded as it approached equilibrium, becoming the first to report a pronounced Mpemba effect experimentally. Furthermore, in collaboration with Chétrite, they also identified the inverse Mpemba effect [1]. In this work, we take a theoretical approach, examining several straightforward potential forms and highlighting the key attributes that lead to strong Mpemba effects depending on the potential configurations.

An overly simplistic heuristic explanation of the Mpemba effect suggests that systems at lower temperatures become trapped in metastable states, unlike identical systems that start at higher temperatures. This explanation rides on the premise that specific metastable states with appropriate geometrical characteristics are essential for the effect to manifest. However, our findings indicate that metastable states are

not a prerequisite for the Mpemba effect to occur. Specifically, in the context of a piecewise-constant potential, both analytical and numerical analyses reveal phase space regions where the Mpemba effect is present, including areas without a notion of metastable states. Our model further demonstrates that the boundaries of these regions correspond to significant changes in eigenvector direction and phase transitions. We also explore methodologies for identifying anomalous relaxation behavior and discuss potential applications for these findings.

The chapter is organized as follows. In section 2.2 we introduce the physical model, section 2.3 defines the Mpemba effect and relevant topological properties of it. In section 2.4 we specify the potential and solve for the Mpemba effect. Section 2.5 contains our main results on the strong Mpemba effect in the case of overdamped-Langevin dynamics in a piecewise-constant potential and 2.6 summarizes the paper.

## 2.2 Model

We consider a particle subject to potential $\tilde{U}(\tilde{x})$, and damping $\tilde{\gamma}$, in a thermal environment, characterized by noise $\tilde{\Gamma}(\tilde{t})$. The mean and the variance of the noise are

$$\langle \tilde{\Gamma}(\tilde{t}) \rangle = 0 \text{ and } \langle \tilde{\Gamma}(\tilde{t}) \tilde{\Gamma}(\tilde{t}') \rangle = 2\tilde{\gamma} k_B \tilde{T}_b \delta(\tilde{t} - \tilde{t}'), \tag{2.1}$$

where $\tilde{T}_b$ is the temperature of the surrounding heat bath and $k_B$ is the Boltzmann's constant. For damping $\tilde{\gamma}$ large compared to inertia, the motion of the particle is described by the overdamped-Langevin equation

$$\frac{d\tilde{x}}{d\tilde{t}} + \frac{1}{\tilde{\gamma}} \frac{d\tilde{U}}{d\tilde{x}} = \frac{\tilde{\Gamma}(\tilde{t})}{\tilde{\gamma}}. \tag{2.2}$$

The evolution of a probability density $\tilde{p}(\tilde{x},\tilde{t})$ of having a particle at position $\tilde{x}$ at time $\tilde{t}$ obeys the Fokker-Planck equation

$$\frac{\partial \tilde{p}}{\partial \tilde{t}} = \frac{\partial}{\partial \tilde{x}}\left[\frac{1}{\tilde{\gamma}}\frac{d\tilde{U}}{d\tilde{x}}\tilde{p}\right] + \frac{2k_B\tilde{T}_b}{2\tilde{\gamma}}\frac{\partial^2 \tilde{p}}{\partial \tilde{x}^2}, \tag{2.3}$$

c.f. [36, 37, 38]. The Fokker-Planck equation arises in many situations, such as in Brownian motion [37, 39], colloids held with optical tweezers [2], chemical reactions [40, 38], fluctuations of the current on a Josephson junction, and stretching of a polymer [41, 42, 43].

It is convenient to use the following normalized coordinate $x$, time $t$, potential $U$ and temperature $T$ defined as

$$x \equiv \frac{2\pi}{L}\tilde{x},\; t \equiv \frac{(2\pi)^2}{L^2}\frac{k_B\tilde{T}_b}{\tilde{\gamma}}\tilde{t},\; U \equiv \frac{\tilde{U}}{k_B\tilde{T}_b},\; T \equiv \frac{\tilde{T}}{\tilde{T}_b}. \tag{2.4}$$

The normalized coordinate is in the domain $x \in \mathcal{D} \equiv [-\pi,\pi]$. Note that the normalized potential $U$ and time $t$ depend on the bath temperature $\tilde{T}_b$. In the new variables the Fokker-Planck equation is

$$\frac{\partial p}{\partial t} = \mathcal{L}_F\, p = -\frac{\partial J}{\partial x}, \tag{2.5}$$

where $\mathcal{L}_F$ is the Fokker-Planck operator

$$\mathcal{L}_F \equiv \frac{\partial}{\partial x}U' + \frac{\partial^2}{\partial x^2}, \tag{2.6}$$

and $J(x,t)$ is the probability current

$$J(x,t) \equiv -e^{-U(x)}[e^{U(x)}p(x,t)]'. \tag{2.7}$$

Here $U' \equiv dU/dx$, and the equilibrium probability density at $T_b = 1$ is

$$\pi(x|T=1) = \left.\frac{e^{-U(x)/T}}{Z(T)}\right|_{T=1}, \tag{2.8}$$

where $Z(T) \equiv \int_{\mathcal{D}} \pi(x|T)\, dx$ is the norm. The Fokker-Planck operator $\mathcal{L}_F$ is not self-adjoint, but it can be transformed into a self-adjoint operator $\mathcal{L}$ with the following transformation

$$\mathcal{L} = e^{\frac{U(x)}{2}} \mathcal{L}_F e^{-\frac{U(x)}{2}} = \frac{\partial^2}{\partial x^2} - V(x), \tag{2.9}$$

where

$$V(x) \equiv e^{\frac{U(x)}{2}} \left( \frac{\partial^2}{\partial x^2} e^{-\frac{U(x)}{2}} \right) = \frac{U'^2}{4} - \frac{U''}{2}, \tag{2.10}$$

for details see e.g. [37]. Finding the spectrum of the Fokker-Planck operator $\mathcal{L}_F$, reduces to solving a Schrödinger eigenvalue problem

$$\mathcal{L}\psi_\mu = \lambda_\mu \psi_\mu. \tag{2.11}$$

The eigenvalues are ordered and non-positive $\lambda_1 = 0 > \lambda_2 \geq \lambda_3 \geq ...$ The general solution with the initial condition $p(x', 0)$ is

$$p(x,t) = \int_{\mathcal{D}} G(x, x', t) p(x', 0)\, dx', \tag{2.12}$$

where the transition probability is

$$G(x, x', t) = e^{-\frac{U(x)}{2} + \frac{U(x')}{2}} \sum_\mu \psi_\mu(x) \psi_\mu^*(x') e^{-|\lambda_\mu| t}, \tag{2.13}$$

and the eigenvectors $\psi_\mu$ fulfil the completeness relation $\sum_\mu \psi_\mu(x)\psi_\mu^*(x') = \delta(x-x')$. The first eigenvector, corresponding to $\lambda_1 = 0$, is $\psi_1(x) = e^{-U(x)/2}/\sqrt{Z(1)}$. Thus the general solution for the probability density is

$$p(x,t) = \frac{e^{-U(x)}}{Z(1)} + \sum_{\mu>1} a_\mu e^{-\frac{U(x)}{2}} \psi_\mu(x) e^{-|\lambda_\mu| t}, \tag{2.14}$$

with

$$a_\mu \equiv \int_{\mathcal{D}} dx' p(x',0) e^{\frac{U(x')}{2}} \psi_\mu^*(x')\, dx'. \tag{2.15}$$

Assuming $\lambda_2 > \lambda_3$ at times $t \gg |\lambda_3|^{-1}$ we have

$$p(x,t) \approx \frac{e^{-U(x)}}{Z(1)} + a_2 e^{-\frac{U(x)}{2}} \psi_2(x) e^{-|\lambda_2| t}. \tag{2.16}$$

## 2.3 The Mpemba effect

Let us choose for the initial condition the equilibrium distribution at temperature $T$, i.e.

$$p(x,0) = \pi(x|T) = \frac{e^{-U(x)/T}}{Z(T)}. \tag{2.17}$$

In this case the overlap coefficients $a_\mu$ are

$$a_\mu(T) = Z^{-1}(T) \int_{\mathcal{D}} dx' e^{-U(x')\left(\frac{1}{T}-\frac{1}{2}\right)} \psi_\mu(x')\, dx'. \tag{2.18}$$

Notice that because of orthogonality of $\psi_\mu$ eigenvectors we get $a_\mu(1) = 0$ as expected (no cooling or heating if $T = T_b = 1$). As $T \to \infty$, $a_\mu$ becomes independent of

temperature, and plateaus to a constant. Assuming that $\lambda_2 > \lambda_3$ the Mpemba effect occurs for $a_2(T)$ non-monotonic as a function of initial temperature $T$ [25]. The strong Mpemba effect occurs for $a_2(T) = 0$ for select $T \neq T_b$, [26]. If $a_2(T) = 0$ for all $T$, then the relaxation to equilibrium does not have that mode and one needs to look at $\mu > 2$ for anomalous relaxations.

### 2.3.1 Parity analysis

One way to check for the strong Mpemba effect in cooling is to check for parity,

$$\mathcal{P}_{\text{dir}} \equiv \left[ -\left.\frac{da_2}{dT}\right|_{T=1} a_2(T=\infty) \right], \tag{2.19}$$

$$\mathcal{P}_{\text{inv}} \equiv \lim_{\varepsilon \to 0^+} \left[ \left.\frac{da_2}{dT}\right|_{T=1} a_2(\varepsilon) \right], \tag{2.20}$$

which was introduced in [26]. There is an odd number of zero crossing of $a_2(T)$ between $T \in (1, \infty)$ if $\mathcal{P}_{\text{dir}} > 0$. From Eq. (2.15) we have

$$a_2(\infty) = \frac{1}{2\pi} \int_{\mathcal{D}} \psi_2(x) e^{\frac{U(x)}{2}}\, dx, \tag{2.21}$$

$$\left.\frac{da_2}{dT}\right|_{T=1} = \frac{Z(2)}{Z(1)} \left[ \langle U\psi_2 \rangle_1 - \langle U \rangle_1 \langle \psi_2 \rangle_2 \right], \tag{2.22}$$

where $\langle g(x) \rangle_T \equiv \int_{\mathcal{D}} g(x) e^{-\frac{U(x)}{T}} [Z(T)]^{-1}\, dx$. Thus the parities of the direct and inverse strong Mpemba effect are

$$\mathcal{P}_{\text{dir}} = \left[ \left( \langle U \rangle_1 \langle \psi_2 \rangle_2 - \langle U\psi_2 \rangle_1 \right) \int_{\mathcal{D}} e^{\frac{U(x)}{2}} \psi_2(x) dx \right], \tag{2.23}$$

$$\mathcal{P}_{\text{inv}} = \lim_{\varepsilon \to 0^+} \left[ \left( \langle U\psi_2 \rangle_1 - \langle U \rangle_1 \langle \psi_2 \rangle_2 \right) \times \right.$$
$$\left. \times \int_{\mathcal{D}} e^{\frac{U(x)}{2} - \frac{U(x)}{\varepsilon}} \psi_2(x) dx \right]. \tag{2.24}$$

## 2.4 Piecewise-constant potential

We examine the occurrence of the Mpemba effect in the context of simple potentials to better understand the conditions under which this phenomenon arises. In scenarios involving symmetric potentials, $V(x)$ and $U(x)$, the eigenvector corresponding to the first excited state, $\psi_2$, is odd. Consequently, for symmetric domains, the overlap coefficient $a_2$, as described by Eq. (2.18), becomes null, indicating the absence of a Mpemba effect associated with this coefficient. Further details can be found in A.0.1 Additionally, in the case of the quadratic potential $U(x) = kx^2/2$, representative of the Ornstein-Ühlenbeck process, we demonstrate in A.0.2 that the Mpemba effect does not manifest.

As we proceed to the next simplest scenario, we introduce an analytically solvable model featuring a piecewise constant potential with three distinct regions. Here, we analytically and numerically derive the areas within the phase space defined by the parameters of the potential, where the system exhibits a Mpemba effect. Our principal findings are detailed in 2.5.

Let us choose the potential as

$$U(x) = \begin{cases} U_1, & x \in [-\pi, -\alpha\pi/2) \\ U_0, & x \in [-\alpha\pi/2, \pi/2] \\ 0, & x \in (\pi/2, \pi] \end{cases}, \tag{2.25}$$

where $U_0$, $U_1$, and $\alpha \in [0, 1]$. Our potential has finite jumps at $-\alpha\pi/2$ and $\pi/2$, and it diverges to infinity at $\pm\pi$. For a finite discontinuity of the potential the probability current must be constant to satisfy the conservation of probability. Assuming we

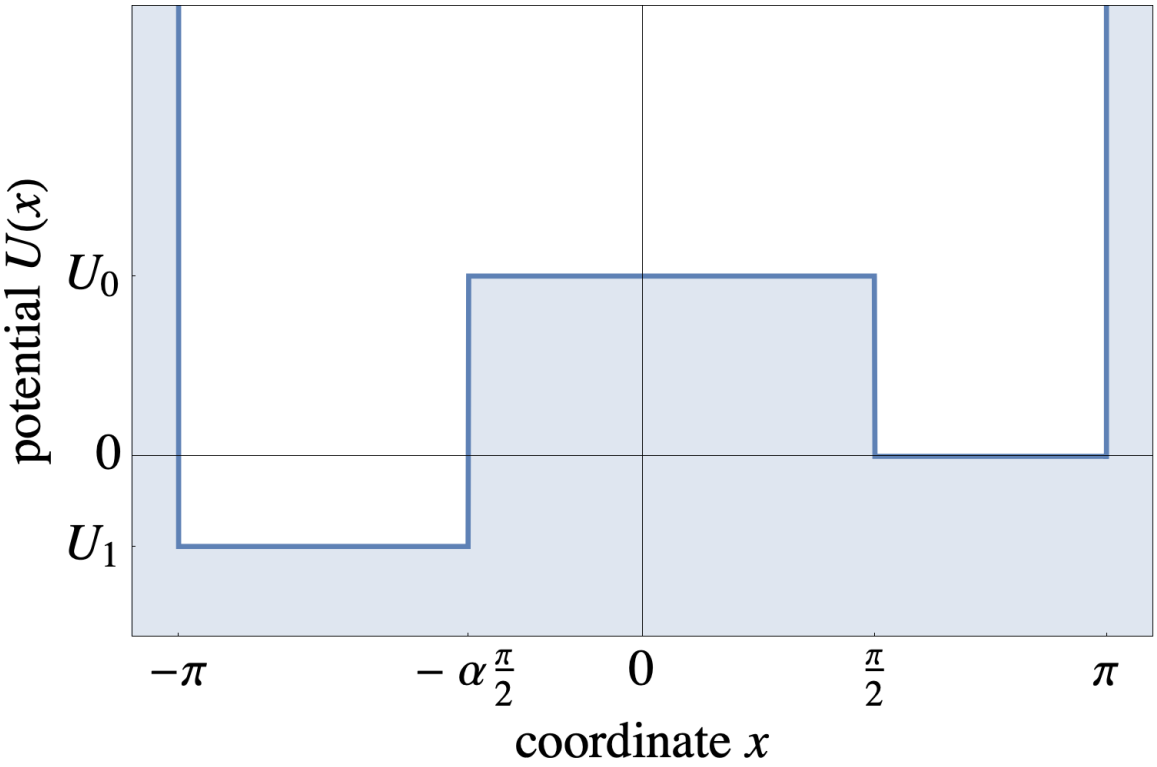


Figure 2.1: Piecewise-constant potential $U(x)$ with parameters $U_0$, $U_1$, and $\alpha \in [0, 1]$.

have a finite jump at $x$ the "jump" conditions are

$$e^{\frac{U(x^+)}{2}}\psi_\mu(x^+) = e^{\frac{U(x^-)}{2}}\psi_\mu(x^-),$$
$$e^{-\frac{U(x^+)}{2}}\left[\psi'_\mu(x^+) + \frac{1}{2}U'(x^+)\psi_\mu(x^+)\right] = e^{-\frac{U(x^-)}{2}}\left[\psi'_\mu(x^-) + \frac{1}{2}U'(x^-)\psi_\mu(x^-)\right]. \tag{2.26}$$

We demand that the potential takes on an infinite positive value at the boundaries of the domain. For a meaningful steady state to exist, it is essential that the probability current is zero at these boundaries, specifically $J(\pm\pi) = 0$.

### 2.4.1 Bistable symmetric rectangular potential well

Let's set $U_1 = 0$, $\alpha = 1$, and explore different values for $U_0$. In this scenario, the potential represents a bistable symmetric rectangular well. The Fokker-Planck equation can be solved analytically [44]. The eigenvector associated with the first excited state is

$$\psi_2(x) = \begin{cases} -\frac{1}{\sqrt{\pi}}\cos[\nu(\pi + x)], & x \in [-\pi, -\frac{\pi}{2}) \\ \frac{1}{\sqrt{\pi}}\sin[\nu x], & |x| \leq \frac{\pi}{2} \\ \frac{1}{\sqrt{\pi}}\cos[\nu(\pi - x)], & x \in (\frac{\pi}{2}, \pi] \end{cases}, \tag{2.27}$$

with $\nu \equiv (2/\pi)\arctan[e^{-U_0/2}]$. We find the relevant eigenvalues are nondegenerate: $\lambda_1 = 0$, $\lambda_2 = \nu^2$, and $\lambda_3 = 1$. The first excited state $\psi_2$ is odd, leading to $a_2 = 0$, because the integral of an odd function over a symmetric domain equals zero. This implies there is no Mpemba effect associated with $a_2$. This finding is consistent with the finding of Kumar and Bechhoefer, who observed that the Mpemba effect is absent for $a_2$ in their experiments with a double-well symmetric potential in a symmetric domain [2].

### 2.4.2 Varying the heights and the widths of a piecewise-constant potential

Let's now consider the cases of $\alpha \in [0,1]$, and vary $U_0$ and $U_1$. The eigenfunctions are

$$\psi_\mu = \begin{cases} A_\mu \cos[\sqrt{\lambda_\mu}(x+\pi)], & -\pi \le x < \frac{-\alpha\pi}{2} \\ B_\mu \cos[\sqrt{\lambda_\mu}x] + C_\mu \sin[\sqrt{\lambda_\mu}x], & \frac{-\alpha\pi}{2} \le x \le \frac{\pi}{2} \\ D_\mu \cos[\sqrt{\lambda_\mu}(x-\pi)], & \frac{\pi}{2} < x \le \pi \end{cases} . \tag{2.28}$$

The zero-current boundary conditions, $\psi'_\mu(\pm\pi) = 0$, are fulfilled by construction. The jump conditions, Eqs. (2.4) and (2.4), and the normalization of $\psi_\mu$'s, specify the coefficients $A_\mu$, $B_\mu$, $C_\mu$ and $D_\mu$. The transcendental equation that specifies $\lambda_2$ is

$$\frac{-e^{U_1}\cos\left[\frac{\sqrt{\lambda_2}\alpha\pi}{2}\right] + e^{U_0}\sin\left[\frac{\sqrt{\lambda_2}\alpha\pi}{2}\right]\tan\left[\sqrt{\lambda_2}\pi\left(1-\frac{\alpha}{2}\right)\right]}{e^{U_1}\cos\left[\frac{\sqrt{\lambda_2}\alpha\pi}{2}\right] - e^{U_0}\sin\left[\frac{\sqrt{\lambda_2}\alpha\pi}{2}\right]\tan\left[\sqrt{\lambda_2}\pi\left(1-\frac{\alpha}{2}\right)\right]} = \frac{\cot\left[\frac{\sqrt{\lambda_2}\pi}{2}\right] - e^{U_0}\tan\left[\frac{\sqrt{\lambda_2}\pi}{2}\right]}{e^{U_0}+1}. \tag{2.29}$$

It is important to note that the width parameter $\alpha$ appears solely within trigonometric functions, thereby limiting its contribution. For a general $\alpha$, an explicit form for $\lambda_2$ cannot be derived. However, explicit forms do exist for the specific cases when $\alpha = 1$ and $\alpha = 0$. In the following sections, we will present analytical results for these two scenarios, along with numerical results applicable to any arbitrary width parameter $\alpha$.

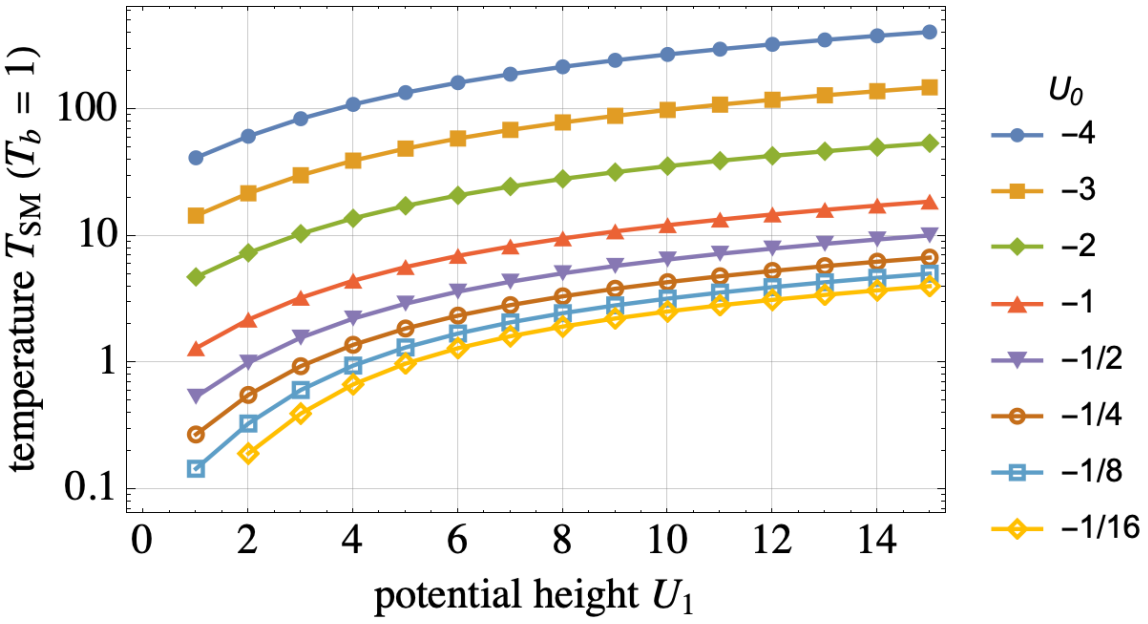


Figure 2.2: The temperature of the strong Mpemba effect $T_{\rm SM}$ as a function of potential parameters $U_0$, $U_1$ and $\alpha = 1$. Here $k_B = 1$ and $T_b = 1$.

**Equal widths of the left and right sections, the $\alpha = 1$ case**

In the case $\alpha = 1$ we have the transcendental equation gives $\lambda_2$ as

$$\lambda_2 = \left[\frac{2}{\pi}\tan^{-1}\left[\sqrt{\frac{2-\tanh\left[\frac{U_0}{2}\right]-\tanh\left[\frac{U_0-U_1}{2}\right]}{2+\tanh\left[\frac{U_0}{2}\right]+\tanh\left[\frac{U_0-U_1}{2}\right]}}\right]\right]^2. \tag{2.30}$$

Plugging in $\psi_2$ and $\lambda_2$, into Eq. (2.18) we get the overlap coefficient $a_2$

$$a_2 = \frac{2\sin\left[\frac{\pi\sqrt{\lambda_2}}{2}\right]}{\pi\sqrt{\lambda_2}} \times \frac{\left(A_2 e^{\frac{U_0}{T}+\frac{U_1}{2}} + 2B_2 e^{\frac{U_0}{2}+\frac{U_1}{T}} + D_2 e^{\frac{U_0}{T}+\frac{U_1}{T}}\right)}{\left(e^{\frac{U_0}{T}+\frac{U_1}{T}} + e^{\frac{U_0}{T}} + 2e^{\frac{U_1}{T}}\right)}.$$

The jump conditions, Eqs. (2.4) and (2.4), and the normalization of $\psi_2$, specify the coefficients $A_2$, $B_2$, $C_2$ and $D_2$. The zeros of the numerator of $a_2$ define the set of temperatures for which we have the strong Mpemba effect [26]. For particular choices of potential parameters $U_0$ and $U_1$, we get the Mpemba effect. The strong

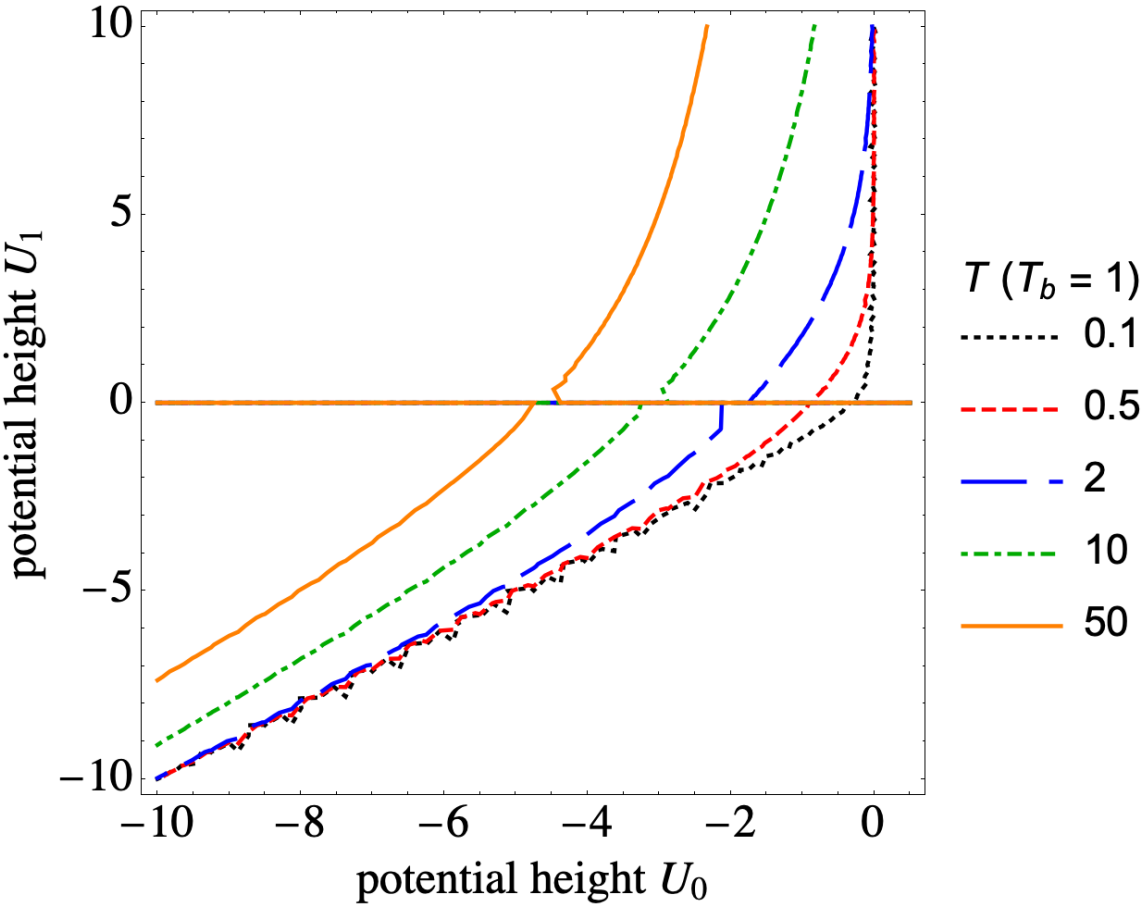


Figure 2.3: The strong Mpemba effect is present along the isolines of $a_2 = 0$ for the potential heights $U_1$, $U_0$, $\alpha = 1$ and initial temperature $T$. Here $T_b = 1$ and $k_B = 1$.

Mpemba temperature $T_{\rm SM}$ as a function of $U_0$, and $U_1$ is shown on Fig. 2.2. The isolines of the strong Mpemba effect in the $U_0U_1-$plane are depicted on Fig. 2.3. On Fig. 2.4 the green region shows the region of existence of the direct strong Mpemba effect (cooling), and the yellow region shows the region of existence of inverse strong Mpemba (heating). In the blue region, there is no strong Mpemba effect. We observe the strong Mpemba effect for $U_1 > U_0$ and $U_0 < 0$, which corresponds to the absence of metastable states. Note that we see the Mpemba effect in the absence of metastable states – this challenges the heuristic explanation attempt described in the introduction, c.f. also [45]

Below in Section 2.5 we argue that the strong Mpemba effect for $\alpha = 1$ happens when the mismatch between the initial probability and the final probability in the left region matches that the mismatch between the initial and final probabilities of the right region.

**Wide left section, the $\alpha = 0$ case**

Above we demonstrated the $\alpha = 1$ case is exactly solvable. Next we obtain an analytic solution for the $\alpha = 0$ case. In this example, the width of the left section is twice the width of the center section and right section. The form of the eigenfunctions is Eq. (2.28), but the eigenvalue $\lambda_2$ is different

$$\lambda_2 = \left[\frac{2}{\pi}\tan^{-1}\left(\sqrt{\frac{e^{U_1-U_0} - \tanh\left[\frac{U_0}{2}\right] + 1}{e^{U_1-U_0} + \tanh\left[\frac{U_0}{2}\right] + 1}}\right)\right]^2, \tag{2.31}$$

and the domains with the strong effect are changed respectively, see Fig. 2.5. Now we see that the region with the strong Mpemba effect is dramatically smaller. It requires fine-tuning the potential to demonstrate the Mpemba effect. However, unlike

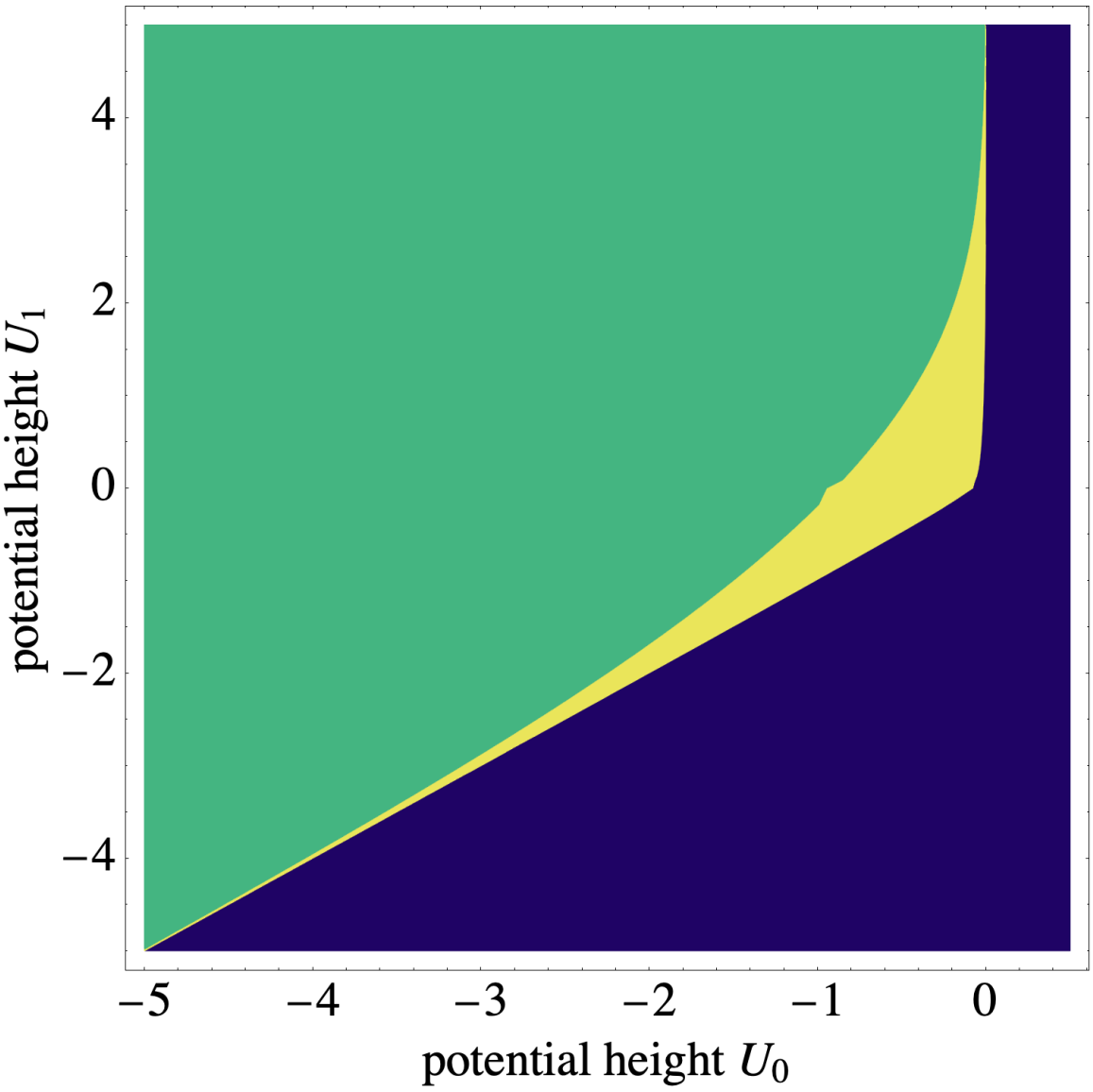


Figure 2.4: The strong Mpemba effect for $\alpha = 1$. In the green region we have the direct strong Mpemba effect (the parity $\mathcal{P}_{\rm dir} > 1$) and in the yellow region we have computed the inverse strong Mpemba effect (the parity $\mathcal{P}_{\rm inv} > 1$, where $\varepsilon = 0.02$). The parities are defined in Eqs. (2.19) and (2.20). In the blue region there is no strong Mpemba effect. Here $T_b = 1$ and $k_B = 1$.

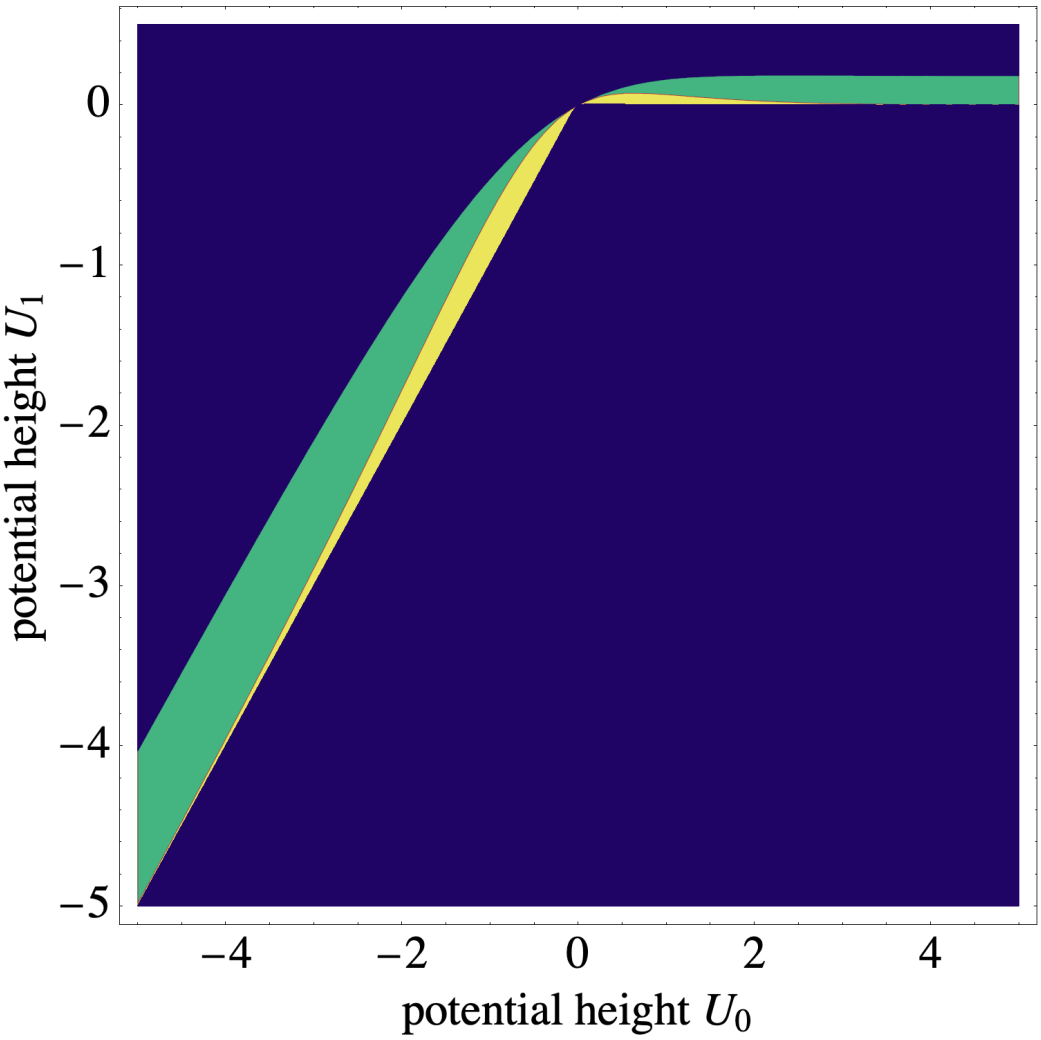


Figure 2.5: The strong Mpemba effect as a function of the potential parameters $U_0$, $U_1$, and $\alpha = 0$. In the green region we have the direct strong Mpemba effect (the parity for the direct effect is $\mathcal{P}_{\rm dir} > 1$; see Eq. (2.19)) and in the yellow region we have the inverse strong Mpemba effect (the parity for the inverse effect is $\mathcal{P}_{\rm inv} > 1$) region. The parity $\mathcal{P}_{\rm inv}$ was computed by choosing $\varepsilon = 0.02$ in Eq. (2.20). In the blue region there is no strong Mpemba effect. Here $T_b = 1$ and $k_B = 1$.

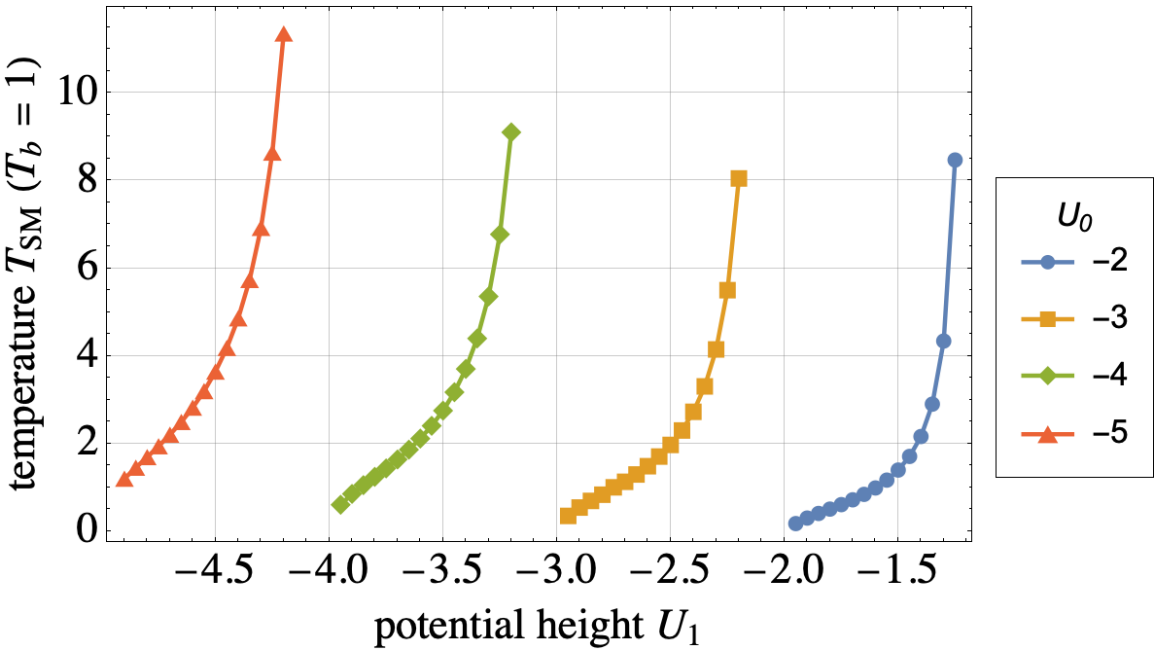


Figure 2.6: The temperature of the strong Mpemba effect $T_{\mathrm{SM}}$ as a function of potential parameters $U_0$, $U_1$, and $\alpha = 0$. Here $T_b = 1$ and $k_B = 1$.

the $\alpha = 1$ case, one now has a Mpemba effect for a barrier in the middle section ($U_0 > U_1$ and $U_0 > 0$) and metastable states, akin in the experiment of Kumar and Bechhoefer [2]. The strong Mpemba temperature $T_{\mathrm{SM}}$ as a function of $U_0$, and $U_1$ is shown on Fig. 2.6. The isolines of the strong Mpemba effect in on the $U_0U_1-$plane are depicted on Fig. 2.7.

**Varying middle section's width, the case $\alpha \in (0, 1)$**

Next, we consider what happens if we change the width of the left and middle piecewise sections, with $\alpha \in (0, 1)$. It is important to note that we are not solving the system perturbatively; we are solving the whole problem for new widths, starting with the transcendental equation given by Eq. (2.29). In the case of arbitrary $\alpha$ Eq. (2.29) does not have an explicit solution for $\lambda_2$, but it is solvable numerically. After the

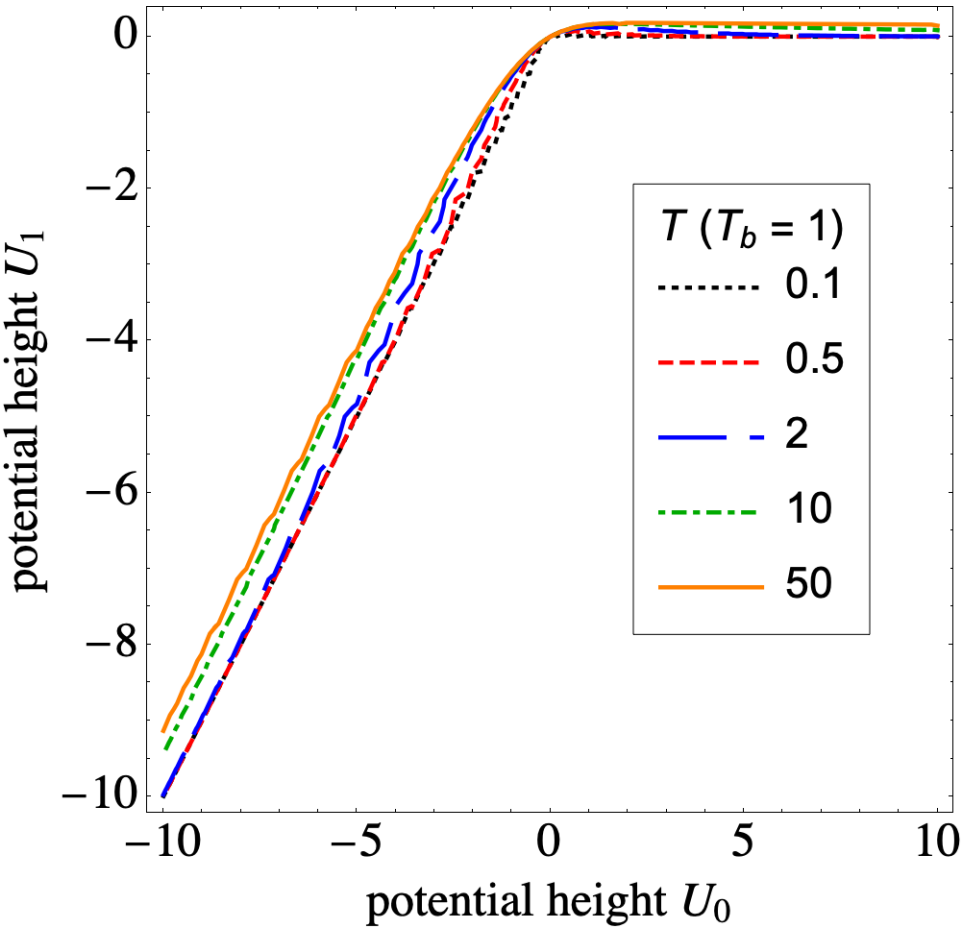


Figure 2.7: The strong Mpemba effect is present along the isolines of $a_2 = 0$ for the potential parameters $U_1$, $U_0$, $\alpha = 0$ and initial temperature $T$. Here $T_b = 1$ and $k_B = 1$.

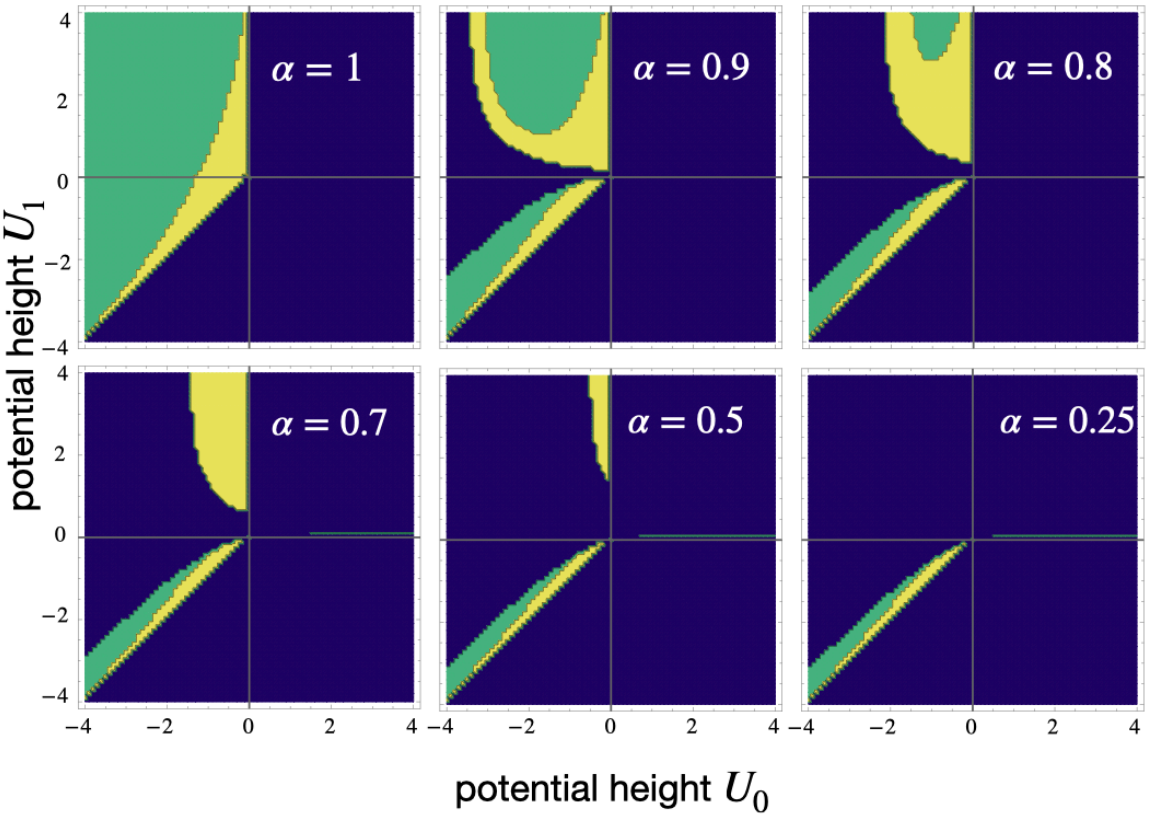


Figure 2.8: The strong Mpemba effect as a function of potential parameters $U_0$, $U_1$, and $\alpha \in [0.25, 1]$. In the green region we have the direct strong Mpemba effect (the parity $\mathcal{P}_{\text{dir}} > 1$) and in the yellow region we have the inverse strong Mpemba effect ($\mathcal{P}_{\text{inv}} > 1$) region. There is no strong Mpemba effect in the blue region. Here we looked for the strong effect between initial temperatures $0.02\,T_b \leq T \leq 200\,T_b$, where $T_b = 1$ and $k_B = 1$. The parity was calculated via Eqs. (2.19) and (2.20).

eigenvalue is obtained, the coefficients $A_2$ $B_2$, $C_2$ and $D_2$ are calculated from the jump conditions, Eqs. (2.4) and (2.4), and the normalization of the eigenvector. Now we can go about calculating $a_2$ numerically and study what happens. In the parity plots Fig. 2.8 we see the behavior changes immediately. This change can be understood through the symmetry breaking of the middle section. The eigenvector for this region is, $B_\mu \cos[\sqrt{\lambda_\mu}x] + C_\mu \sin[\sqrt{\lambda_\mu}x]$. When we integrate this eigenvector over a symmetric domain, as we do in the $\alpha = 1$ case, the contribution of the $\sin[\sqrt{\lambda_\mu}x]$ piece always vanishes. By changing $\alpha$, we break this symmetry and now $\sin[\sqrt{\lambda_\mu}x]$ term in the middle section, $-\alpha\pi/2 \leq x \leq \pi/2$, will also contribute to the overlap $a_2$.

## 2.5 General remarks on the strong Mpemba effect for the piecewise-constant potential

### 2.5.1 Regions of the direct and strong Mpemba effect

Here the direct and inverse strong Mpemba effect regions are disjoint, see Fig. 2.8, while in general, the effects can coexist. For example, in Glauber dynamics on the mean-field antiferromagnet on a complete bipartite graph, there is a region where one has both strong Mpemba effects [26].

Also, note that the region where we have the inverse effect in this range of parameters seems smaller than where we have the direct effect. It results from a temperature unit scale we have imposed on the problem by setting $T_b = 1$. Namely, there is less "room" to create non-zero curvature between the $T_b$ and zero temperature, then between $T_b$ and infinity, which corresponds to less phase space area for the inverse strong Mpemba effect than the direct strong Mpemba effect.

### 2.5.2 Ratio of the mismatch in equilibrium probabilities in the flanking regions

To shed some intuition on when we see the strong Mpemba effect we look at the difference of the equilibrium probabilities for the particle to be at the left and the right region at the bath temperature $T_b$ and the temperature of the strong Mpemba effect $T_{\rm SM}$. The equilibrium probability of a particle being in region $\mathcal{D}_i$ is

$$\Pi_i(T) \equiv \int_{\mathcal{D}_i} \pi(x|T)dx, \tag{2.32}$$

where $\mathcal{D}_1 = [-\pi, -\alpha\pi/2)$ is the left, $\mathcal{D}_0 = [-\alpha\pi/2, \pi/2]$ is the middle and $\mathcal{D}_2 = (\pi/2, \pi]$ is the right region. The ratio of the difference in equilibrium probabilities is defined as

$$R \equiv \frac{\Pi_1(T_b) - \Pi_1(T_{\rm SM})}{\Pi_2(T_b) - \Pi_2(T_{\rm SM})}. \tag{2.33}$$

From Fig. 2.9 we notice that for left and right regions of the same width, $\alpha = 1$ case, the ratio $R = 1$. In this case, we have the strong Mpemba effect only if there is a difference between the initial and final probabilities in the left region, matching that of the right region. Also, $R = 1$, can be used as an implicit formula for $T_{\rm SM}$.

For flanking regions of different widths, $\alpha < 1$, the ratio $R$ is less than $R(\alpha = 1) = 1$. I.e., in this case, we have the strong Mpemba effect when the wider region contains less probability mismatch than the narrower region – how much less depends on all of the parameters of the potential, that is $R(U_0 - U_1, U_0, \alpha)$. Namely, we see from Fig. 2.9 that the ratio $R$ is a function of both the gap $U_0 - U_1$ and $U_0$. As we make the left region wider, reduce $\alpha$, the dependence on $U_0$ becomes weaker compared

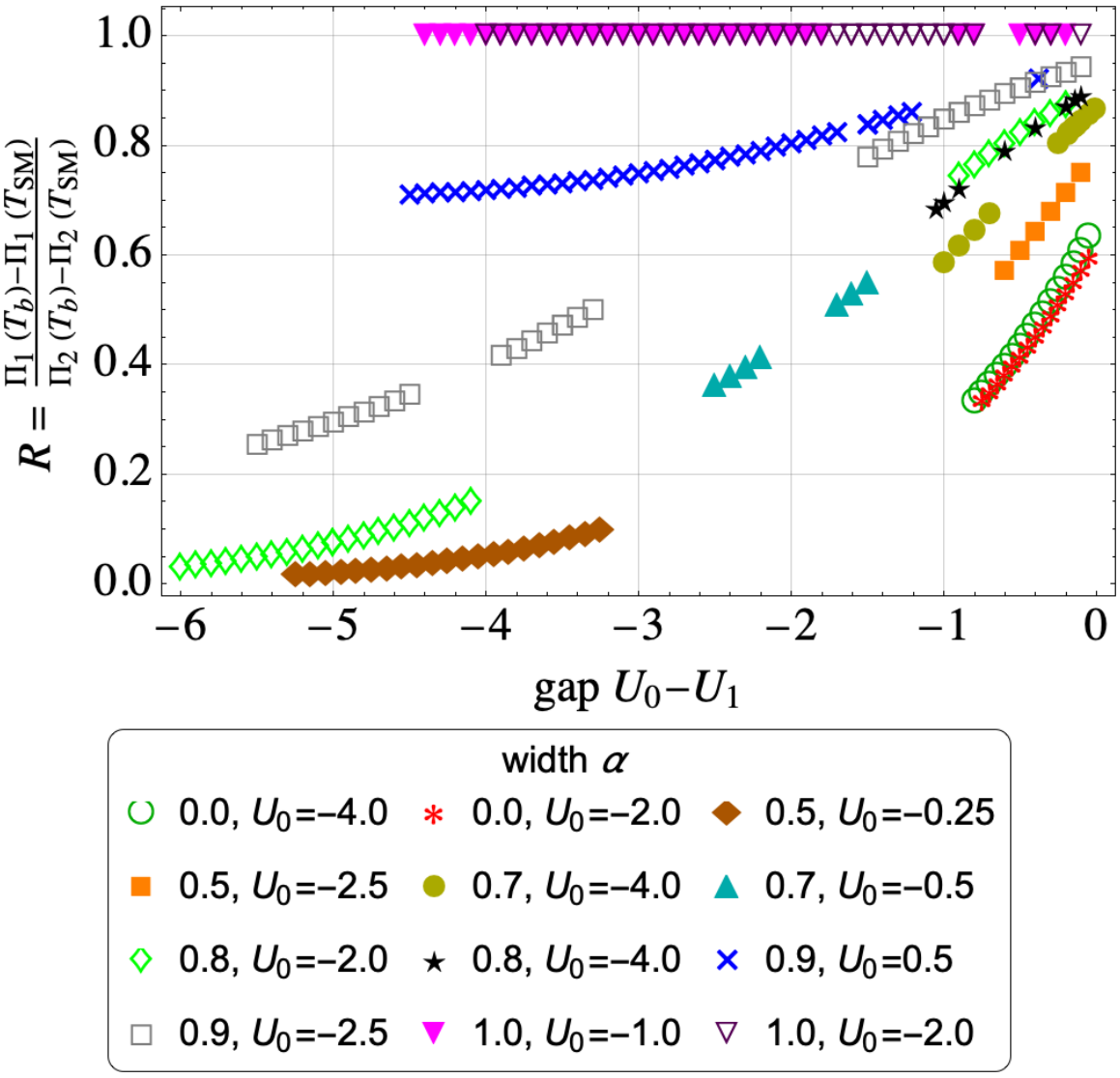


Figure 2.9: Ratio of difference of equilibrium probabilities at the bath temperature, $T_b$, and the temperature where we have the strong Mpemba effect, $T_{\rm SM}$, for the left region (1) and the right region (2) as a function of the gap $U_0 - U_1$, $U_0$ and $\alpha$. Here $T_b = 1$ and $k_B = 1$. We notice that the ratio $R$ is equal to 1 for $\alpha = 1$. In other cases, $\alpha \in [0, 1)$, the ratio depends on both the gap $U_0 - U_1$ and $U_0$.

to the dependence on the gap $U_0 - U_1$.

Note that in the case of the metastable Mpemba effect, described in [1, 2], the authors see the effect for potentials that simultaneously satisfy $\Pi_1(T_b) = \Pi_1(T_{\mathrm{SM}})$ and $\Pi_2(T_b) = \Pi_2(T_{\mathrm{SM}})$, which is quite different from our case. Indeed, for the piecewise-constant potential that we are considering, metastability is not needed to have the effect. Even more, for $\alpha = 1$, we do not have the effect if we have metastability.

### 2.5.3 Topological considerations

The existence of the strong Mpemba effect could be thought of as a topological invariant [26]. Namely, it is a non-trivial intersection of the locus of points corresponding to the equilibrium distribution at different temperatures and the $a_2 = 0$ hyperplane. The number of times this locus of points intersects the $a_2 = 0$ hyperplane is the intersection number and was named the Mpemba index by the authors of [26]. As a topological invariant, the Mpemba index can change under perturbations, but its modulo two cannot. Our results show agreement with this assertion. In our analysis of the piecewise-constant potential, we show that the strong Mpemba effect cannot be removed or introduced without changing the Mpemba index modulo two, which can only happen if, as laid out in [26]:

(i) The perturbation changes the ordering of the eigenvalues – it causes $\lambda_3$ to become larger than $\lambda_2$.

(ii) The perturbation causes $a_2(0)$ or $a_2(\infty)$ or both to change sign. For this to occur, the eigenvector $\psi_2$ must change "direction."

(iii) There is a phase transition. For example, the ground state of the system

changes.

We obtain the full spectrum of eigenvalues analytically and conclude that eigenvalues $\lambda_2$ and $\lambda_3$ do not cross in our case; thus, (i) never happens. In our case, removing or introducing the strong Mpemba effect requires that the system goes through a change of the direction of the eigenvector (ii) or through a phase transition (iii), or both.

Fig. 2.4, Fig. 2.5, and Fig. 2.8 provide a simple phase diagrams. The green, yellow, and blue regions are divided by domain walls, demarking the region of existence of the direct, the inverse strong Mpemba effect, and the absence of both effects, respectively.

For equally wide outer sections, in the $\alpha = 1$ case, one can only get a strong Mpemba on a part $U_0 < 0$ half-plane where $U_0 < U_1$ (see Fig. 2.4). In this case, one cannot get a strong Mpemba effect in $a_2$ if the middle section is a barrier. Regardless of how small one makes the middle section, i.e. $U_0$, it cannot be the highest potential height. The symmetry of the problem protects this. It seems that as if one needs remove the metastable states for the effect to occur. Likewise, choosing $U_0 < 0$ and crossing the $U_1 = U_0$ line toward $U_1 < U_0$ introduces a metastable state and removes the strong Mpemba effect. However, note that simply "removing" metastable states will not introduce the effect; in the region $U_1 < U_0 < 0$, there is no strong Mpemba effect, despite the absence of metastable states.

In the case that the outer potential sections have different widths, the $\alpha \neq 1$ case, there now exists additional domain walls, compared to the $\alpha = 1$ case, where the Mpemba index modulo two can change, see Fig. 2.5 and Fig. 2.8. As before, these domain walls correspond to the eigenvector changing the direction and to changes of the ground state.

The line between the direct and the inverse effect (between green and yellow

regions on the phase diagrams on Fig. 2.4, Fig. 2.5, and Fig. 2.8) corresponds to two zeros of $a_2$, one at $T > T_b$ and the other at $T = T_b$, merging into one at $T = T_b$ and the becoming two distinct zeros again where one is now at $T < T_b$ and the other remains at $T = T_b$.

To conclude, by studying how a Brownian particle diffuses on a potential energy landscape, we see how the particle behaves vastly differently depending on the geometry of the potential landscape. Intuitively this is to be expected, but what is interesting is that there are particular initial temperatures for which the system relaxes exponentially faster than when starting from other temperatures. By studying this phenomenon in our piecewise-constant potential, we see that this behavior is protected by symmetries present in our problem and is robust to perturbations. Together, these provide intuition on the dynamical behavior of our Brownian particle. The described exotic behavior could be considered a topological phase because the system's behavior is topologically protected against perturbations.

Additionally, out of the three cases which change the Mpemba index, stated in 2.5, the phase transitions and the crossing of eigenvalues are properties of the potential and bath only; they do not depend on the initial conditions, while as the eigenvector some changes of direction are significant for specific initial conditions. Thus one could use eigenvalue crossings and phase transitions to gauge the domains which might yield the Mpemba effect. Such explorations might be useful for experimental and numerical applications.

## 2.6 Summary

We studied the occurrence of the Mpemba effect in several simple potentials. We show that there is no Mpemba effect for symmetric potentials in symmetric domains related to the first excited state. We further show that to find a Mpemba effect, one needs to go beyond a quadratic potential to polynomials of higher degrees or make the diffusion coefficient spatially dependent.

Next, we solved analytically and numerically the case of a piecewise-constant potential with variable height and variable width sections. We analyzed the existence of the strong Mpemba effect as a function of the parameters of the potential and remarked on the topological aspects of the strong effect. In particular, we found that in the case of equal-width outer sections and a variable height of the sections, there seems to be no strong Mpemba effect if the system has metastable states. I.e., the middle section cannot be a barrier between the two wells. If the outer sections are not of equal width, this condition is relaxed, and we can also have the Mpemba effect with metastable states present. In summary, we challenge the intuition that for the strong Mpemba effect, one needs metastable states. Instead, we demonstrate by our example that it sometimes becomes more challenging to have a Mpemba effect if the potential contains metastable states. The phase diagrams that we obtained show manifestly different relaxation behavior on every line that denotes a change of the deepest well.

Moreover, in the case of equal-width outer sections we found that the strong Mpemba effect occurs when the ratio of the mismatch between initial and final probabilities in the two outer sections is equal.

A particle diffusing in a potential landscape is a frequent effective description in

phenomenological theories. For an arbitrary potential, the problem is not analytically tractable. We chose this conceptually simple situation to gain intuition on anomalous relaxation processes and nonmonotonicity in relaxation times. We looked at a piecewise-constant potential, where we could solve for the dynamics of the probability distribution function exactly. We analyzed the connection between the occurrence of the strong Mpemba effect and the parameters of the potential. Based on topological considerations, we have identified the domains in the phase space, formed by the potential parameters, where one might expect to see the effect. These are areas on whose boundaries where there is a phase change (in our case, the deepest well changes) or where the eigenvector changes the direction significantly compared to the initial condition. In our example, for the phase space parameters that we checked, the areas with the strong Mpemba effect seemed simply connected. Studying the topology of such regions would be an exciting future avenue of study.

Understanding better when the Mpemba effect occurs will enable us to design auxiliary potential traps, such as with electromagnetic fields or optical lattices, that could facilitate optimal cooling and heating of our system and allow better preparation of a system in a particular state.

# Chapter 3

# Mpemba effect in terms of mean first passage times

## 3.1 Introduction

Rapid changes in temperature can lead to unexpected thermal relaxation behaviors in physical systems. A notable instance of such an anomaly is the Mpemba effect. This phenomenon occurs when a system initially set to a higher temperature surpasses an identical system at a lower, yet still warm, temperature, leading it to equilibrate more swiftly with a cold environment [25]. A similar effect has been observed during heating processes as well [25, 1]. When comparing two identical systems as they relax to their surroundings, one might intuitively expect that the system with a closer temperature to the environment would thermalize more rapidly. However, this is not always the case. The Mpemba effect has been documented in various materials including water [4, 3], clathrate hydrates [5], magnetic systems [6], polymers [7], and colloidal particle systems [2]. Additionally, numerical studies have indicated its presence in spin-glasses [9], systems lacking equipartition [10], driven granular gases [11, 12, 13, 14, 15, 16, 17, 18], cold gases [19], quantum systems [20, 21, 22], molecular gases [23, 24], and antiferromagnets [25, 26, 27, 28, 29]. The widespread nature of these observations suggests that the effect is quite general, prompting significant exploration in

theoretical studies [25, 26, 30, 31, 32, 33, 34].

The significance of the Mpemba effect lies in its potential to enhance our understanding of such "shortcuts" to thermalization, which could provide insights into broader concepts within nonequilibrium statistical mechanics. Practically, it holds relevance for optimizing heating and cooling protocols and for effective phase space sampling, making it a topic of interest across both scientific and industrial domains. To investigate the Mpemba effect as a representative case study, we utilize overdamped Langevin dynamics applied to a double-well potential. This approach has significant applications, including in chemical reactions, polymers, colloids, escape from metastable states, models of quantum tunneling, and scalar field theories. The classic Kramers' escape problem, related to a classical point particle in a potential with a metastable state, has been extensively studied [39, 46, 47, 48, 49], yet the conditions for the emergence of the Mpemba effect within this framework remain unclear.

In this chapter, we establish the necessary conditions for the Mpemba effect within the small-diffusion limit of overdamped Langevin dynamics on a double-well potential, expressing the conditions in terms of mean first passage times. Our findings align with the experimental results reported by Kumar and Bechhoefer [2], who explored the Mpemba effect in a colloidal system subjected to thermal quenching in water.

The structure of this chapter is as follows: we will first introduce the model and the Mpemba effect, followed by the derivation of the necessary conditions for the effect. Our analytical results are derived under the assumptions of small diffusion and large barrier limits, where the Kramers' problem can be solved analytically. Lastly, we will confirm our results through Monte Carlo simulations of Langevin dynamics.

## 3.2 Model

### 3.2.1 Overdamped Langevin dynamics and Fokker-Planck equation

We examine the overdamped Langevin dynamics of a particle situated within a double-well potential $U$, as illustrated in Fig. 3.1, while immersed in a thermal bath of solvent molecules. The trajectory of the particle, denoted as $\mathrm{x}(t)$, obeys

$$\gamma \frac{d}{dt}\mathrm{x}(t) = -\frac{1}{m}U'[\mathrm{x}(t)] + \Gamma(t), \tag{3.1}$$

the force is represented by $-U' \equiv -dU/d\mathrm{x}$, while $\gamma$ denotes the friction coefficient, and $\Gamma(t)$ signifies the thermal noise per unit mass. In scenarios where the time significantly exceeds the particle-solvent collision time, $\Gamma(t)$ adheres to Gaussian statistics, characterized by $\mathbb{E}[\Gamma(t)] = 0$ and $\mathbb{E}[\Gamma(t)\Gamma(t')] = 2\gamma(k_B T_b/m)\delta(t-t')$. The diffusion coefficient is given by $k_B T_b/m\gamma$. For the purposes of our analysis, we set the Boltzmann constant and particle mass to unity ($k_B = 1$, $m = 1$). The corresponding Fokker-Planck (FP) equation articulates the evolution of the probability density, $p(x,t)$, representing the probability of finding a particle at a specific coordinate $x$ at time $t$,

$$\partial_t p(x,t) \quad = \tfrac{1}{\gamma}\partial_x \left\{ [U'(x) + T_b \partial_x]\, p(x,t) \right\} \equiv \mathcal{L}\, p(x,t), \tag{3.2}$$

where $\mathcal{L}$ is the FP operator. We also denote the probability current density, $j(x,t)$, as $\partial_t p(x,t) \equiv -\partial_x j(x,t)$. The system is closed and we thus have reflective boundary

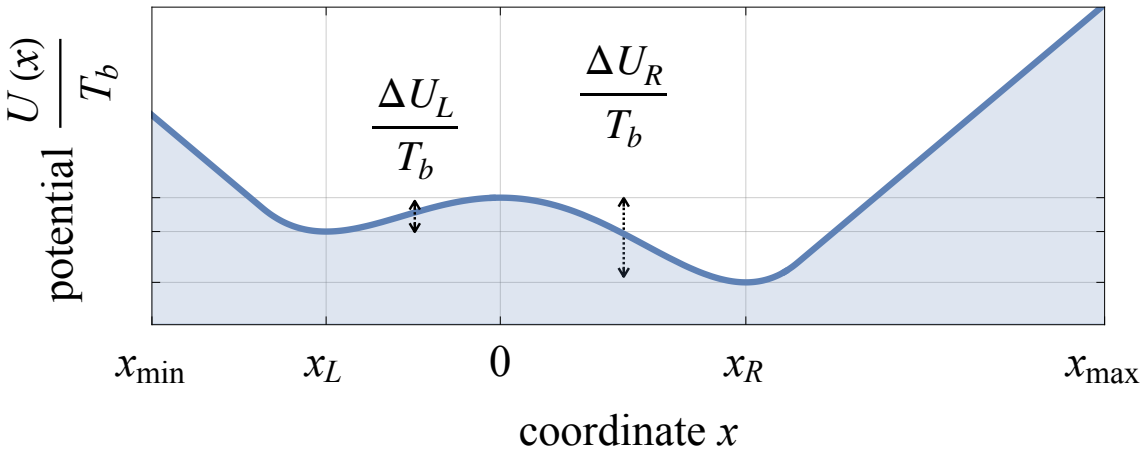


Figure 3.1: Double-well potential $U(x)$ with the barrier centered at $x = 0$, and minima at $x_L$ and $x_R$. The barrier heights are $\Delta U_L$ and $\Delta U_R$.

conditions. The stationary distribution is the Boltzmann distribution,

$$\pi_{T_b}(x) = \frac{1}{Z(T_b)} e^{-\frac{U(x)}{T_b}}, \tag{3.3}$$

where $Z(T_b) \equiv \int_{x_{\min}}^{x_{\max}} \exp[-U(x)/T_b]\, dx$ is the partition function.

The scalar product is defined as $\langle u, v\rangle \equiv \int_{x_{\min}}^{x_{\max}} u(x)v(x)\, dx$ and the adjoint operator of the FP operator is denoted $\mathcal{L}^\dagger = \gamma^{-1}[-U'\partial_x + T_b\partial_x^2]$. The corresponding eigenvalue problems can be expressed as: $\mathcal{L}v_i = \lambda_i v_i$ and $\mathcal{L}^\dagger u_i = \lambda_i u_i$. The relationship between the eigenfunctions is given by $u_i(x) = \exp[U(x)/T_b]v_i(x)$. The eigenvalues are arranged in order, with $\lambda_1 = 0$ representing the eigenvalue corresponding to $\pi_{T_b}$, while the remaining eigenvalues are negative: $0 > \lambda_2 \geq \lambda_3 \geq \ldots$ The probability density $p(x, t)$ is introduced as follows:

$$p(x, t) = \pi_{T_b}(x) + \sum_{i>1} a_i e^{\lambda_i t} v_i(x), \tag{3.4}$$

with overlap coefficients

$$a_i \equiv \frac{\langle u_i, p_{\text{init}} \rangle}{\langle u_i, v_i \rangle}, \tag{3.5}$$

and $p_{\text{init}}$ is the initial condition.

### 3.2.2 Strong and weak Mpemba Effect

We begin by assuming that the system is in equilibrium at temperature $T$, denoted as $\pi_T$. We then examine scenarios where there is a gap between the second and third eigenvalues, specifically $\lambda_2 > \lambda_3$. The strong Mpemba effect is observed when the overlap $a_2$, as defined in Eq. (3.5), is equal to zero. Which is expressed mathematically as:

$$\langle u_2 \rangle_T = 0. \tag{3.6}$$

Here $\langle \cdot \rangle_T$ represents the equilibrium expectation value at temperature $T$.

The strong Mpemba effect is defined by jump in relaxation time from $-\lambda_2^{-1}$ to $-\lambda_3^{-1}$, leading to exponentially accelerated relaxation process toward equilibrium. It occurs for initial conditions that are orthogonal to the slowest relaxation mode. The concept of the strong Mpemba effect was established by Klich, Raz, Hirschberg, and Vucelja in [26], and experimentally first observed by Kumar and Bechhoefer [2]. The strong Mpemba effect implies the weak Mpemba effect, which happens when $a_2$ is a non-monotonic function of initial temperature $T$ [25]. Specifically, this condition is

met when $\partial_T a_2 = 0$, which for finite $T$ reduces to

$$\langle u_2 U \rangle_T - \langle u_2 \rangle_T \langle U \rangle_T = 0. \tag{3.7}$$

We will proceed to determine $\lambda_2$ and $u_2$.

## 3.3 Spectrum of the adjoint Fokker-Planck operator

For the spectrum of the adjoint FP operator, we look at the following eigenvalue problem

$$\partial_x \left[ e^{-\frac{U(x)}{T_b}} \partial_x u_i(x) \right] = \frac{\gamma \lambda_i}{T_b} e^{-\frac{U(x)}{T_b}} u_i(x). \tag{3.8}$$

Integrating the equation from $x_{\min}$ to $x$ twice and using the conservation of probability, we have

$$u_i(x) = u_i(x_{\min}) \times \left[ 1 + \frac{\gamma \lambda_i}{T_b} \frac{\int_{x_{\min}}^{x} e^{\frac{U(y)}{T_b}} \, dy \int_{x_{\min}}^{y} e^{-\frac{U(z)}{T_b}} u_i(z) \, dz}{u_i(x_{\min})} \right]. \tag{3.9}$$

For details, see the supplementary material. Similarly integrating twice from $x$ to $x_{\max}$ and using the boundary condition $u_i'(x_{\max}) = 0$, we get another expression for $u_i$,

$$u_i(x) = u_i(x_{\min}) \alpha_i \times \left[ 1 + \frac{\gamma \lambda_i}{T_b} \frac{\int_{x}^{x_{\max}} e^{\frac{U(y)}{T_b}} \, dy \int_{y}^{x_{\max}} e^{-\frac{U(z)}{T_b}} u_i(z) \, dz}{u_i(x_{\max})} \right],$$

with $\alpha_i \equiv u_i(x_{\max})/u_i(x_{\min})$.

In the small-diffusion limit the eigenfunction $u_i$ over the domain $\mathcal{D}_L \equiv [x_{\min}, 0]$ can be more accurately approximated starting from Eq. (3.9) than Eq. (3.10). Conversely, over the domain $\mathcal{D}_R \equiv [0, x_{\max}]$, it is preferable to utilize Eq. (3.10). By imposing the continuity condition for $u_i$ at $x = 0$, we determine the eigenvalue

$$\frac{\gamma\lambda_i}{T_b} = (1-\alpha_i)\left[\alpha_i \frac{\int_0^{x_{\max}} e^{\frac{U(y)}{T_b}}\, dy \int_y^{x_{\max}} e^{-\frac{U(z)}{T_b}} u_i(z)\, dz}{u_i(x_{\max})} - \frac{\int_{x_{\min}}^{0} e^{\frac{U(y)}{T_b}}\, dy \int_{x_{\min}}^{y} e^{-\frac{U(z)}{T_b}} u_i(z)\, dz}{u_i(x_{\min})}\right]^{-1}. \tag{3.10}$$

In the following derivation, we will identify the first nonzero eigenvalue, $\lambda_2$, along with its corresponding left eigenfunction, $u_2$. The magnitude of $\lambda_2$ signifies the switching rate between the two wells. The Kramers' problem presents an analytical solution in the regime of small diffusion and large barriers, as referenced in, c.f. [37, 50]. It is important to note that both barriers illustrated in Fig. 3.1 must be significantly larger than the diffusion factor, specifically $|\Delta U_L| \gg T_b$ and $|\Delta U_R| \gg T_b$. In this scenario, the transition rate between the wells is minimal, indicating that $\lambda_2$ is small. We utilize this to determine $\lambda_2$ and $u_2$. In the zeroth approximation, diffusion is negligible, resulting in no transitions between the wells, thus $\lambda_2^{(0)} = 0$. This condition leads to the conclusion that $u_2$, defined in Eqs. (3.9) and (3.10), is a step function,

$$u_2^{(0)} = \begin{cases} u_2(x_{\min}), & x \in \mathcal{D}_L \\ u_2(x_{\max}), & x \in \mathcal{D}_R \end{cases}. \tag{3.11}$$

In this instance, we observe a breakdown of ergodicity.

It is crucial to highlight that we have centered the potential to establish a local

maximum at $x = 0$. The coefficient $\alpha_2^{(0)}$ is derived from the requirement that $u_2'(x)$ remains continuous at $x = 0$. In the zeroth-order approximation, the condition of continuity at $x = 0$ yields the following results:

$$\alpha_2^{(0)} = -\int_{x_{\min}}^{0} e^{-\frac{U(z)}{T_b}}\, dz \Big/ \int_{0}^{x_{\max}} e^{-\frac{U(z)}{T_b}}\, dz \equiv -\Pi_L(T_b)/\Pi_R(T_b), \tag{3.12}$$

where we label with $\Pi_L(T_b)$ and $\Pi_R(T_b)$ the probabilities of the particle being in left and right well at temperature $T_b$. By substituting $u_2^{(0)}$, Eq. (3.11), within the precise formula for $\lambda_2$, Eq. (3.10), we arrive at the following result.

$$\frac{\gamma\lambda_2^{(1)}}{T_b} = -\frac{Z(T_b)}{\Pi_R(T_b)\mathcal{A}_L(0)+\Pi_L(T_b)\mathcal{A}_R(0)}, \tag{3.13}$$

where we denoted

$$\mathcal{A}_R(x) \equiv \textstyle\int_x^{x_{\max}} e^{\frac{U(y)}{T_b}}\, dy \int_y^{x_{\max}} e^{-\frac{U(z)}{T_b}}\, dz, \tag{3.14}$$

$$\mathcal{A}_L(x) \equiv \textstyle\int_{x_{\min}}^{x} e^{\frac{U(y)}{T_b}}\, dy \int_{x_{\min}}^{y} e^{-\frac{U(z)}{T_b}}\, dz. \tag{3.15}$$

The eigenvector is

$$u_2^{(1)}(x) \propto \begin{cases} 1 + \frac{\gamma\lambda_2^{(1)}}{T_b}\mathcal{A}_L(x), & x \in \mathcal{D}_L \\ \alpha_2^{(1)} + \alpha_2^{(0)}\frac{\gamma\lambda_2^{(1)}}{T_b}\mathcal{A}_R(x), & x \in \mathcal{D}_R \end{cases}. \tag{3.16}$$

From continuity of $u_2(x)$ at $x = 0$, we have $\alpha_2^{(1)} = \alpha_2^{(0)}$.

The values for $\lambda_2$ and $u_2$ can also be derived by analyzing the ground state and the lowest eigenfunction of the adjoint FP operator, employing the inverted potential $-U(x)$ alongside absorbing boundary conditions. It is important to note that there

exists a precise mapping between these two problems [37]. The following section presents the initial nonzero corrections to $\lambda_2$. For clarity, we will omit the superscripts for $u_2$, $\lambda_2$, and $\alpha_2$. Before proceeding further, it is instructive to express $\mathcal{A}_L(x)$ and $\mathcal{A}_R(x)$ in terms of mean first passage times.

## 3.4 Mean first passage time

A typical scenario for analyzing Mean First Passage Time (MFPT) involves tracking particles as they exit a specific domain for the first time never returning, as detailed in references like [50]. Let's consider the domain denoted as $\mathcal{D}_R$. The movement of the particles is described by the Langevin equation Eq. (3.1). Assuming our starting point is $x_0 \in \mathcal{D}_R$, we define the first passage time as the moment when the particle exits the domain. To determine the MFPT, we concentrate on trajectories that remain within the boundaries of $\mathcal{D}_R$ up to time $t$. The distribution of such particles follows the Fokker-Planck (FP) equation given by

$$\partial_t \tilde{p} = \tilde{\mathcal{L}}\tilde{p}, \tag{3.17}$$

where we set $\tilde{\mathcal{L}} = \mathcal{L}$. The inclusion of the tilde indicates that the initial and boundary conditions differ from those discussed elsewhere in the paper.

The initial condition is given by $\tilde{p}(x,0) = \delta(x-x_0)$, where $x_0 \in \mathcal{D}_R$. The boundary conditions are defined as follows: $\tilde{j}(x_{\max}) = [\tilde{p}' + U'\tilde{p}]_{x=x_{\max}} = 0$ and $\tilde{p}(0,t) = 0$. The total number of points remaining in $\mathcal{D}_R$ at time $t$ is expressed by the equation:

$$\tilde{P}(t,x_0) = \int_{\mathcal{D}_R} \tilde{p}(x,t)\,dx. \tag{3.18}$$

The number of points that have yet to leave by time $t$, but do leave during the interval $(t, t+dt)$, is given by:

$$\tilde{P}(t, x_0) - \tilde{P}(t+dt, x_0) = \rho(t, x_0)dt, \tag{3.19}$$

where $\rho(t, x_0)$ represents the distribution of first passage times. The MFPT is defined as the first moment of $t$ with respect to $\rho(t, x_0)$:

$$\tau_R(x_0) = \int_0^\infty t\rho(t, x_0)\, dt = \int_0^\infty \tilde{P}(t, x_0)\, dt. \tag{3.20}$$

In the one-dimensional case, $\tau_R$ can be calculated explicitly (refer to the supplementary material), yielding:

$$T_b\gamma^{-1}e^{\frac{U(x)}{T_b}}\partial_x e^{-\frac{U(x)}{T_b}}\partial_x\tau_R(x) = -1, \tag{3.21}$$

with a boundary condition of $\tau_R(0) = 0$, indicating that any initial point on the boundary exits immediately. We further assume that the MFPT at $x = x_{\max}$ approaches a constant, which leads to $\tau'(x_{\max}) = 0$. Upon integrating Eq. 3.21 twice for the right domain, we obtain:

$$\mathcal{A}_R(x) = T_b\gamma^{-1}\left[\tau_R(x_{\max}) - \tau_R(x)\right], \tag{3.22}$$

for $x \in \mathcal{D}_R$. The derivation for the left domain, $\mathcal{D}_L$, follows a similar procedure. The MFPT $\tau_L$ satisfies the equation:

$$T_b\gamma^{-1}e^{\frac{U(x)}{T_b}}\partial_x e^{-\frac{U(x)}{T_b}}\partial_x\tau_L(x) = -1, \tag{3.23}$$

with boundary conditions $\tau_L'(x_{\min}) = 0$ and $\tau_L(0) = 0$. By integrating this equation twice for $x \in \mathcal{D}_L$, we derive:

$$\mathcal{A}_L(x) = T_b \gamma^{-1} \left[\tau_L(x_{\min}) - \tau_L(x)\right]. \tag{3.24}$$

Utilizing Eq. 3.24 and 3.22, we can express the eigenvalue as:

$$\lambda_2 = -\frac{Z(T_b)}{\Pi_R(T_b)\tau_L(x_{\min}) + \Pi_L(T_b)\tau_R(x_{\max})}. \tag{3.25}$$

In the small-diffusion limit, the exponential integrals in $Z(T_b)$, $\tau_R(x_{\max})$, and $\tau_L(x_{\min})$ can be accurately approximated using Laplace's method. Therefore, in this limit, $\lambda_2$ simplifies to the sum of Kramers' rates from one well to another, as detailed in the supplementary material and compared to the work of [37]. Having derived the expression for $u_2$ (refer to Eq. (3.16) in terms of the MFPT, we can now state the necessary conditions for the Mpemba effect.

## 3.5 Conditions for the Mpemba effect

### 3.5.1 Strong Mpemba effect

Plugging in the expression for $u_2$, as defined in Eq. (3.16), into Eq. (3.6), we derive the condition for the strong Mpemba effect:

$$0 = \left(\frac{\Pi_L(T)}{\Pi_L(T_b)} - \frac{\Pi_R(T)}{\Pi_R(T_b)}\right) + \frac{\gamma\lambda_2}{T_b}\left(\langle\mathcal{A}_L\rangle_{L,T}\frac{\Pi_L(T)}{\Pi_L(T_b)} - \frac{\Pi_R(T)}{\Pi_R(T_b)}\langle\mathcal{A}_R\rangle_{R,T}\right),$$

where $\langle\cdot\rangle_{X,T}$ denotes the average over $\mathcal{D}_X$ with the probability distribution $\pi(T)Z(T)/\Pi_X(T)$, with $X$ representing either $L$ or $R$. In the limit of vanishingly small $\gamma\lambda_2/T_b$, and utilizing the relation $\Pi_L + \Pi_R = 1$, the expression simplifies to:

$$\Pi_L(T) = \Pi_L(T_b), \tag{3.26}$$

which aligns with the observations made by Kumar and Bechhoefer in their experiment [2]. Specifically, they noted that the strong Mpemba effect manifests when the probability of a particle residing in a well remains constant between the initial and bath temperatures. Therefore, under conditions of small $\gamma\lambda_2/T_b$, the strong Mpemba effect emerges when the equilibrium probability of being in a well is predominantly established at the outset. A plausible explanation for this phenomenon is that, particularly in scenarios involving large barriers, relaxing the probability density within each well can occur more rapidly than transitioning between wells. Consequently, the strong Mpemba effect is most pronounced when the system starts with an optimal allocation of probability across the wells. Additional corrections that are linear in $\gamma\lambda_2/T_b$ provide insights into how this condition relates to the MFPT. An example of the strong Mpemba effect and use of Eq. (3.26) is shown in Fig. 3.2.

### 3.5.2 Weak Mpemba effect

After substituting $u_2$ from Eq. (3.16) into Eq. (3.7), we arrive at the condition for the weak Mpemba effect given by:

$$0 = \quad W^{(0)} + \tfrac{\gamma\lambda_2}{T_b} W^{(1)}, \tag{3.27}$$

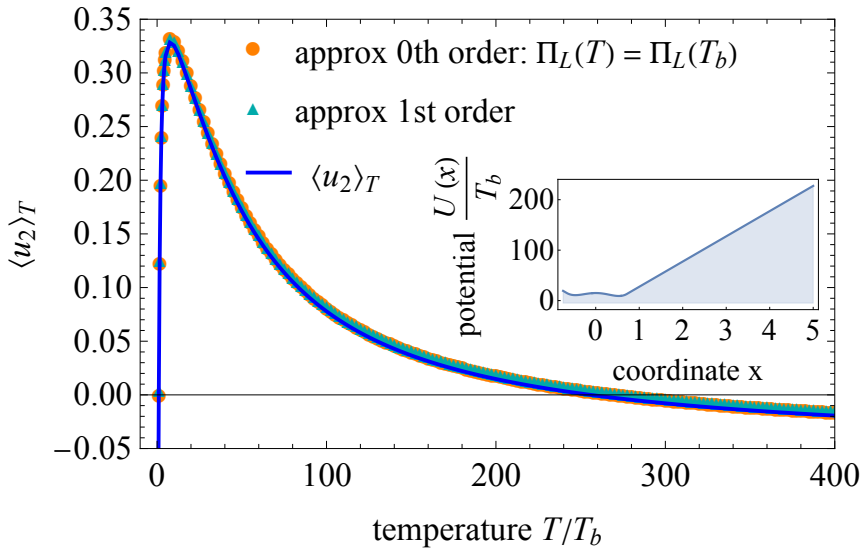


Figure 3.2: An example of a strong Mpemba effect at $T \approx 256\,T_b$. The small-diffusion parameters are: $T_b/|\Delta U_L| = 0.24$ and $T_b/|\Delta U_R| = 0.17$. The eigenvalue is $\lambda_2 \approx -0.287$ numerically and $\lambda_2^{(1)} \approx -0.284$ with our approximation. The inset shows the potential. The condition for the strong Mpemba effect stated in Eq. (3.6) (blue line) and approximated with Eq. (3.26) (orange circles are $0^{\text{th}}$ order and cyan triangles are $1^{\text{st}}$ order approximation). In the zeroth order, we neglected terms proportional to $\gamma\lambda_2/T_b$ in Eq. (3.26). Both orders agree well with the numerics.

where we define $W^{(0)}$ as:

$$W^{(0)} \equiv \langle U \rangle_{L,T} \frac{\Pi_L(T)}{\Pi_L(T_b)} - \frac{\Pi_R(T)}{\Pi_R(T_b)} \langle U \rangle_{R,T} - \langle U \rangle_T \left( \frac{\Pi_L(T)}{\Pi_L(T_b)} - \frac{\Pi_R(T)}{\Pi_R(T_b)} \right), \tag{3.28}$$

and for $W^{(1)}$:

$$W^{(1)} \equiv \langle U\mathcal{A}_L \rangle_{L,T} \frac{\Pi_L(T)}{\Pi_L(T_b)} - \frac{\Pi_R(T)}{\Pi_R(T_b)} \langle U\mathcal{A}_R \rangle_{R,T} - \langle U \rangle_T \left( \langle \mathcal{A}_L \rangle_{L,T} \frac{\Pi_L(T)}{\Pi_L(T_b)} - \frac{\Pi_R(T)}{\Pi_R(T_b)} \langle \mathcal{A}_R \rangle_{R,T} \right). \tag{3.29}$$

When considering a very small value for $\gamma\lambda_2/T_b$, the condition for the Mpemba effect simplifies to $W^{(0)} = 0$. Here, the dependence on the MFPT is encapsulated in $\lambda_2$ and $W^{(1)}$. An illustration of the weak Mpemba effect and the application of Eq. (3.27) can be found in Fig. 3.3.

The necessary conditions for the Mpemba effect, denoted as Eqs. (3.26) and (3.27), articulate the relationship between the MFPT, mean energy, and the correlation between the MFPT and energy that must be satisfied for the effect to manifest. These equations represent the principal findings of this letter.

### 3.5.3 No Mpemba effect for a two-level system

It is important to note that by simplifying the diffusion problem in a double-well potential to a two-level system where the two states correspond to the minima of the potential, the Mpemba effect is not observed. Within the framework of a two-level system, it becomes evident that Eqs. (3.26) and (3.27) are valid only under the condition that $T = T_b$. This outcome aligns with the requirements for the Mpemba effect, which necessitates at least three eigenvectors and a gap ($\lambda_2 > \lambda_3$).

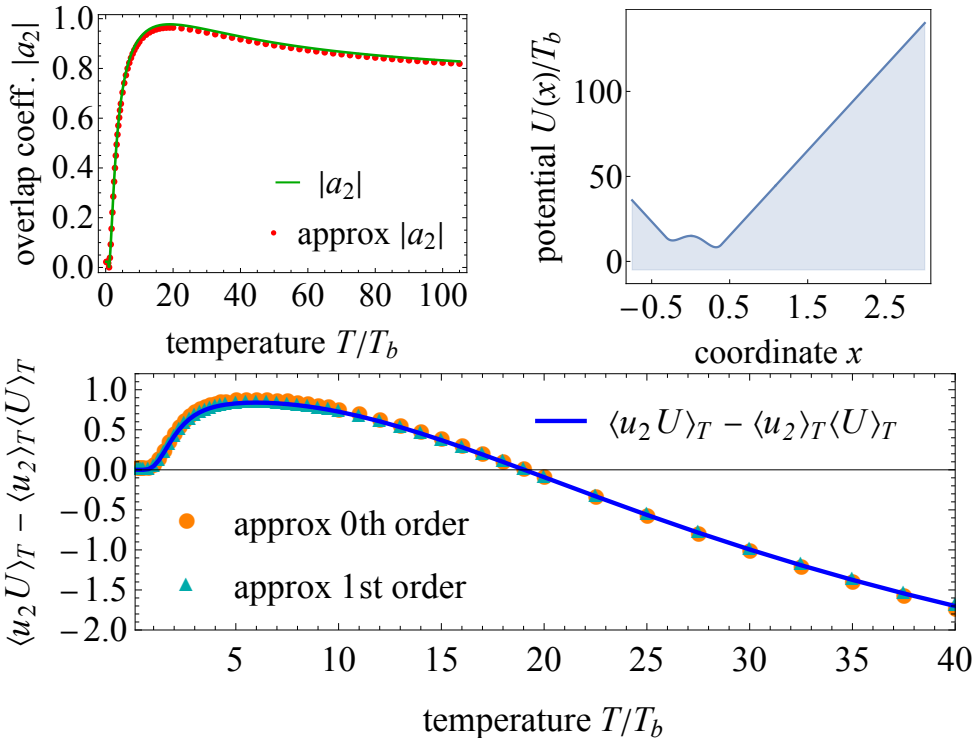


Figure 3.3: (top left) The overlap coefficient $a_2$ obtained numerically (green), and by using approximate $u_2$, Eq. (3.16) (red circles). At initial temperature $T \approx 19\,T_b$ the overlap $a_2$ has a local maximum, which is the hallmark of the weak Mpemba effect. (top right) The potential with small-diffusion parameters: $T_b/|\Delta U_L| = 0.36$ and $T_b/|\Delta U_R| = 0.13$. The eigenvalue is $\lambda_2 \approx -0.92$ numerically and $\lambda_2^{(1)} \approx -0.89$ with our approximation. (bottom) The condition for the weak Mpemba effect stated in Eq. (3.7) (blue line) and approximated with Eq. (3.27) (to $0^{\text{th}}$ order: orange circles and $1^{\text{st}}$ order: teal triangles). In the zeroth order, we neglected terms proportional to $\gamma\lambda_2/T_b$ in Eq. (3.27). Both orders agree well with the numerics.

## 3.6 Stochastic simulations

We set out to validate our theoretical results from the FP analysis, specifically Eqs. (3.26) and (3.27), with respect to overdamped Langevin dynamics. To illustrate our findings, we will utilize the potentials shown in Fig. 3.2 and Fig. 3.3 to simulate the motion of an overdamped Langevin particle. We implement the algorithm introduced in [51], simulating $N = 300,000$ trajectories for each initial condition, using a time step of $\delta t = 5 \times 10^{-4}$ over 500,000 time steps. The distance from equilibrium is calculated as $L_1 = \int_{x_{\min}}^{x_{\max}} |p(x,t) - \pi_{T_b}(x)| dx$, following the method applied by Kumar and Bechhoefer [2]. While we approximate the FP equation using the eigenfunction expansion defined in Eq. (3.4), we can only achieve accurate results for the first few eigenfunctions. As a result, the initial values along the y-axis of the figures below may not align perfectly. Nonetheless, our numerical approximation of the FP equation, analytical results, and stochastic simulations are in agreement. Refer to Fig. 3.4 and Fig. 3.5 for more details.

## 3.7 Generalizations

Our findings extend to scenarios involving spatially-dependent diffusion, thereby predicting the Mpemba effect for potentials that are multiples of the original potential. The approximate solutions for the largest nonzero eigenvalue and eigenfunction can also be adapted to accommodate multiple barriers, as outlined below.

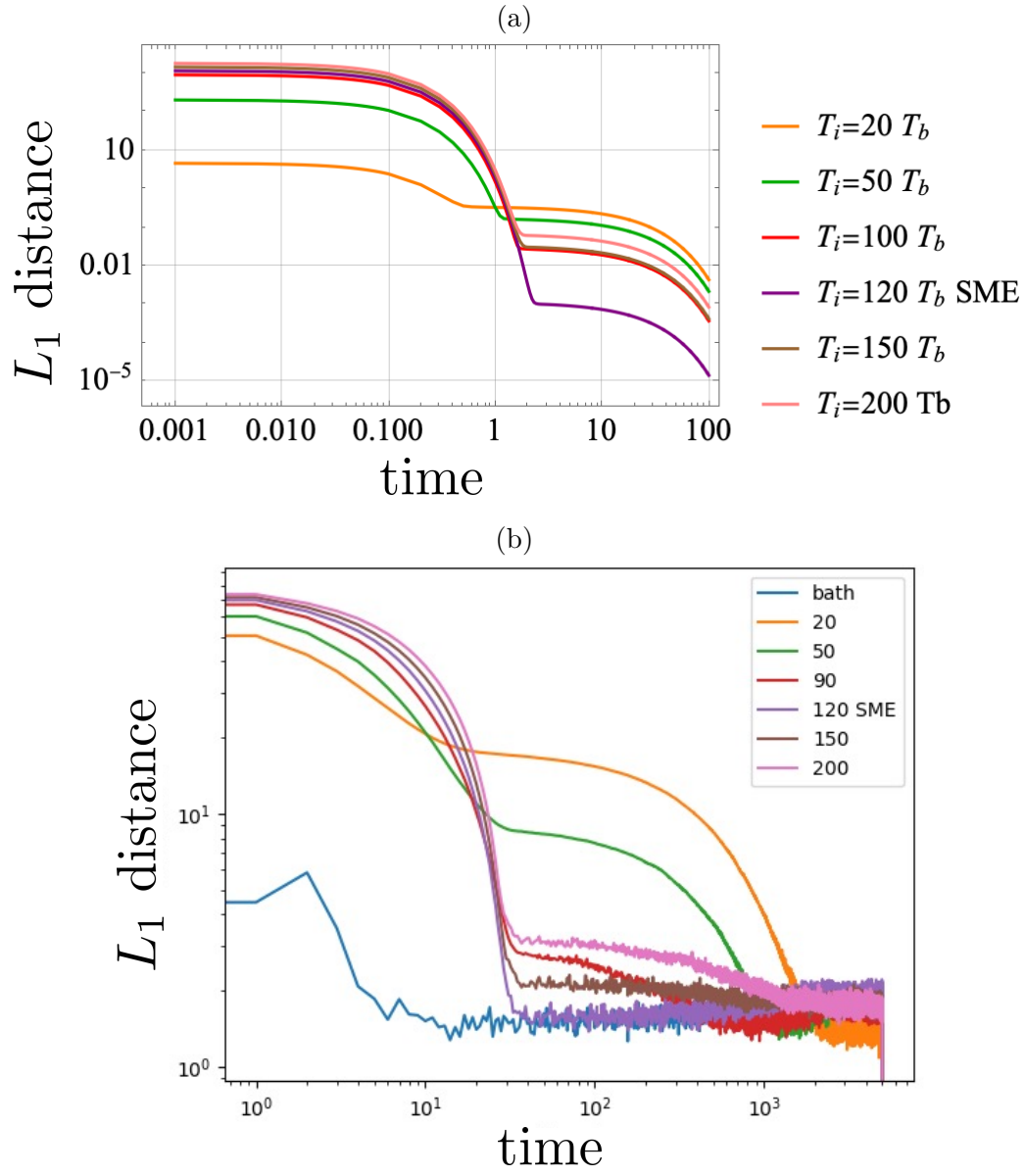


Figure 3.4: Showing the numerical solutions (a) for the Strong Mpemba effect (SME) obtained from the FP equation vs the stochastic simulations (b). Here we are simulating $N = 300,000$ trajectories and calculating the $L_1$ distance at each instance in time. In both figures you can see that $T_i = 120T_b$ is the situation that reaches equilibrium the fastest. This initial condition is the SME. The parameters are $\gamma = 17, T_b = 1.2, \lambda_2 = -0.035$, the potential $U(x)$ is the inset of Fig. 3.2, and we are only using the first $i = 6$ eigenfunctions in the expansion Eq. (3.4). In this case the first order correction to Eq. (3.26) is small and the SME occurs when $\Pi_{L,R}(T_i) = \Pi_{L,R}(T_b)$

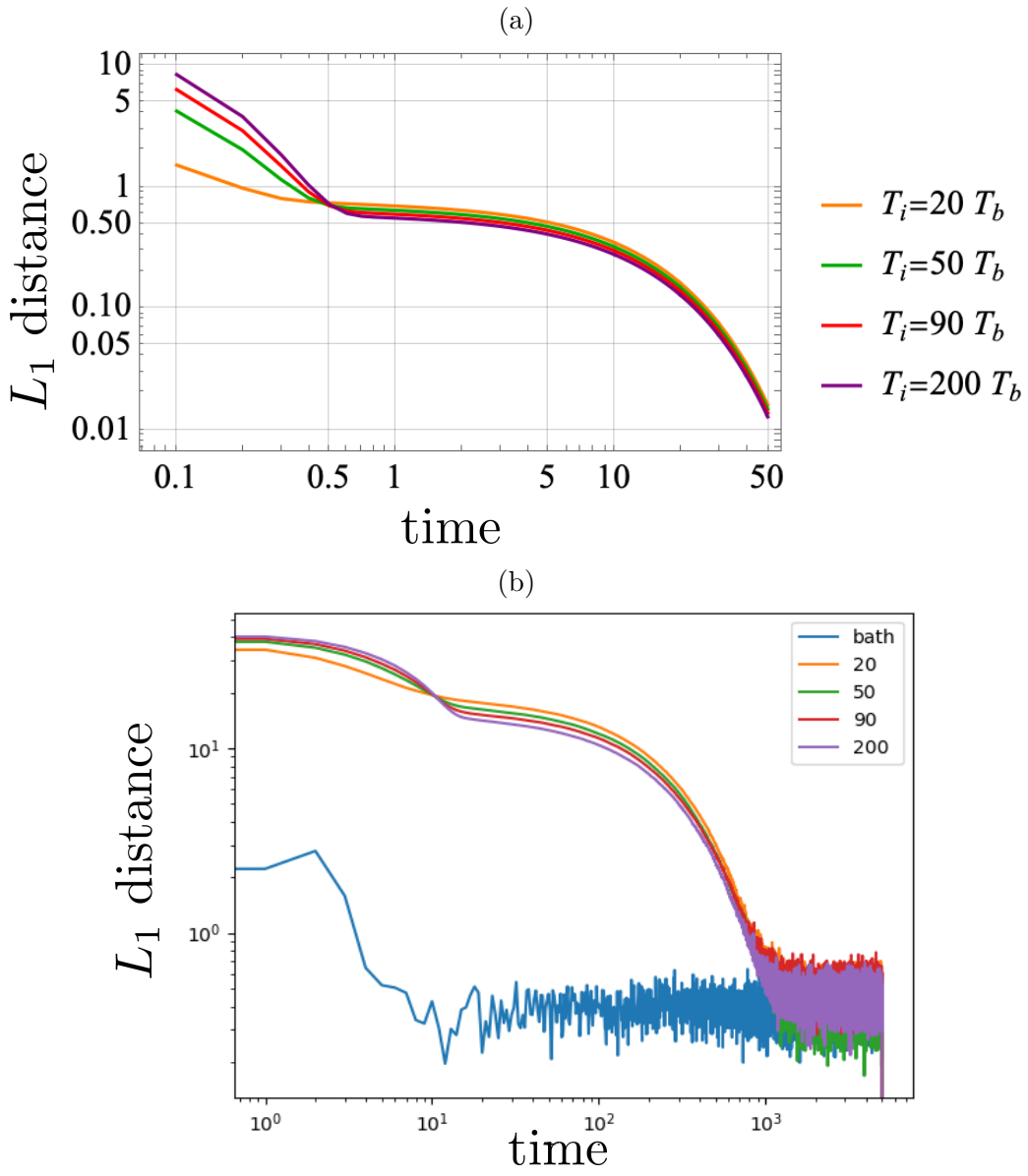


Figure 3.5: (a) Showing the numerical solutions (right) obtained from the FP equation. (b) Stochastic simulations for the Weak Mpemba effect (WME). Here we are simulating $N = 300,000$ trajectories and calculating the $L_1$ distance at each instance in time. In this case $\gamma = 17, T_b = 1.2$, the potential $U(x)$ is the top right of Fig. 3.3, and we are only using the first $i = 6$ eigenfunctions in the expansion Eq. (3.4). In this case there is no SME, and only WME.

### 3.7.1 Spatially dependent diffusion

For a one-dimensional Fokker-Planck equation, the diffusion coefficient that depends on the coordinate can always be redefined to a constant value, $D(T_b) > 0$, as shown in works like [37]. If we denote the original coordinate as $\tilde{x}$, where the diffusion coefficient is given by $\tilde{D}(\tilde{x}, T_b)$, the new coordinate $x$ relates to it through the equation: $D(T_b) = \left(\frac{dx}{d\tilde{x}}\right)^2 \tilde{D}(\tilde{x}, T_b)$. The relationship between the new and old coordinates is expressed as follows:$x(\tilde{x}) = \int_{\tilde{x}_0}^{\tilde{x}} d\tilde{y} \left(\frac{D(T_b)}{\tilde{D}(T_b,\tilde{y})}\right)^{1/2}$. Here, the choice of $\tilde{x}_0$ influences the value of $D$. The potential in transformed coordinates is described by the equation

$$-\frac{1}{\gamma}U'(x) = \frac{dx}{d\tilde{x}}\left(-\frac{1}{\gamma}\tilde{U}'(\tilde{x})\right) + \left(\frac{d^2x}{d\tilde{x}^2}\right)\tilde{D}(\tilde{x}, T_b). \tag{3.30}$$

Given this transformation and the presence of a Strong Mpemba effect ($a_2 = 0$) at the temperatures $\{T_{\text{init}} = T, T_b\}$, we can conclude that there is also a Strong Mpemba effect observed for the force $-\tilde{U}'(\tilde{x})$, the diffusion coefficient $\tilde{D}(\tilde{x}, T_b)$, and the same temperature conditions, $\{T_{\text{init}} = T, T_b\}$.

### 3.7.2 Scaling argument

Since the temperature is always related to the potential in a consistent way, we can use the same expression for the Boltzmann distribution and the eigenfunction $u_2$ for the pairs $\{U, T\}$ and $\{\kappa U, \kappa T\}$, where $\kappa$ represents a constant. Therefore, a Strong Mpemba effect for the potential $U$, the diffusion coefficient $T_b/\gamma$, and the temperatures $\{T_{\text{init}} = T, T_b\}$ suggests a Strong Mpemba effect for the potential $\kappa U$, the diffusion $\kappa T_b/\gamma$, and the temperatures $\{T_{\text{init}} = \kappa T, \kappa T_b\}$.

### 3.7.3 Multiple barriers

It's important to note that the approximation method for finding the second eigenvalue and eigenfunction in the case of a double-well potential can be easily extended to potential scenarios with multiple minima in the small-diffusion limit. However, determining the conditions for the Mpemba effect in such potentials necessitates a more detailed analysis.

## 3.8 Discussion

We explore the essential conditions required for the Mpemba effect by examining overdamped Langevin dynamics within a double-well potential framework. Our research identifies particular initial temperatures that can lead to the Mpemba effect, which we illustrate through integral equations outlining the probabilities of occupancy in either well and the mean first passage times. The exponential integrals we encounter can be easily addressed using Laplace's method.

Concerning the Strong Mpemba effect, our primary observations agree with the experimental findings documented by Kumar and Bechhoefer [2]. Their studies reveal that this effect manifests when the probabilities of being in a well at the initial temperature coincide with those at the bath temperature. In cases where barriers are substantial, the speed at which the probability distribution adjusts within a well far exceeds that of transitions between wells. Thus, it appears plausible that the Strong Mpemba effect emerges from initial conditions that possess the "right amount" of probability in the wells—akin to what is observed in equilibrium.

Furthermore, we have established the criteria for the weak Mpemba effect, which

would be interesting to explore in experiments. Given that overdamped Langevin dynamics offer a versatile and phenomenologically rich framework applicable to a variety of systems, the physical implications of the conditions prompting the Mpemba effect across different scenarios are indeed captivating.

Lastly, we replicate the experimental conditions of Kumar and Bechhoefer [2] through Monte Carlo simulations. Our results affirm that the theoretical conditions derived from the Fokker-Planck equation correspond well with the statistics obtained from simulating over-damped Langevin dynamics for both the weak and Strong Mpemba effect.

# Chapter 4

# Optimal transport and anomalous thermal relaxations

## 4.1 Introduction

In the preceding two chapters, we have sought to understand the Mpemba effect through the lens of optimizing initial conditions. By optimization, we refer to the selection of initial conditions that facilitates the relaxation process in the shortest possible time frame. This relaxation may be perceived as a transition from one distribution, $\pi(T_i)$, to another, $\pi(T_b)$. In this chapter, we will adopt an alternative viewpoint regarding the Mpemba effect. Specifically, we will hold the initial distribution, $\pi(T_i)$, and the final conditions, $\pi(T_b)$, constant while varying the dynamics of the process. This approach aims to elucidate how we can transform the initial distribution into the final one by optimizing the cost-effectiveness of the protocol employed. Traditionally, the Mpemba effect has implied that cost-effectiveness refers to achieving outcomes "as swiftly as possible." However, starting in this chapter, we will redefine cost-effectiveness in terms of minimizing dissipation, or in other words, reducing entropy production. We will illustrate that the same protocol responsible for what we have previously referred to as the Strong Mpemba effect also yields a cost-effective transport protocol. In this context, we will establish a relationship between

the two phenomena, particularly within the frameworks of Markov jump processes and continuous Langevin dynamics.

Optimal transport is a rich mathematics and statistics problem concerned with the optimal way of transporting a distribution from a source to a target function in a finite amount of time. The problem has a long history, starting with Monge 1781, who formalized it and illustrated with an example of the most economical way of transporting soil from one place to another [52]. Major advances and connections to linear programming were later made by Kantorovich [53, 54]. The applications of the specific solution to the optimal problem span a variety of fields, such as, e.g., statistics and machine learning [55], molecular biology [56], classical mechanics [57], linguistics [58] and computer vision [59]. Recently geometrical [60], thermodynamical [61], and topological [62] interpretations of the aspects of the optimal transport problem were made. The thermodynamical interpretation is especially relevant in stochastic thermodynamics [63].

Besides optimal routes to a target distribution, fast routes are also of interest. One such "shortcut" is the Mpemba effect – a counter-intuitive relaxation process in which a system starting at a hot temperature cools down faster than an identical system starting at an initially lower temperature when both are coupled to an even colder bath. An analogous effect exists in heating. By now Mpemba effect was seen in water [3], colloidal systems [2, 1], polymers [7], magnetic alloys [6], clathrate hydrates [5], granular fluids [17, 13], spin glasses [9], quantum systems [20], nanotube resonators [64], cold gasses [19], mean-field antiferromagnets [26], systems without equipartition [10], molecular dynamics of water molecules [65], driven granular gasses [18], and molecular gasses [23]. The Mpemba effect was formulated for a general Markovian system in [25]. The strong variant of the effect, the so-called

Strong Mpemba effect, was introduced in [26] and experimentally observed in [2]. Optimal heating strategy applications were discussed in [66]. The Mpemba effect in the overdamped limit of a particle diffusing on a potential landscape was studied in [25, 30, 67, 68, 69]. Other theoretical advances involving the Mpemba phenomenon link it to phase transitions [34], relaxations to nonequilibrium steady states [32], Otto cycle efficiency [33], stochastic resetting [31], random energy models [26], quantum analogs in Lindblad dynamics [20, 22, 70], and quantum analogs related to symmetry breaking [71]. Recently the effects of the type of coupling between the system and the bath [28, 27], effects of dynamics [72] and of eigenvalue crossings [29] on the phenomenon were studied.

The Mpemba effect can be viewed as an optimization of the initial condition. However, in scenarios where the initial conditions are fixed, sometimes we can vary the dynamics and obtain an analogous effect starting from the same initial condition but with different dynamics [72]. Below we refer to this similar effect as the Mpemba effect. In that case, our initial and final points in the probability distribution space are fixed, and the situation starts to resemble a problem of transport from a source to a target. Here we ask if there are cases in which the same dynamics corresponds to the optimal transport, i.e., minimal entropy production and the Mpemba effect. Our enabling examples are the two main paradigms of stochastic thermodynamics – a particle diffusing over a potential landscape with overdamped-Langevin dynamics and a Markov jump process. Surprisingly, the strong variant of the Mpemba effect in certain discrete cases coincides with the optimal transport. Below we show that the results depend on the large time we are looking at, the relaxation modes, and net probability currents.

The chapter is organized as follows. We first introduce the notation relevant to

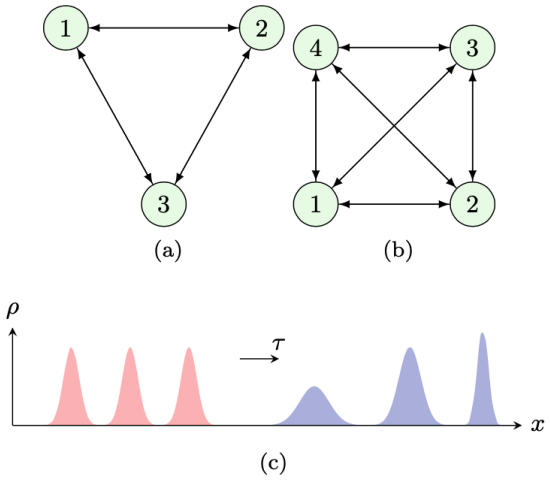


Figure 4.1: (a) Fully connected graph $\mathcal{G}(\mathcal{V}, \mathcal{E})$ with 3 edges and vertices. (b) Larger graph that could resemble a biophysical network, distribution network of some organization, or perhaps a computer network linking different servers. (c) There is some distribution of stuff that must be transported across the network in (a). The optimal transport protocol would be the most cost efficient way to do so in the finite amount of time $\tau$

Markov jump processes. Next, we present the optimal transport and the Wasserstein distance as a good measure of optimal transport. We continue by introducing the Mpemba effect. Afterward, we discuss anomalous thermal relaxations and optimal transport for a particle diffusing on a potential landscape, a three-state, and four-state Markov jump process. We finish with a discussion of the results.

## 4.2 General setup

Although we consider both continuous and discrete examples, we will first introduce the the concepts and notations of optimal transport, mobility, and the Mpemba effect on Markov jump processes.

We consider a Markov jump process on a graph $\mathcal{G}(\mathcal{V}, \mathcal{E})$, with vertices $\mathcal{V}$, and

edges $\mathcal{E}$ (see Fig. 4.1), which obeys the Master equation

$$\partial_t p = R\, p, \tag{4.1}$$

where $p_x(t)$ is the probability of finding the system is state $x \in \Omega$ at time $t$, and $R$ is the rate matrix, with $R_{xy}$ as the transition rate from $y$ to $x$ labeled as an edge $\mathcal{E}$ in the graph. Each state $x$ is a vertex on the graph characterized by energy $E_x$. Examples of Eq. (4.1) include chemical reaction networks, open quantum systems, birth-death populations, and biophysical and flow networks [73, 74]. We consider rate matrices that obey Detailed Balance (DB),

$$R_{xy}\pi_y^{T_b} = R_{yx}\pi_x^{T_b}. \tag{4.2}$$

where $\pi^{T_b}$ is stationary solution of the system described by the Master equation. We assume that the stationary system corresponds to thermal equilibrium and is give by the Boltzmann distribution $\pi_{T_b,x} = \frac{1}{Z(T_b)} e^{-\beta_b E_x}$, with $Z(T_b) = \sum_{x\in\Omega} \exp\left[-\beta_b E_x\right]$ as the partition sum. Below we label $\beta_b = 1/(k_B T_b)$ and set the Boltzmann constant to be unity, $k_B = 1$. We look at cases where, given two probability distributions, at initial time $t = 0$ and at the finite final time, $\tau$, and a protocol specifying the dynamics, there is an optimal transport protocol between the two, which minimizes the entropy production. The solution to the optimal transport problem provides an optimal transport plan between the source and target distributions. The *Wasserstein distance* is a metric in the space of probability distributions useful in quantifying the optimality of the transport. Other names for this metric are the *Monge-Kantorovich distance* or the *earth mover's distance*. The Wasserstein metric was extensively studied, and has thermodynamics [61], geometric [60], topological [62], and fluid mechanics [75, 76, 77]

interpretations. The discrete $L_1$ Wasserstein metric is defined

$$\mathcal{W}_1(p^A, p^B) = \min_{p^{AB}} \sum_{x,y\in\Omega} C_{xy}\, p^{AB}_{xy}, \tag{4.3}$$

where $C_{xy}$ is the cost function, $p^{AB}_{xy}$ is a joint distribution, with marginals corresponding to $p^A_x$ and $p^B_y$, and the minimum is taken over a set of all admissible couplings, see e.g. [53, 54]. Eq. (4.3) allows us to introduce the concept of an optimal transport protocol which transforms out initial state, $p^A$ into the final state, $p^B$. The Wasserstein distance $\mathcal{W}_1(p^A, p^B)$ is bounded from above by

$$\mathcal{W}_1(p^A, p^B) \leq \mathcal{J}(\tau) \leq \mathcal{C}_{\sigma m}(\tau) \leq \mathcal{C}_{\Sigma\mathcal{M}}(\tau), \tag{4.4}$$

with $\mathcal{J}(\tau)$ as the flow cost,

$$\mathcal{J}(\tau) \;\equiv\; \int_0^\tau \sum_{\substack{x>y \\ x,y\in\Omega}} |j_{xy}(t)|dt, \tag{4.5}$$

where $j_{xy}(t) = R_{xy}p_y(t) - R_{yx}p_x(t)$ is the amount of current in each edge $\mathcal{E}$. Eq. (4.2) demands that the net current $j_{xy}(t) = 0$ at thermodynamic equilibrium. Upper bound $\mathcal{C}_{\sigma m}(\tau)$ depends on the entropy production rate and dynamical mobility $\mathcal{C}_{\sigma m}(\tau) \equiv \int_0^\tau \sqrt{\sigma(t)m(t)}dt$, where

$$\sigma(t) = \sum_{x>y} j_{xy}(t) \ln\left[\frac{R_{xy}p_y(t)}{R_{yx}p_x(t)}\right] = \sum_{x>y} m_{xy}(t)\left[f_{xy}(t)\right]^2, \tag{4.6}$$

$$m_{xy} = \frac{j_{xy}}{f_{xy}} = \frac{R_{xy}p_y(t) - R_{yx}p_x(t}{\ln\left[(R_{xy}p_y(t)\right] - \ln\left[R_{yx}p_x(t)\right]}, \tag{4.7}$$

and

$$m(t) = \sum_{x>y} m_{xy}(t) \tag{4.8}$$

Eq. (4.6), Eq. (4.7), and Eq. (4.8) allows one to introduce the microscopic analogs of the Onsager coefficients, $m_{xy}(t)$, as the entropy production rate can be expressed as a quadratic form of generalized forces $f_{xy}(t)$, and current $j_{xy}(t)$ . Upper bound $\mathcal{C}_{\Sigma\mathcal{M}}(\tau)$ in Eq. (4.4) is simply the time averaged entropy production and kinetic cost, $\mathcal{C}_{\Sigma\mathcal{M}}(\tau) \equiv \Sigma(\tau)\mathcal{M}(\tau) = \langle\sigma\rangle_\tau\langle m\rangle_\tau$, where we have defined the time average of a qunaity as $\langle\mathbf{x}\rangle_\tau = \int_0^\tau \mathbf{x}(t)dt$. See Appendix B and [61] for more details. The Wasserstein distance is bounded below,

$$\mathcal{W}_1\left[p^A, p^B\right] \geq \mathcal{T}\left[p^A, p^B\right], \tag{4.9}$$

by the total variation distance $\mathcal{T}$,

$$\mathcal{T}\left[p^A, p^B\right] \equiv \frac{1}{2}\sum_{x\in\Omega}\left|p_x^A - p_x^B\right|. \tag{4.10}$$

In essence, the Wasserstein metric is a measure of how efficient the protocol given by $R$ in the Master equation transforms the initial state into the final one. This efficiency is bounded by the flow cost Eq. (4.5), or the integral amount of current in each edge $\mathcal{E}$ during the process. The flow cost and Wasserstein distance are next upper bounded by a $\mathcal{C}_{\sigma m}(\tau)$, which is proportional to the integral product of entropy production Eq. (4.6), times the dynamic mobility Eq. (4.8). The entropy production is a measure of the thermodynamic dissipation present in the systems, while the mobility plays the role of response in the network. Likewise, $\mathcal{C}_{\Sigma\mathcal{M}}(\tau)$, tells us that

the distance between $p^A$ and $p^B$ is bounded by the time averaged entropy production times the average kinetic cost. Interestingly, the two quantities are not totally independent. You cannot make one small while keeping the other fixed. These facts have been of large interest lately to the statistical mechanics community. These so called Thermodynamic uncertain relations, have been extensively studied and we direct the reader to [78] for details.

In the continuous case, there is a beautiful fluid mechanics interpretation of the optimal transport problem, given by Benamou and Brenier [75, 76, 77]. Suppose the evolution of the probability density, $p(x,t)$, is governed by a continuity equation,

$$\partial_t p(x,t) + \partial_x[v(x,t)p(x,t)] = 0, \tag{4.11}$$

then the $L_2-$Wasserstein distance from $p^A = p(0)$ at initial time $t = 0$ to $p^B = p(\tau)$, at final time, $\tau$, is given by the so-called the Benamou-Brenier formula,

$$\mathcal{W}_2(p^A, p^B) = \min_v \sqrt{T_b \tau \Sigma(\tau)}, \tag{4.12}$$

where the total entropy production during period $\tau$ is

$$\Sigma(\tau) = \frac{1}{T_b}\int_0^\tau \int_{\mathcal{D}} [v(x,t)]^2 \, p(x,t) dx dt, \tag{4.13}$$

[63]. The Wasserstein distance $\mathcal{W}_2(p^A, p^B)$ is minimum is over all smooth paths $\{v(t)\}_{0\leq t\leq\tau}$, subject to Eq. (4.11)

In the next section we will introduce anomalous thermal relaxation and the Mpemba effect on a graph.

## 4.3 Mpemba effect

The Mpemba effect occurs when a system prepared at initial temperature $T_h$ and immersed in a bath of temperature $T_b$ relaxes faster down to the bath's temperature than a replica of the same system starting at $T_w$, where $T_b \leq T_w \leq T_h$, [25]. An analogous effect also occurs in heating, and it is called the inverse Mpemba effect [25].

Below we specify what we mean by the Mpemba effect on a classical discrete case, where the relaxation is governed by the Master equation Eq. (4.1). The generalization to continuous systems evolving with Eq. (4.11). Note that we restrict our considerations to systems with Markov property, i.e., the system's future state depends only on the present state. However, one can also consider systems with memory. Sometimes the Mpemba effect on systems with Markov property is called the Markovian Mpemba [25].

At large times a probability distribution of a relaxing system, evolving according to Eq. (4.1), that is initiated at temperature $T$, $p(0) = \pi^T$, is characterized by

$$p(t) = \pi^{T_b} + \sum_{i>1} a_i v_i e^{\lambda_i t}, \tag{4.14}$$

where $\lambda_i$ are the eigenvalues of $R$, $v_i$ are the right eigenvectors of $R$, and $a_i$ are the overlap coefficients of the left eigenvector $u_i$ of the rate matrix $R$ and the initial condition,

$$a_i \equiv \frac{\langle u_i, \pi^T \rangle}{\langle u_i, v_i \rangle}, \tag{4.15}$$

The eigenvalues of $R$ are ordered and nonpositive, $\lambda_1 = 0 > \lambda_2 \geq \lambda_3 \geq ....$ We assume that there is a gap between $\lambda_2$ and $\lambda_3$, thus in the long time limit, the evolution of

the system is

$$p(t) \approx \pi^{T_b} + a_2 v_2 e^{\lambda_2 t}. \tag{4.16}$$

The Mpemba effect occurs when the overlap coefficient $a_2$ with respect to initial conditions is nonmonotonic [25]. That is if comparing two identical systems, prepared at $T_h$ and $T_w$, in their independent relaxation to thermal equilibrium at $T_b$, we have the Mpemba effect for $T_h \geq T_w \geq T_b$ and $|a_2(T_h)| \leq |a_2(T_w)|$. The Mpemba effect is the most pronounced if the slowest mode is orthogonal to the initial conditions, i.e., if $a_2(T_h) = 0$. In this case, the relaxation of the system approaches the equilibrium state from the direction of $v_3$, and there is a jump in the relaxation time from $-1/\lambda_2$ to $-1/\lambda_3$ at $T_h$. We refer to the case where there is no projection of the slow mode to the initial conditions as the Strong Mpemba effect.

### 4.3.1 Distance-from-equilibrium

Distance-from-equilibrium should satisfy the following properties [25]: (i) during a relaxation process, the distance should monotonically decrease with time, (ii) the distance from a Boltzmann distribution at $T$ to equilibrium at $T_b$ is a monotonically increasing function of $|T - T_b|$, with, in general, different pre-factors for cooling and heating, and (iii) the distance is a continuous and convex function of $p(t)$. The suitable choices are, for example, the Kulback-Leibler divergence and $L_1$ norm, [25, 68]. We define them below.

The *Kullback-Leibler* (KL) *divergence* [79], is defined as

$$D_{\mathrm{KL}}\left(p(t)||\pi^{T_b}\right) \equiv \sum_{x\in\Omega} p_x(t) \ln\left[\frac{p_x(t)}{\pi_x^{T_b}}\right]. \tag{4.17}$$

It can be thought of as the "entropic distance," by which we mean the total amount of entropy production in a relaxation process, starting from $p(t)$ and ending at $\pi^{T_b}$,

$$\int_t^\infty \sigma(t')\,dt' = \Sigma(\infty) - \Sigma(t), \tag{4.18}$$

see e.g. [25]. With Eq. (B.11), the above expression can be written as

$$\int_t^\infty \sigma(t')\,dt' = \sum_{x\in\Omega}\left\{\beta_b E_x\left[p_x(t) - \pi_x^{T_b}\right] + p_x(t)\ln p_x(t) - \pi_x^{T_b}\ln \pi_x^{T_b}\right\}, \tag{4.19}$$

which is the KL divergence, Eq. (4.17), hence

$$D_{\mathrm{KL}}\left(p(t)||\pi^{T_b}\right) = \Sigma(\infty) - \Sigma(t). \tag{4.20}$$

The $L_1-norm$ is

$$\left|\left|p(t), \pi^{T_b}\right|\right|_1 = \sum_{x\in\Omega}\left|p_x(t) - \pi_x^{T_b}\right|. \tag{4.21}$$

Note that $L_1$-norm is twice the *total variation distance* $\mathcal{T}$, see Eq. (4.10).

Next, we extend our definitions to the continuous case and show how for over-damped Langevin dynamics with metastability, the Mpemba effect and the optimal transport protocol in general do not coincide.

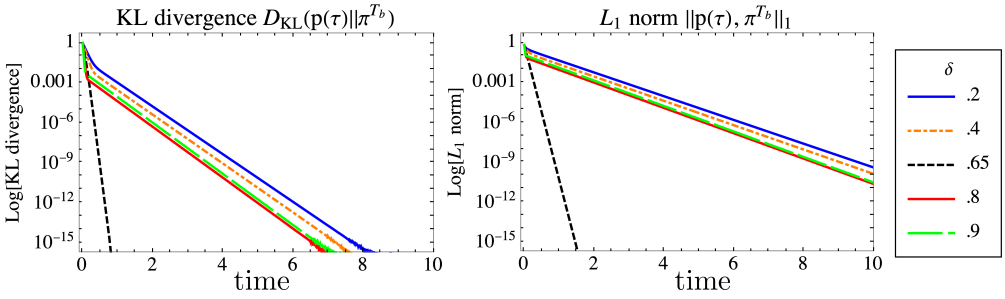


Figure 4.2: The figure above shows how a shortcut in the relaxation time can be measured using two different notions of distance. On the left, we plot the KL divergence on a *Log* scale vs time, and on the right we show the same behavior using the $L_1$ norm. The beginning and end points are the same for each curve, but each system has different dynamics, $\delta$. We see the dynamics with no overlap on the second slowest eigenfunction, $\delta = 0.65$, approach thermal equilibrium exponentially faster.

## 4.4 Examples

### 4.4.1 Particle diffusion on a potential landscape

Our intuition would suggest faster relaxation would be associated with higher entropy production, and therefore would not be optimal. Essentially, you cannot be fast and optimal for the same dynamics. This is ineed what we find for the case of a overdamped particle diffusing on a potential energy surface.

Let us consider a Brownian particle subject to a potential force $-U' \equiv -dU/dx$ and suppose that the particle is subject to overdamped Langevin dynamics

$$\gamma \frac{d}{dt}\mathrm{x}(t) = -\frac{1}{m}U'[\mathrm{x}(t)] + \Gamma(t), \tag{4.22}$$

where $\mathrm{x}(t)$ is particle's trajectory, $\gamma$ is the friction coefficient, and $\Gamma(t)$ is the thermal noise per unit mass. In the limit of instantaneous collisions, we can assume that the

thermal noise has Gaussian statistics, with

$$\mathbb{E}[\Gamma(t)] = 0, \quad \mathbb{E}[\Gamma(t)\Gamma(t')] = 2\gamma \frac{k_B T_b}{m} \delta(t - t'), \tag{4.23}$$

c.f. [37, 80, 81]. The diffusion coefficient is $k_B T_b / m\gamma$. We set the Boltzmann constant, $k_B = 1$, mass, $m = 1$, and friction constant, $\gamma = 1$, to unity. The probability density, $p(x, t)$ to find the particle at time $t$ and coordinate $x$, obeys the Fokker-Planck (FP) equation,

$$\partial_t p(x, t) = \mathcal{L}_{\text{FP}}\, p(x, t), \tag{4.24}$$

$$\mathcal{L}_{\text{FP}} \equiv \partial_x \left[ U'(x) + T_b \partial_x \right], \tag{4.25}$$

where $\mathcal{L}_{\text{FP}}$ is the FP operator. We assume that the system is closed, $x \in \mathcal{D} \equiv [x_{\min}, x_{\max}]$. In this case, the probability is conserved, and we have reflective boundary conditions, which means that the current probability density, $j(x, t)$, defined as $\partial_t p(x, t) = -\partial_x j(x, t)$, is zero at the boundaries, i.e. $j(x_{\min}, t) = j(x_{\max}, t) = 0$. The stationary distribution is the Boltzmann distribution,

$$\pi^{T_b}(x) = \frac{1}{Z(T_b)} e^{-\frac{U(x)}{T_b}}, \tag{4.26}$$

where $Z(T_b) \equiv \int_{x_{\min}}^{x_{\max}} \exp[-U(x)/T_b]\, dx$ is the partition function. We assume that the system is initially at thermal equilibrium at temperature $T$,

$$p(x, 0) = \pi^T(x). \tag{4.27}$$

The continuity equation, Eq. (4.11), with the mean local velocity of the process

x(t),

$$v(x,t) \equiv \frac{j(x,t)}{p(x,t)} = -U'(x) - T_b \partial_x \ln p(x,t). \tag{4.28}$$

is a FP equation, Eq. (4.24). From Eqs. (4.13) and (4.28) the entropy production is explicitly is

$$\Sigma(\tau) = \int_{\mathcal{D}} dx \Big\{ \beta_b U(x) \left[ \pi^T(x) - p(x,t) \right] + \pi^T(x) \ln \pi^T(x) - p(x,t) \ln p(x,t) \Big\}. \tag{4.29}$$

In the case of Eq. (4.24) the minimum of dissipative dynamics can always be achieved with a potential velocity $v$, i.e., a potential force [75, 76, 77, 61].

To search for the Mpemba effect we should look at the distance from equilibrium, for example, the KL divergence. Using Eqs. (4.20) and (4.29), the KL divergence can be written as

$$D_{\mathrm{KL}} \left( p(\tau) || \pi^{T_b} \right) = \int_{\mathcal{D}} dx \Big\{ \beta_b U(x) (p(x,t) - \pi^{T_b}(x)) + p(x,t) \ln p(x,t) - \pi^{T_b}(x) \ln \pi^{T_b}(x) \Big\}. \tag{4.30}$$

By restricting our consideration to a range of initial temperatures, one can ask about the instances of minimal KL divergence and minimal total entropy production at times $\tau \gg \max\{t_M, -\lambda_2^{-1}\}$, where $t_M(T)$ is the largest time when a pair $D_{\mathrm{KL}}-$curves, from the considered set of initial conditions $\{T_i\}$, cross.

For the example initially introduced in [25], we compute KL divergence and the total entropy production. The potential is shown on Fig. 4.3a. At large times, here $\tau\gamma = 10^4$, we observe that for a range of initial temperatures, $T \in [T_{\max}, 10\, T_{\max}]$, that the total entropy production is a monotonically decreasing function of the KL

divergence – resulting in minimal KL divergence and maximal total entropy production at $10\,T_{\max}$ and maximal KL divergence and minimal total entropy production at $T_{\max}$; see Fig. 4.3d. Hence the optimal transport in time $\tau$ for a range of initial temperatures $T \in [T_{\max}, 10\,T_{\max}]$ happens for $T = T_{\max}$, but this is also the "slowest" trajectory, as it is farthest from equilibrium at the chosen time $\tau\gamma = 10^4$. While the "fastest" trajectory, the closest to equilibrium at $\tau$, among those labeled with initial conditions from $T \in [T_{\max}, 10\,T_{\max}]$ is the one starting at $10\,T_{\max}$, at the same time this trajectory also has the highest total entropy production of the set. To summarize, the above example shows a case of an often "antipodal" relation between the "optimal" transport (minimal total entropy production) and "fast" relaxation (here, the Mpemba effect).

The optimal transport problem is typically defined with a well-defined starting point $p^A$ and well-defined end $p^B$ after a finite time $\tau$. The optimal transport is the one that minimizes the total entropy production by altering the dynamics with specified control parameters. Above, we did not change the dynamics; instead, we considered a range of initial conditions, and we asked which initial condition minimizes the total entropy production and, after a large but finite time $\tau$, how far away from the equilibrium distribution is the probability distribution at time $\tau$.

Next, suppose we vary the potential in a continuous manner with a time-dependent control parameter, $\delta(t)$, and let us assume the potential variations are with fixed temporal endpoints, $U[\delta(t=0)] = U[\delta(t=\infty)]$. Also, suppose that among different variations of $\delta(t)$, there is a protocol, $\delta_{\rm SM}(t)$, such that there is no overlap to the slowest mode, i.e., for that protocol, $a_2 = 0$, and the KL divergence is minimal,

$$\min_{\delta(t)} D_{\rm KL}\left(p(\tau)||\pi^{T_b}\right). \tag{4.31}$$

Here $\tau$ is a sufficiently large time, meaning $\tau \gg \max\{t_M, -\lambda_2^{-1}\}$, where $t_M(T)$ is the largest time when a pair $D_{\mathrm{KL}}-$curves, from the considered set of protocols conditions $\{\delta(t)\}$, cross. The KL divergence at $\tau$ is the difference between the entropy production at infinity and at $\tau$, Eq. (4.20). Since the entropy production at infinity only depends on the initial condition and the equilibrium, see Eq. (4.29), the minimum KL divergence corresponds to maximal total entropy production. Thus, for potential variations with fixed temporal endpoints, the Strong Mpemba effect and optimal transport generically would not happen for the same dynamics.

In the previous chapters we saw that the Mpemba effect represents a shortcut in the time for a system to reach thermal equilibrium. Usually this effect is measured as a crossing in distance functions, where the hot system overtakes the colder and initially closer system. In cases where there is a strong Mpemba effect, i.e. $a_2(T_i) = 0$, the initial conditions correspond to exponentially faster approach to the target distribution. Our main result in this chapter, which we detail in the next section, is when considering discrete networks, with the initial and final distribution fixed, you can find situations where varying the dynamics so $a_2(\delta) = 0$, corresponds to both faster approach to the target distribution, and is also the most efficient transport protocol. See Fig. 4.2 and Fig. 4.4. For example, in a chemical reaction network, once can transform the initial concentrations into different concentrations both faster and most efficiently. This result is quite unexpected, as most of our intuition suggests that driving a system faster would be associated with high entropy production, and be a less efficient protocol. Similarly, in the adiabatic limit, you will produce no entropy as you change one system into another, but this protocol requires that the process takes an infinite amount of time. This result is similar in nature to the Braess's paradox, in which one finds that adding links between two distant nodes on a graph

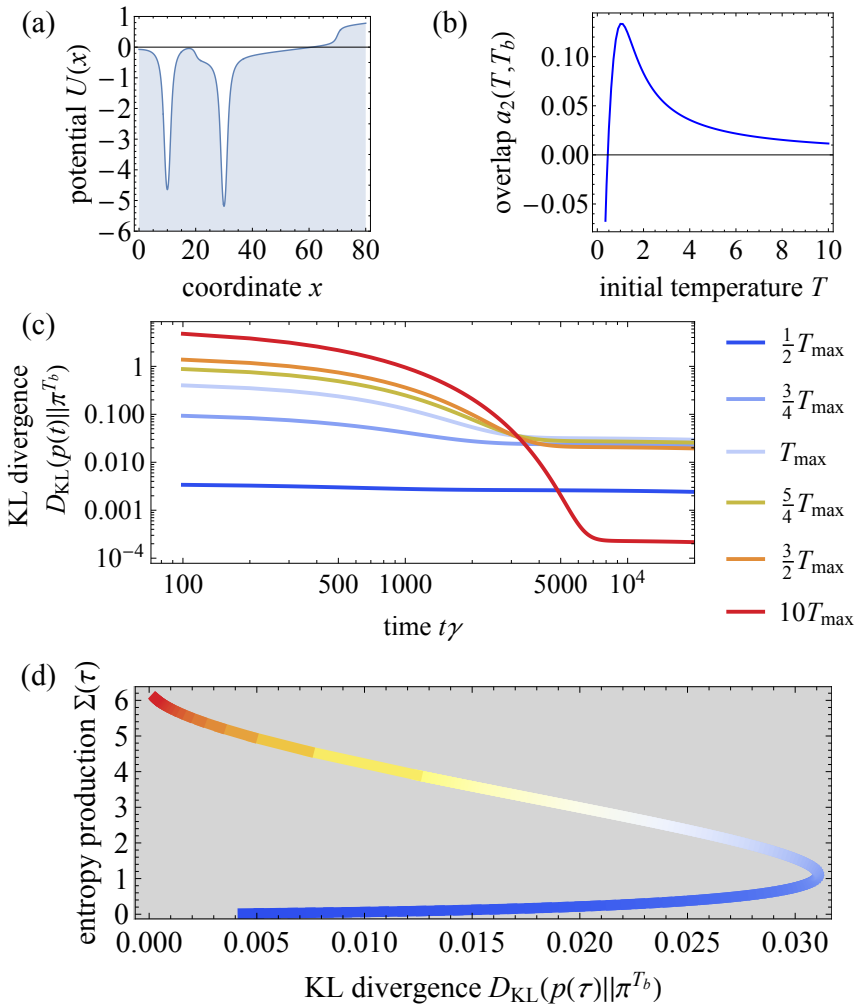


Figure 4.3: (a) A one dimensional potential, previously considered in [25] with overdamped-Langevin dynamics, Eq. (4.22) and diffusion constant proportioanl to $T_b = 0.45$. (b) The overlap coefficient $a_2$ is non-monotonic, indicating a Mpemba effect, and has a maximum at $T_{\max} = 1.0462$. The eigenvalues are: $\lambda_2 = -2.5 \times 10^{-6}$ and $\lambda_3 = -0.001$. (c) The time dependence of the KL divergence, $D_{\mathrm{KL}}(p(t)||\pi^{T_b})$ is computed with approximate $p(t) \approx \pi^{T_b} + a_2 v_2 e^{\lambda_2 t} + a_3 v_3 e^{\lambda_3 t}$. The crossings of the KL divergence curves indicated the Mpemba effect – for example, the process starting at $10\,T_{\max}$ (red) by $\tau\gamma = 10^4$ overtakes all shown curves. The process starting at $T_{\max}$ (lightest blue) has maximal KL divergence. Therefore the closest to equilibrium at $\tau\gamma = 10^4$ is the process starting at $10\,T_{\max}$ (red) and the farthest is one starting at $T_{\max}$ (lightest blue). (d) The parametric plot of the total entropy production $\Sigma(\tau)$ with KL divergence $D_{\mathrm{KL}}(p(\tau)||\pi^{T_b})$ at $\tau\gamma = 10^4$. In the interval $T \in [T_{\max}, 10\,T_{\max}]$ we have for $T_{\max}$ the minimum of $\Sigma(\tau)$ and maximum of $D_{\mathrm{KL}}$, and for $10\,T_{\max}$ the maximum of $\Sigma(\tau)$ and minimum of $D_{\mathrm{KL}}$. Here, within the chosen interval, the optimal transport is at $T_{\max}$, but the "fastest" (closest to equilibrium at $\tau$) trajectory has the highest entropy production (at $10\,T_{\max}$).

leads to a longer search time as opposed to a shorter one. Authors in [74] found that by adding more edges to a graph the search time worsened, and that there is an optimal amount of nodes and topology to have. In would be interesting to explore how these two problems are related.

### 4.4.2 Three-level system

We consider a fully connected three-level system with energies $\{E_1, E_2, E_3\}$. The Mpemba effect on such systems was already considered in [25] and recently as a function of dynamics in [72]. We define the clockwise direction as $1 \to 2 \to 3 \to 1$ and clockwise the transition rates are

$$R_{21} = \gamma e^{-\frac{1}{2}\beta_b(E_2-E_1)},\ R_{13} = \gamma e^{-\frac{1}{2}\beta_b(E_1-E_3)}, \tag{4.32}$$

$$R_{32}(\delta) = \gamma e^{-\beta_b(E_3-E_2)\delta}, \tag{4.33}$$

where $\gamma^{-1} = 1$ sets the unit of time, and $R_{32}$ has an additional control parameter, $\delta \in [0, 1]$, for its magnitude. Detailed Balance(DB), sets the corresponding "counter-clockwise" transitions. DB does not prescribe the dynamics; it just sets the ratio between the forward and backward rates. By changing $\delta$, we change the magnitude of the rates between states 2 and 3 – because of DB, this local change affects all of the currents $j_{xy}$. While in a larger graph, only currents connected to the two nodes involved are affected. The parameter $\delta$ is often called the load factor, and it has been studied in the context of molecular motors [82, 83, 84], differential mobility [85], Markov jump processes [86], and recently by the authors, in the context of anomalous thermal relaxations [72]. The conservation of probability sets the diagonal elements

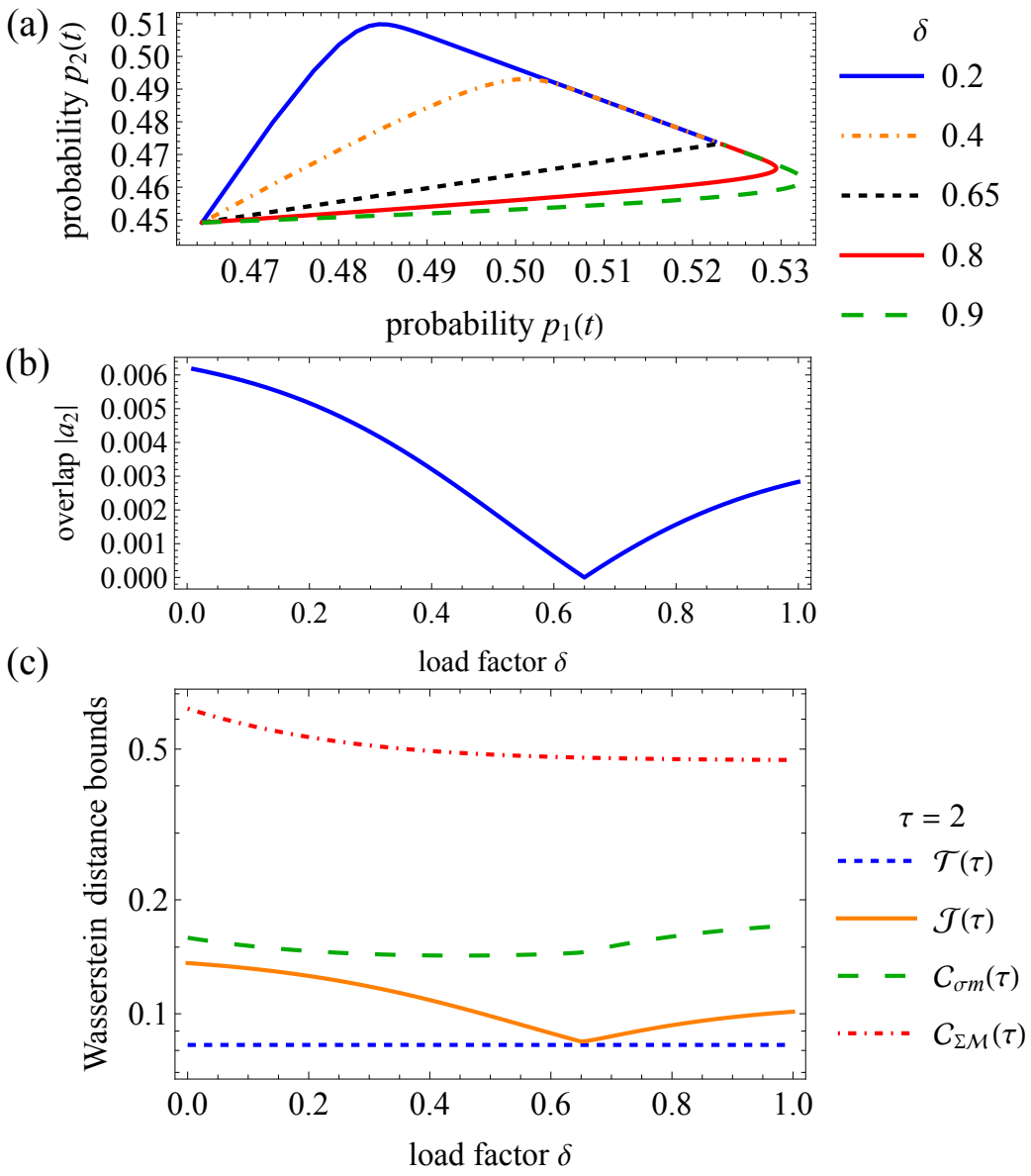


Figure 4.4: (a) Relaxation trajectories of probabilities of state occurrences, $p_1(t)$ and $p_2(t)$, for a three-level system. The energies of the system are $\{0, 0.1\,T_b, 5\,T_b\}$, the initial temperature is $T = 2.97\,T_b$ and $\tau = 2/\gamma$ (with $T_b = 1$ and $\gamma = 1$). Different colors represent different dynamics, parameterized by the load factor $\delta$, introduced in Eq. (5.36). The dashed black line is for $\delta_{\rm SM} = 0.65$, which corresponds to the Strong Mpemba effect. The relaxation with $\delta_{\rm SM}$ is along a straight line, as the projection on the second eigenvector is zero. (b) The overlap $|a_2|$ vanishes for $\delta_{\rm SM} = 0.65$, which corresponds to the Strong Mpemba effect. (c) Total variation distance $\mathcal{T}(\tau)$, flow cost $\mathcal{J}(\tau)$ and upper bounds $\mathcal{C}_{\sigma m}(\tau)$ and $\mathcal{C}_{\Sigma\mathcal{M}}(\tau)$ as a function of the load factor $\delta$. The optimal transport has a minimal flow cost. In this example, the minimal flow cost and the Strong Mpemba effect happen at the same load factor, $\delta = \delta_{\rm SM}$.

– the columns of the $R$ matrix sum to zero, i.e.

$$R_{xx} = -\sum_{\substack{y\in\Omega \\ y\neq x}} R_{yx}, \quad \forall x \in \Omega. \tag{4.34}$$

In general, the rate matrix depends on the properties of the system, the environment, and time. However, we restrict our considerations below to rate matrices that depend solely on the bath temperature, $T_b$, and a control parameter specifying the dynamics, which we introduce below. Lastly, note that the three-level system considered here is fully connected. Thus, the Wasserstein distance is equal to the total variation distance, see Eq. (4.9).

We look at a situation where for the given initial temperature $T$ and bath temperature $T_b$, there is a Strong Mpemba effect at load factors $0 < \delta < 1$. We observe that in the cases where the gap between $\lambda_2$ and $\lambda_3$ is large, $(\lambda_2 - \lambda_3)/\tau \ll 1$, the flow cost $\mathcal{J}(\tau)$ has a minimum at the same load factor as the overlap coefficient $|a_2|$, indicating that in that case, the optimal transport is the one where the Strong Mpemba occurs as shown in Fig. 4.4. The dynamic state mobility $m(\tau)$ saturates at large times because it is proportional to the difference in activities, Eq. (B.14). Thus the even later times' contributions to the bounds $\mathcal{C}_{\sigma m}(\tau)$ and $\mathcal{C}_{\Sigma\mathcal{M}}(\tau)$ are mainly entropic – due to the entropy production rate and the entropy production.

For smaller gaps or shorter times, the contribution of the fast mode also matters, and the entropy production rate is not minimal for the same load factor as the occurrence of the Strong Mpemba effect. Looking at larger times $\tau$, in this case, does make things more entropy-dominated and slow-mode-dominated. Mobility likewise again saturates in finite time.

### 4.4.3 Four-level system

Similarly, for a fully-connected four-state system Fig. 4.1(b), we confirm the minimum of the flow cost and Strong Mpemba effect happen at the same load factor $\delta$, see Fig. 4.5. We also show that the gap between the two slowest decaying modes, $\lambda_2$ and $\lambda_3$ does not need to be as large as in the three-level system in Fig. 4.7. This is expected because you have a higher dimensional manifold, and even when $a_2(\delta) \to 0$, you still relax along the $v_2$ and $v_3$ directions. However, we note that in the case of the four-state system, things can be more complicated as the eigenvalues of the rate matrix can cross [29].

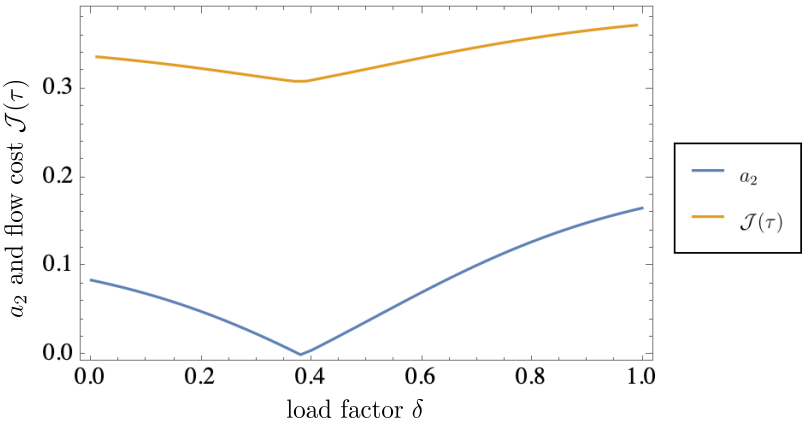


Figure 4.5: Showing that the minimum of the flow cost $\mathcal{J}(\tau)$ happens at the same point where $a_2$ as a function of the load factor $\delta$. Here $E_4 = 4., E_1 = 0, E_2 = 3.4, E_3 = 0.1, \beta_b = 1$, and $T_i = 5.0$

### 4.4.4 Overlap of optimality and strong Mpemba effect

We define a notion of distance to measure the degree of separation between optimal protocol and SM protocol as the *Degree of seperation* $D_{OS} = |\delta_{\mathcal{J}_{min}} - \delta_{a_2=0}|$. We observe a highly regular but counter-intuitive behavior of $D_{OS}$ with increasing eigen-

value gap in the three-level system Fig. 4.6. The four level system behavior, is very

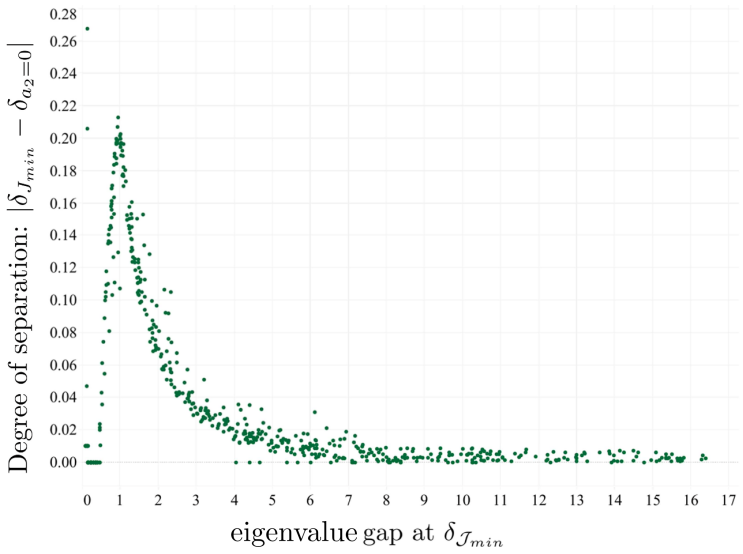


Figure 4.6: A notion of distance is defined to measure the Degree of separation between optimal protocol and SM protocol as $D_{OS} = |\delta\mathcal{J}_{min} - \delta a_2 = 0|$. A highly regular but counter-intuitive behavior of DOS with increasing eigenvalue gap is observed. For a larger eigenvalue gap, the optimal transport and Strong Mpemba protocols overlap; that is, DOS is small. The above data is for a three-level system at $\beta_b = 1$,with energy spectrum $E_0 = 0$, $E_2 = 0.18, 0 < E_3 < 5$, and for initial temperatures $1 < \beta^{-1} < 15$.

similar, and has the same shape. However, the gap between $|\lambda_2 - \lambda_3|$ does not need to be as dramatic as in the three-level system.

## 4.5 Discussion

In discrete systems, a small change in the long time limit of the dynamic state mobility might influence a large change in the total entropy dissipation, while in the overdamped Langevin case, the long time limit of the dynamic state mobility is constant with respect to the considered dynamics changes, and proportional to the diffusion constant, $T_b$. The two cases also differ in the allowable probability currents –

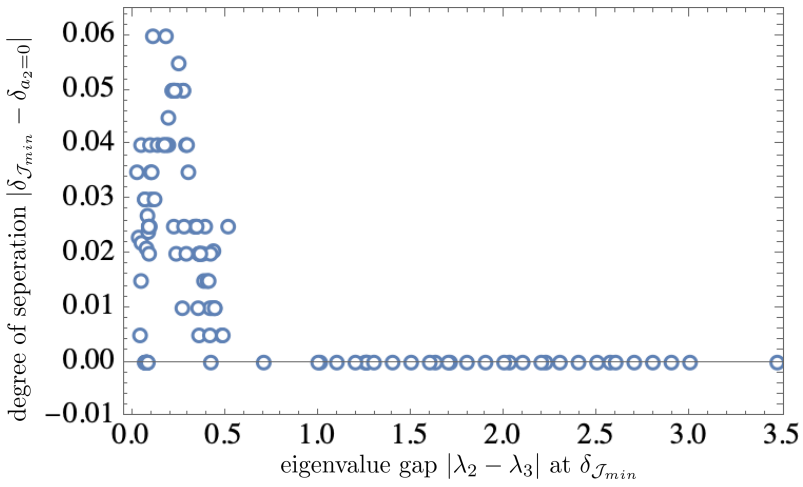


Figure 4.7: $D_{OS} = |\delta\mathcal{J}_{min} - \delta a_2 = 0|$ for the graph in Fig. 4.1(b). We see a similar structure like the three-level system Fig. 4.6, but less dramatic. Here $\beta_b = 1$,with energy spectrum $E_1 = 0$, $E_4 = 4.0, 0.05 < E_3 < 0.1$, and $0.05 < E_2 < 3.7$ and for initial temperatures $1 < \beta^{-1} < 20.0$. This plot was made with 120 random samples of the 4-D parameter space.

in the continuous cases considered, the probability currents are continuous, while in the discrete case, we can have quite a wide distribution of currents restricted only by detailed balance.

We find seemingly counter-intuitive cases in which the Strong Mpemba effect and the minimal Wasserstein distance occur at the same load factor. The exponentially faster relaxation to thermal equilibrium also occurs with minimal entropy production for specific types of dynamics. We argue that such a scenario is highly surprising, especially considering our continuous paradigm – the overdamped Langevin dynamics with continuous variations of continuous potential, where the Strong Mpemba effect is generally observed together with a high entropy production.

More work is needed to verify our findings in a discrete case for a larger reaction network and to specify what kind of variations of the dynamics are needed to observe the Mpemba effect and the optimal transport for the same protocol. Another

consideration is the size of the system and the relative size of the perturbation of the dynamics needed to have the optimal transport and Mpemba effect happen for the same protocol.

Somewhat conceptually related to our results are the results of elastic network alterations where even small local perturbations in specific networks can change their macroscopic responses, flow, and functionality of these networks, see, e.g., and references within [73].

Like optimal transport, the Mpemba effect could be helpful in designing efficient samplers, optimal heating and cooling protocols, and preparations of state. Real-world applications of our findings will depend on the feasibility of altering the dynamics in such a way as to have both the Mpemba effect and optimal transport. Separately, we note that the authors of [74] the authors studied how optimal search protocols are related to the topology of the network, and found an analog of Braess's Paradox. By adding links between topologically distant vertices, they actually increase the search time as opposed to decreasing it. In chapter 3. we saw how the conditions for the Mpemba effect can be expressed in terms of mean first passage times. It would be interesting to study how the Mpmeba effect, the dynamics, the search time, and optimal transport plans are all related.

# Chapter 5

# Effect of dynamics on anomalous thermal relaxations and information exchange

## 5.1 Introduction

In chapters 2. and 3., we have sought to better understand why the Mpemba occurs. Specifically, in the case of an overdamped particle diffusing in a potential energy landscape. We found that the effect can happen in systems without metastability, and in chapter 3. derived the conditions to observe the Mpemba effect in terms of mean first passage times. In chapter 4., we observed a relation between the Mpemba effect, and optimal transport protocols by changing the dynamics in discrete Markov jump processes. In this chapter we will show an application of how changing the dynamics allows one to take advantage of the Mpemba effect, in the context of a Maxwell's demon. We will show how Maxwell's "neat figured being," a information engine like device, can use the Mpemba effect to optimize the performance of both the work extracted, act a faster information eraser, and all without sacrificing efficiency. We will also study the occurrence of the Mpemba effect in Markov jump process on a small networks.

Markov jump processes have extensive applications across various fields, including physics, chemistry, biology, statistics, finance, and sociology. These processes serve as effective models for investigating chemical reaction networks [87, 88, 89], magnetic systems [90], as well as ecological and evolutionary dynamics [91, 92]. They are also pivotal in the study of enzyme kinetics [92], diffusion on lattices [37, 80, 93], and the modeling of stock markets [94], cloud cover [95], and social processes [96].

In particular, linear kinetic networks are crucial in biological contexts, functioning as kinetic pathway networks, metabolic models of the microbiome, and ecological and evolutionary networks pertaining to biological or clonal species [91, 92]. Moreover, these networks have significant relevance in chemistry and physics, appearing in processes such as isomerizations, the behavior of quantum dots, catalysis [92, 97], protein functionality [98], and models of molecular motors [82].

The widespread applications of Markov jump processes highlights the significance of efficient thermal relaxation in both scientific research and practical applications. Potential applications include enhanced sampling methods, optimized heating and cooling protocols, and more effective relaxation techniques for achieving specific polymer configurations. We will investigate the Mpemba effect in Markov jump processes, showing the phase space for small graphs when there is a strong forward, inverse, or both at the same time. We also note an example of how such a "shortcut", can have applications.

The dynamics play a crucial role in characterizing out-of-equilibrium phenomena [82, 84, 85, 86]. A well-known approach in this context is Glauber dynamics, which is computationally advantageous due to its ability to bound transition rates [99]. Nonetheless, employing capped rates can result in overlooking significant effects, such as negative motility [85], where an increase in force results in decreased

mobility, and alterations in the microscopic free energy landscape of the motor influenced by force [82, 83, 84]. To gain a more profound understanding of the Mpemba effect, we investigate the impact of dynamics on anomalous thermal relaxations. For this study, we utilize Markov jump processes within linear reaction networks, introducing a one-dimensional family characterized by a control parameter known as the *load distribution factor*, which allows for variations in the dynamics. Our findings demonstrate that changes in the load distribution factor significantly influence the regions of phase space in which the Mpemba effect is observed.

We also investigate the influence of dynamics on anomalous thermal relaxation alongside the exchange of information, which is recognized as a valuable thermodynamic resource. The foundational work establishing that *information is physical* [100] significantly advanced the connection between information theory and statistical physics.

In stochastic thermodynamics [63, 101], the two are often indelible, with examples of thermodynamic efficiencies in the presence of information exchange [102, 103, 104, 105], information-carrying molecules in chemical systems [106], and Maxwell's demons setups [107, 108, 109, 110, 111]. Our paradigm is a three-level Markov jump process that interacts with a tape kept at a finite temperature. Our setup is a Maxwell demon setup. Our main result is that choosing the dynamics with which the device has a strong variant of the Mpemba effect can stabilize and increase the device's power output without sacrificing efficiency.

The chapter is organized as follows. In Section 5.2, we introduce the unimolecular reactions. Next, we focus on a three-level Markov jump process on a ring and study the Mpemba effect in this system. In Section 5.5, we present the results on the effect of the dynamics on our system. Lastly, in section 5.7 we illustrate the results and

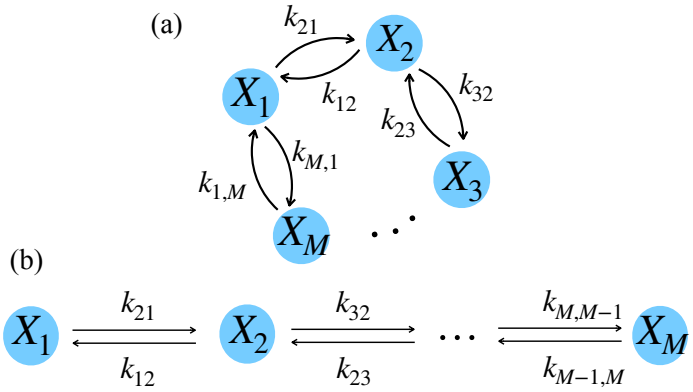


Figure 5.1: Examples of linear reaction networks of reactants on a ring (a) or with fixed ends (b). Unlike the networks in the previous chapter, these networks are not fully connected.

their application on an example of an autonomous Maxwell demon interacting with a tape kept at finite temperature. We end with a discussion in section 5.8

## 5.2 Model

We focus on the linear reaction networks of $M$ reactants, with $X_i$ as distinct reactants, which can represent, for example, molecules, conformations of a molecule, atomic levels, or energy levels. A set of reactions

$$\left\{ X_i \underset{k_{ij}}{\overset{k_{ji}}{\rightleftarrows}} X_j \middle| i, j \in [1, M] \right\}, \tag{5.1}$$

where, $k_{ij}$ is the reaction rate from $X_j$ to $X_i$, and defines a reaction network. Special cases of such networks include reactants on a ring or a line interval; see Fig. 5.1. Each reactant $X_i$ has internal energy $\epsilon_i$. We assume the system is closed and the total number of reactants is conserved, $N = n_1 + n_2 + ... + n_M$. A system state is described by its occupation numbers $\boldsymbol{n} = (n_1, n_2, ..., n_M)$ of respective reactants

$\{X_1, X_2, ..., X_M\}$. The system has $L = \binom{N+M-1}{N}$ states. We consider a system that is immersed in a thermal bath of temperature $T_b$; thus, the rates $k_{ij}$ obey Detailed Balance (DB)

$$\frac{k_{ij}}{k_{ji}} = e^{-\beta_b(\epsilon_i - \epsilon_j)}, \tag{5.2}$$

where $\beta_b \equiv (k_B T_b)^{-1}$ is the inverse temperature of the bath. The Boltzmann constant is taken to be unity, $k_B = 1$. The Master equation governing the dynamics is

$$\partial_t p_{\boldsymbol{n}}(t) = \sum_{m \in \Omega} R_{\boldsymbol{nm}}\, p_{\boldsymbol{m}}(t) \tag{5.3}$$

where $p_{\boldsymbol{n}}(t)$ is the probability to be at state $\boldsymbol{n}$ at time $t$ and $R_{\boldsymbol{nm}}$ is the transition rate from $\boldsymbol{m}$ to $\boldsymbol{n}$. The rate matrix $R$ obeys DB, and in general, it depends on the particulars of the system and the environment. Here we restrict our considerations to rate matrices that depend on the temperature $T_b$ and a load distribution factor $\delta$ that controls the magnitudes of the transitions. The general form of the rate matrix obeying DB is

$$R_{\boldsymbol{nm}} = \begin{cases} \Gamma e^{-\beta_b(B_{\boldsymbol{nm}} - E_{\boldsymbol{m}})}, & \boldsymbol{n} \neq \boldsymbol{m} \\ -\sum_{\boldsymbol{l} \neq \boldsymbol{n}} R_{\boldsymbol{lm}}, & \boldsymbol{n} = \boldsymbol{m} \end{cases}, \tag{5.4}$$

where $E_{\boldsymbol{n}} = \sum_{i=1}^{M} n_i \epsilon_i$ is the energy of the state $\boldsymbol{n}$, $B_{\boldsymbol{nm}} = B_{\boldsymbol{mn}}$ is interpretable as a "barrier" between $\boldsymbol{m}$ and $\boldsymbol{n}$, and $\Gamma^{-1}$ sets the unit of time [112]. The rate matrix obeys the eigenvalue equations

$$R\,\boldsymbol{v}_\mu = \lambda_\mu \boldsymbol{v}_\mu \qquad \text{and} \qquad \boldsymbol{u}_\mu R = \lambda_\mu \boldsymbol{u}_\mu, \tag{5.5}$$

where $\boldsymbol{v}_\mu$ is a right eigenvector, $\boldsymbol{u}_\mu$ is a left eigenvector, and $\lambda_\mu$ is the corresponding eigenvalue. The eigenvalues are real and labelled in descending order such that $\lambda_1 = 0 > \lambda_2 \geq \lambda_3 \geq \ldots$. The first eigenvalue, $\lambda_1 = 0$, corresponds to the thermal equilibrium at the bath temperature $T_b$,

$$\pi_{\boldsymbol{n}}^{T_b} \propto e^{-\beta_b E_{\boldsymbol{n}}}. \tag{5.6}$$

The two eigenvectors are related as $(\boldsymbol{u}_\mu)_{\boldsymbol{n}} = e^{\beta_b E_{\boldsymbol{n}}}(\boldsymbol{v}_\mu)_{\boldsymbol{n}}$, and $R$ can be symmetrized [26]. The probability of the system being in state $\boldsymbol{n}$ at time $t$ is

$$p_{\boldsymbol{n}}(t) = \pi_{\boldsymbol{n}}^{T_b} + \sum_{\mu=2}^{L} a_\mu(T, T_b) e^{\lambda_\mu t} (\boldsymbol{v}_\mu)_{\boldsymbol{n}}, \tag{5.7}$$

here $a_\mu$ is the overlap (or projection) of $\boldsymbol{u}_\mu$ on the initial conditions. We take the initial condition to be thermal equilibrium at temperature $T$, $\boldsymbol{\pi}^T$, i.e.

$$a_\mu(T, T_b) = \frac{\sum_{\boldsymbol{n}\in\Omega} (\boldsymbol{u}_\mu)_{\boldsymbol{n}} \pi_{\boldsymbol{n}}^T}{\sum_{\boldsymbol{m}\in\Omega} (\boldsymbol{u}_\mu)_{\boldsymbol{m}} (\boldsymbol{v}_\mu)_{\boldsymbol{m}}}. \tag{5.8}$$

At large times, if the system has $\lambda_2 > \lambda_3$ gap, the evolution of $\boldsymbol{p}(t)$ is dominated by the first two terms

$$\boldsymbol{p}(t) \approx \boldsymbol{\pi}^{T_b} + a_2(T, T_b) e^{\lambda_2 t} \boldsymbol{v}_2. \tag{5.9}$$

Non-monotonic behavior of $a_2$ with respect to the initial temperature $T$ leads to a Weak Mpemba effect in the system [25], and zeros of $a_2$ indicate a jump in the relaxation time and a Strong Mpemba effect [26]. The Strong Mpemba effect implies the Weak Mpemba effect.

Below we focus on Strong Mpemba effect occurrence, i.e., zeros of $a_2$. As the Strong Mpemba effect is topological, it is convenient to check for parity of the direct (effect in cooling) and inverse (effect in cooling) effects,

$$\mathcal{P}_{\rm dir} = -\left[\left.\frac{\partial a_2}{\partial T}\right|_{T=T_b} a_2(T=\infty,T_b)\right], \tag{5.10}$$

$$\mathcal{P}_{\rm inv} = \lim_{\varepsilon\to 0^+}\left[\left.\frac{\partial a_2}{\partial T}\right|_{T=T_b} a_2(T=\varepsilon,T_b)\right], \tag{5.11}$$

see [26]. There is an odd number of zero crossings of $a_2$ between $T\in(1,\infty)$ if $\mathcal{P}_{\rm dir}>0$ and an odd number of zero crossings of $a_2$ between $T\in(\varepsilon,1)$ if $\mathcal{P}_{\rm inv}>0$. An odd number of zero crossings gives a lower bound for the occurrence of the Strong Mpemba effect.

## 5.3 Single-particle picture

The dynamics of a single particle jumping through $M$ states can be modeled as a Markov jump process

$$\frac{d}{dt}q_i(t)=\sum_{j=1}^{M}Q_{ij}q_j(t), \tag{5.12}$$

where $q_i(t)$ is the probability of the particle being in state $i$ (of type $X_i$), at time $t$, and $Q_{ij}$ is the transition probability from $j$ to $i$. The eigenvalue problem is

$$Q\,\boldsymbol{w}_\mu=\nu_\mu\boldsymbol{w}_\mu \qquad \text{and} \qquad \boldsymbol{x}_\mu\,Q=\nu_\mu\boldsymbol{x}_\mu. \tag{5.13}$$

The eigenvalues are ordered and $\nu_1 = 0 > \nu_2 \geq \nu_3 \geq \cdots \geq \nu_M$. The left and the right eigenvalues related as $(\boldsymbol{x}_\mu)_i = e^{\beta_b \epsilon_i}(\boldsymbol{w}_\mu)_i$. The probability vector $\boldsymbol{q}(t)$ is thus

$$\boldsymbol{q}(t) = \boldsymbol{\rho}^{T_b} + \sum_{\mu>1}^{M} b_\mu e^{\nu_\mu t} \boldsymbol{w}_\mu, \tag{5.14}$$

where

$$\boldsymbol{q}(0) = \boldsymbol{\rho}^T = \frac{1}{Z_1(T)} \left( e^{-\beta\epsilon_1}, e^{-\beta\epsilon_2}, \ldots, e^{-\beta\epsilon_M} \right), \tag{5.15}$$

is the initial condition, with $Z_1 = \sum_{i=1}^{M} \exp[-\beta\epsilon_i]$ being the partition sum, and the coefficients $b_\mu(T, T_b)$ represent the overlap between the initial conditions and the $\mu-$th left eigenvector of $Q$, $\boldsymbol{x}^\mu$:

$$b_\mu(T, T_b) = \frac{\boldsymbol{x}_\mu \cdot \boldsymbol{\rho}^T}{\boldsymbol{x}_\mu \cdot \boldsymbol{w}_\mu}. \tag{5.16}$$

In the long time limit, assuming $\nu_2 > \nu_3$, we have

$$\boldsymbol{q}(t) \approx \boldsymbol{\rho}^{T_b} + b_2(T, T_b)\, e^{\nu_2 t}\, \boldsymbol{w}_2. \tag{5.17}$$

In the above expression, only the $b_2$ overlap coefficient depends on the initial temperature $T$.

## 5.4 Multi-particle picture

The probability of having $N$ molecules in state $\boldsymbol{n}$ is

$$p_{\boldsymbol{n}}(t) = \frac{N!}{n_1!n_2!...n_M!}\left[q_1(t)\right]^{n_1}\left[q_2(t)\right]^{n_2}...\left[q_M(t)\right]^{n_M}. \tag{5.18}$$

Substituting for each $q_i(t)$ its long time limit we get that the term corresponding to the second eigenvector is

$$a_2(T,T_b)(\boldsymbol{v}_2)_{\boldsymbol{n}} = b_2(T,T_b)\frac{N!}{n_1!n_2!\ldots n_M!}\prod_{i=1}^{M}\left[\rho_i^{T_b}\right]^{n_i}\sum_{j=1}^{M} n_j\frac{(\boldsymbol{w}_2)_j}{\rho_j^{T_b}}, \tag{5.19}$$

where eigenvectors $\boldsymbol{v}_2$, $\boldsymbol{\rho}^{T_b}$, and $\boldsymbol{w}_2$ depend solely on $T_b$. The second eigenvalue is $\lambda_2 = \nu_2$.

In $M \leq 5$, it is possible to find the coefficients $(\boldsymbol{w}_2)_i$ analytically, as one eigenvalue is always zero (ground state) and the polynomial left is of order $M-1$.

The Mpemba effect property is determined by the non-monotonicity of coefficients $b_2(T,T_b)$ with respect to $T$. Hence, to infer the existence of the Mpemba effect, it is enough to look at $N=1$, and the results will also be valid in the thermodynamic limit (large $N$ limit). Thus below, we focus on $N=1$. Note that we know the full probability distribution in this case

$$p_{\boldsymbol{n}}(t) = \prod_{i=1}^{N}\left[\frac{\langle n_i(t)\rangle^{n_i}}{n_i!}e^{-\langle n_i(t)\rangle}\right], \tag{5.20}$$

where $\sum_i n_i = N$, and $\langle n_i\rangle \equiv \sum_{\boldsymbol{n}} p_{\boldsymbol{n}}(t)\, n_i$, is the average occupancy of state $i$ at time $t$. In the case of linear reaction networks, the full statistics are determined with only averages of $\langle n_i(t)\rangle$ and higher moments do not contribute [89, 88].

## 5.5 Specifying the dynamics

Detailed Balance does not determine the dynamics; it only sets the ratio of the forward and backward microscopic rates between two states

$$\frac{k_{ij}}{k_{ji}} = e^{-\beta_b(\epsilon_i - \epsilon_j)}. \tag{5.21}$$

The choice of rates sets the dynamics. To study the influence of the dynamics on the Mpemba effect, we introduce the so-called load distribution factor, $\delta$. This control parameter has been previously studied in molecular motors [82, 84], negative differential mobility [85], and Markov jump processes [86]. For example, for a cyclic system, $M-$states on a ring, we define $\delta$ as follows

$$\begin{aligned} k_{21} = e^{-\beta_b(\epsilon_2-\epsilon_1)(1-\delta)} \quad &, \quad k_{12} = e^{\beta_b(\epsilon_2-\epsilon_1)\delta}, \\ k_{32} = e^{-\beta_b(\epsilon_3-\epsilon_2)(1-\delta)} \quad &, \quad k_{23} = e^{\beta_b(\epsilon_3-\epsilon_2)\delta}, \\ &\vdots \\ k_{1,M} = e^{-\beta_b(\epsilon_M-\epsilon_1)(1-\delta)} \quad &, \quad k_{M,1} = e^{\beta_b(\epsilon_M-\epsilon_1)\delta}. \end{aligned} \tag{5.22}$$

That is, the rates clockwise (CW), $1 \to 2 \to \cdots \to M \to 1$, get a factor $(1-\delta)$ and the rates of transitions in counter-clockwise (CCW) direction get $\delta$. The load distribution factor varies between $\delta \in [0, 1]$.

For $N = 1$, $E_i = \epsilon_i$, and the barriers $B_{ij}$ can be expressed with the load distribu-

tion factor $\delta$ as

$$\begin{aligned} B_{12} &= B_{21} = E_2(1-\delta) + E_1\delta, \\ B_{32} &= B_{23} = E_3(1-\delta) + E_2\delta, \\ B_{13} &= B_{31} = E_1(1-\delta) + E_3\delta. \end{aligned} \tag{5.23}$$

Next, we look at cases with two-, three-, and four-level systems. There is no Mpemba effect in the two-level system, as one needs at least three eigenvectors to observe the effect, see Appendix C .

## 5.6 Three-level system

### 5.6.1 Three-level cyclic system

For the three-level system on a ring, the single-particle rate matrix is

$$Q = \begin{pmatrix} -k_{21} - k_{31} & k_{12} & k_{13} \\ k_{21} & -k_{12} - k_{32} & k_{23} \\ k_{31} & k_{32} & -k_{13} - k_{23} \end{pmatrix}. \tag{5.24}$$

The eigenvalues are

$$\lambda_1 = 0, \qquad \lambda_{2,3} = \frac{1}{2}\left(k_{\text{tot}} \pm \Delta\right), \tag{5.25}$$

with $k_{\text{tot}} \equiv \sum_{i,j=1;i\neq j}^{3} k_{ij}$,

$$\Delta \equiv \sqrt{(\kappa_1 + \kappa_2 + \kappa_3)^2 - 4\kappa_1\kappa_3}, \tag{5.26}$$

and $\kappa_1 \equiv k_{12} - k_{13}$, $\kappa_2 \equiv k_{21} - k_{23}$, and $\kappa_3 \equiv k_{31} - k_{32}$. The second right eigenvector of $Q$, $\boldsymbol{w}_2$, is

$$\begin{aligned} (\boldsymbol{w}_2)_1 &= -\kappa_1 - \kappa_2 - \kappa_3 + \Delta, \\ (\boldsymbol{w}_2)_2 &= -2\kappa_3 - (\boldsymbol{w}_2)_1, \\ (\boldsymbol{w}_2)_3 &= 2\kappa_3. \end{aligned} \tag{5.27}$$

As it should be, since $\boldsymbol{w}_2 \cdot \boldsymbol{u}_1 = 0$, the entries of $\boldsymbol{w}_2$ sum to 0.

### Regions of the Strong Mpemba Effect

**Enhanced transition rate – the "highway picture"** – We observe the Strong Mpemba effect if two levels are close to each other, that is if $|\epsilon_i - \epsilon_j| = \mathcal{O}(T_b)$. The Strong Mpemba regions in the phase space plots correspond to the rate of going from the highest to the lowest energy level being larger than all of the other rates. Suppose the reaction rates are pictured as "roads," where the width of the road determines a higher rate, in the regions of Strong Mpemba effect in the phase space plots of $M = 3$. In that case, the "road" going from the highest single particle energy state to the lowest single energy particle state becomes a "highway" compared to all the other roads, see thick lines on Fig. 5.2. For example, for $\delta = 0$ and $\epsilon_1 = 0$, the CCW rates are 1, while the CW rates are: $k_{21} = \exp[-\beta_b \epsilon_2]$, $k_{32} = \exp[-\beta_b(\epsilon_3 - \epsilon_2)]$, and $k_{13} = \exp[-\beta_b \epsilon_3]$. The regions of occurrence of the Strong Mpemba effect are

$$\text{region I: } \epsilon_3 > \epsilon_2 > 0, \qquad |\epsilon_2| \sim \mathcal{O}(T_b), \tag{5.28}$$

$$\text{region II: } \epsilon_2 > 0 > \epsilon_3, \qquad |\epsilon_3| \sim \mathcal{O}(T_b), \tag{5.29}$$

$$\text{region III: } 0 > \epsilon_3 > \epsilon_2, \qquad |\epsilon_3 - \epsilon_2| \sim \mathcal{O}(T_b), \tag{5.30}$$

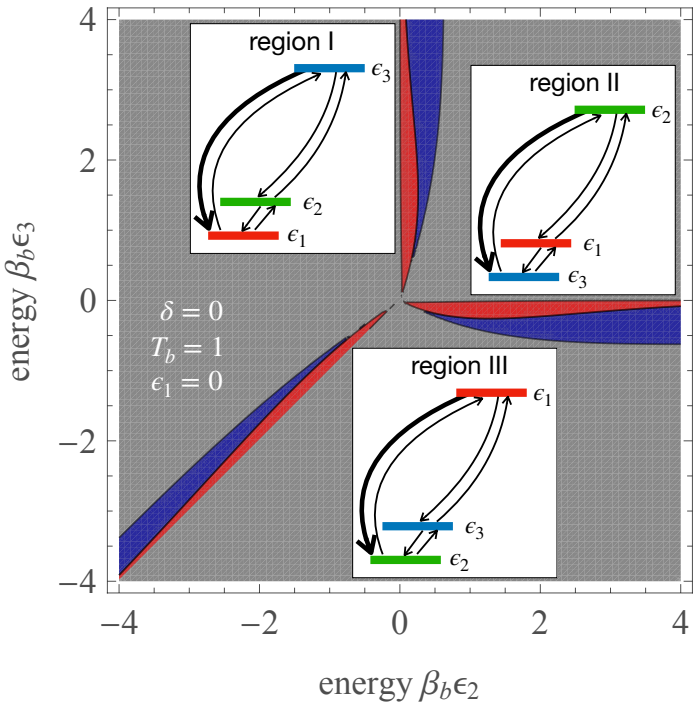


Figure 5.2: The phase space of energies $\epsilon_2$ and $\epsilon_3$ showing regions with the Strong Mpemba effect. The blue regions correspond to the lower bound for the Strong Mpemba effect in cooling ($\mathcal{P}_{\text{dir}} = 1$), the red for the Strong Mpemba effect in heating ($\mathcal{P}_{\text{inv}} = 1$), and in the gray regions, there is no effect. The red and blue regions also correspond to the transition rate, $k_{ij}$, from the highest energy level to the lowest, being the global maximum of the rates (thick arrows). In the text, we refer to this enhanced transition rate as the "highway." The bath temperature is $T_b = 1$, $\epsilon_1 = 0$, and the load distribution factor is $\delta = 0$.

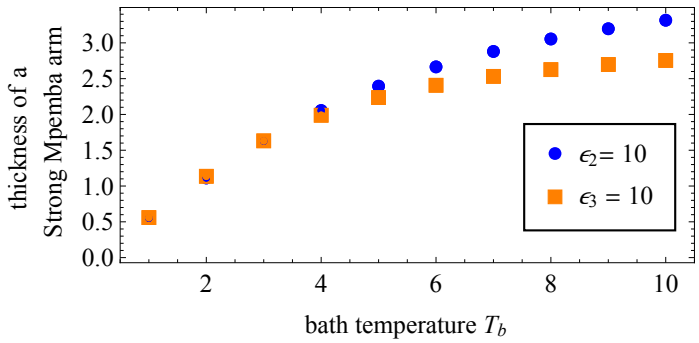


Figure 5.3: Thickness Strong Mpemba arms at $\epsilon_2 = 10$ and $\epsilon_3 = 10$ for bath temperature $T_b \in [1, 10]$. The parameters of the plot are $\epsilon_1 = 0$ and $\delta = 0$.

as can be seen on Fig. 5.2. We do not have the effect of any two energies being the same. In all three regions, it is the transition from the highest level to the lowest level that is the highest rate of the six (in region I: $k_{13} > 1$; in region II: $k_{32} > 1$, and $k_{21} > 1$ in region III). The "arms" corresponding to the Strong Mpemba thicken to $\sim \mathcal{O}(T_b)$ thickness at the widest part Fig. 5.2. Changing the bath temperature scales the Strong Mpemba regions in the phase space in a way such that the thickness of the arms increases monotonically with the bath temperature, see Fig. 5.3.

**Non-overlapping regions and a unique solution for the Strong Mpemba effect temperature** – The regions of the Strong Mpemba effect (blue and red on Fig. 5.2) do not overlap in the three-level cyclic system. The numerator of the overlap coefficient $b_2$, see Eq. (5.16), is

$$\boldsymbol{x}_2 \cdot \boldsymbol{\rho}^T = (\boldsymbol{x}_2)_1 + [(\boldsymbol{x}_2)_2 - (\boldsymbol{x}_2)_1]\, \rho_2^T + [(\boldsymbol{x}_2)_3 - (\boldsymbol{x}_2)_1]\, \rho_3^T ,$$

where we used that $\sum_i \rho_i^T = 1$ and $\sum_i (\boldsymbol{x}_2)_i = 0$. The condition for the Strong Mpemba effect is that the numerator of the overlap coefficient $b_2$ is zero at $T \neq T_b$. Given that it is zero at $T = T_b$, the Strong Mpemba effect condition can be written

as

$$[(\boldsymbol{x}_2)_2 - (\boldsymbol{x}_2)_1]\left(\rho_2^T - \rho_2^{T_b}\right) + [(\boldsymbol{x}_2)_3 - (\boldsymbol{x}_2)_1]\left(\rho_3^T - \rho_3^{T_b}\right) \;=\; 0. \tag{5.31}$$

For there to be a nontrivial zero, all three components of $\boldsymbol{x}_2$ should be non-zero, and no pair should be equal to each other; if it were, it would imply $T = T_b$, see Eq. (5.31). Thus, we can rewrite the above equation as

$$\frac{\rho_2^T - \rho_2^{T_b}}{\rho_3^T - \rho_3^{T_b}} \;=\; \frac{1 - \frac{(\boldsymbol{x}_2)_1}{(\boldsymbol{x}_2)_2}}{2 + \frac{(\boldsymbol{x}_2)_1}{(\boldsymbol{x}_2)_2}}. \tag{5.32}$$

Given that the Boltzmann distribution is a monotonic function of the temperature, the equation has at most one solution for $T \neq T_b$.

In contrast to the three-level system, a four-level system on a ring can have both Strong Mpemba effects (in cooling and heating) for the same set of parameters and even multiple zeros of the overlap $b_2$ above or below $T_b$, see Fig. 5.4. Note that the four-level system also has cases where the eigenvalues cross [113].

**Chirality** – Notice that the three-level cycle has the following symmetry: for $\epsilon_1 = 0$, the systems with $\delta$ and $1 - \delta$ are equivalent if $\epsilon_2 \rightleftarrows \epsilon_3$. Thus, it is sufficient to study the system for $\delta \in \left[0, \frac{1}{2}\right]$. The rates $k_{ij}$ possess a chirality, see Eq. (5.22). In this case, then $\delta = 1/2$ is the only value at which chirality is not specified, and thus, as such, the Strong Mpemba effect there has to be zero. From Fig. 5.5, we see that the phase space plots for the Strong Mpemba regions are mirror-symmetric about $\delta = 1/2$. For $\delta = 0$, the arms are the thickest, which gradually thins out in a continuous manner as $\delta \to 1/2$. At $\delta = 1/2$, the regions for Strong Mpemba disappear completely. As $\delta$ moves away from $1/2$, the arms of opposite chirality reappear and gradually thicken

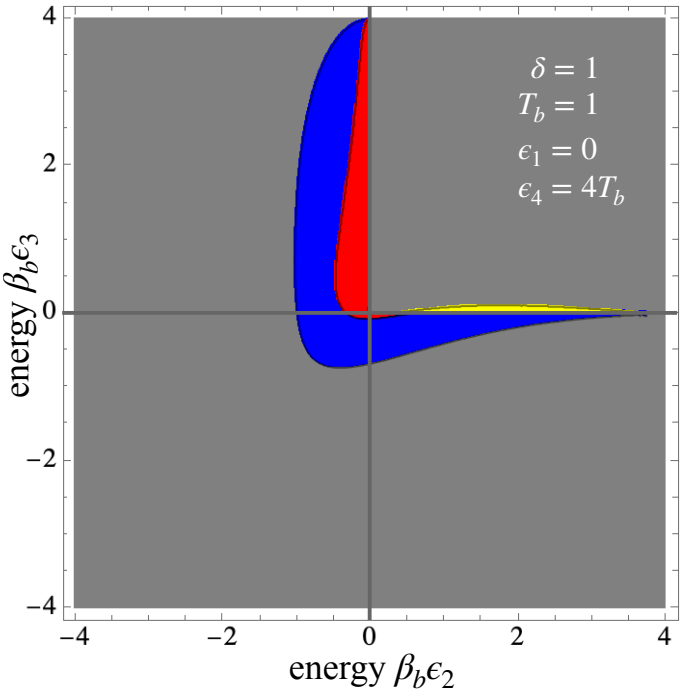


Figure 5.4: Phase space section of the Strong Mpemba effect in a four-level system on a ring with fixed energies $\epsilon_1 = 0$ and $\epsilon_4 = 4T_b$. Here $T_b = 1$ and $\delta = 1$. The Strong Mpemba effect occurs in the yellow region in heating and cooling. In the blue region, we have the Strong Mpemba effect in cooling only and the red region in heating only. In the gray region, there is no Strong Mpemba effect.

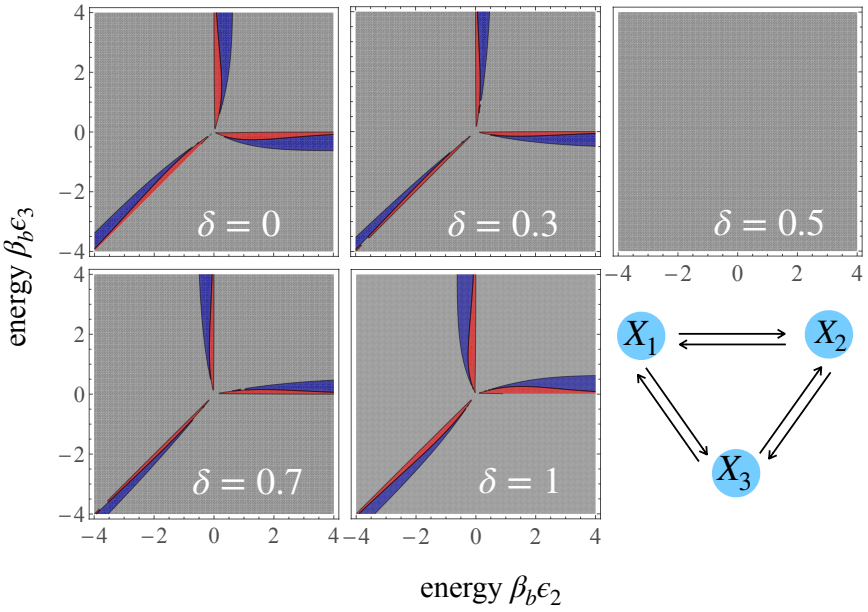


Figure 5.5: Phase space plot showing regions with the Strong Mpemba effect as $\delta$ changes from 0 to 1 for a three-level system on a ring. The parameters are $T_b = 1$, $\epsilon_1 = 0$.

in a continuous manner as $\delta \to 1$. Here, the Strong Mpemba effect appears in the regions where we have an enhanced transition from the highest to the lowest state, as a result of "symmetry breaking."

For different topologies, such as the three-level system with open ends and the four-level on a ring system, we no longer have the chiral symmetry of the rates, and there is a Strong Mpemba effect for the "symmetric load" of $\delta = 1/2$. For example, in the three-level case with open ends, the phase space where the Strong Mpemba occurs at $\delta = 1/2$ in one connected region, see Fig. 5.6.

**Appearance of islands** – Here, we assume a pair of rates has a prefactor, $k = const$. We single out the pair of rates $k_{21}$ and $k_{12}$,

$$k_{21} = ke^{-\beta_b(\epsilon_2-\epsilon_1)(1-\delta)}, \qquad k_{12} = ke^{-\beta_b(\epsilon_2-\epsilon_1)\delta}, \tag{5.33}$$

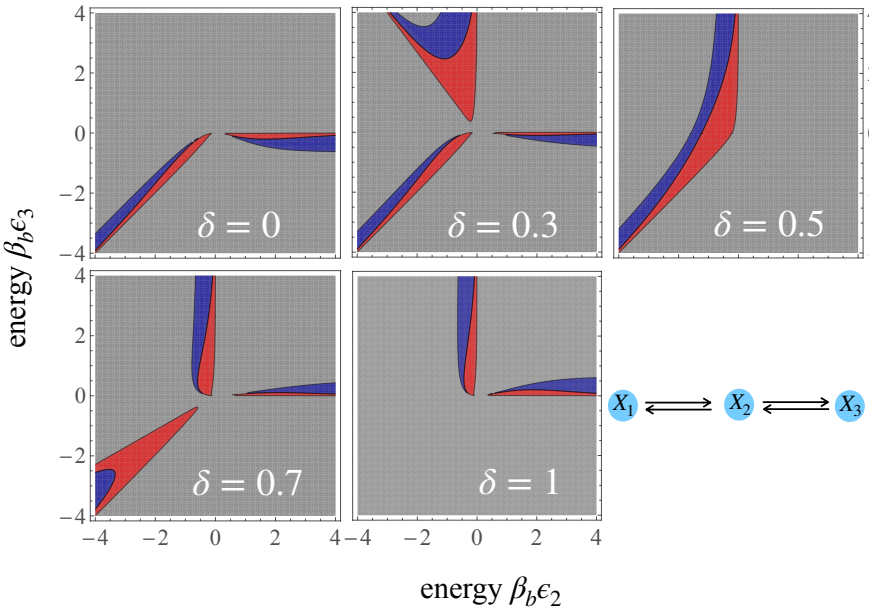


Figure 5.6: Phase space plot showing regions with the Strong Mpemba effect as $\delta$ changes from 0 to 1 for a three-level system with open ends. The parameters are $T_b = 1$, $\epsilon_1 = 0$.

and the other rates we set by Eq. (5.22). As a rate decreases, one of the arms translates to infinity along its axis while the other two arms vary minutely. Reading the top row of Fig. 5.7 from right to left, we see that the arm along $\epsilon_2 = \epsilon_3$ pulls back. Here we have $k_{12} < 1$ and constant, while the other two CCW rates are set to unity (i.e., $\delta = 0$). This observation can be explained using the "highway picture" as follows: for varying the reaction rate, $k_{12}$, the arm that translates to infinity corresponds to the condition where $0 > \epsilon_3 > \epsilon_2$ thus, the "highway" exists from state 1 to 2 and the highest rate is $k_{21}$. As $k_{12}$ decreases, $k_{21}$ also decreases due to DB. In order to maintain $k_{21}$ as the maximal rate of the six, the decrease needs to be compensated for, which can be done by decreasing $\epsilon_2$ so that the contribution from $\exp[-\beta_b\epsilon_2]$ is large enough. Thus $k_{21}$ becomes the highest rate after a sufficiently small $\epsilon_2$, enough to compensate for the decrease in $k_{21}$; hence the translation of the arm along the $\epsilon_2 = \epsilon_3$ axis. On the other hand, increasing, such that $k_{12} > 1$ and $\delta = 0$, while the

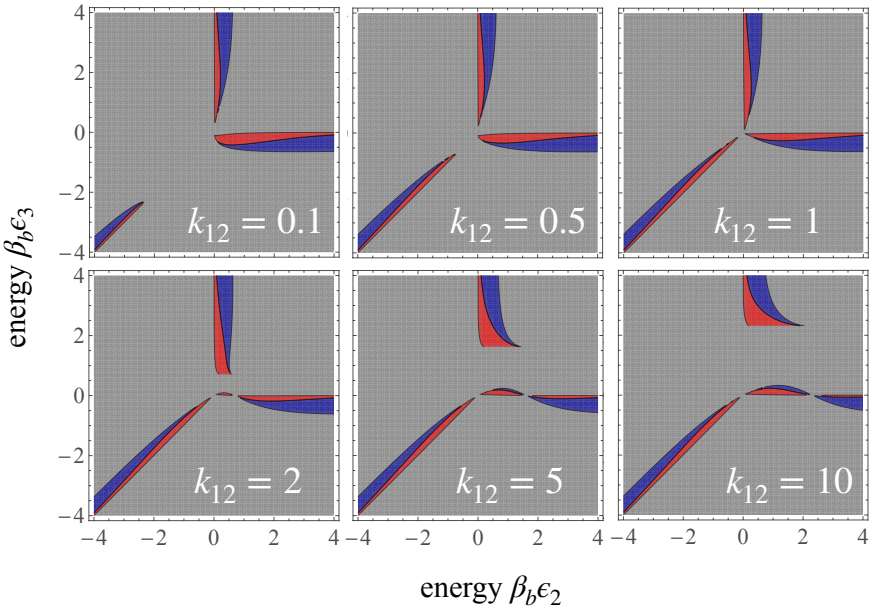


Figure 5.7: Phase space section showing the Strong Mpemba effect in cooling (blue), heating (red), and no effect (gray) for a three-level system on a ring and parameters $T_b = 1$, $\delta = 0$, $\epsilon_1 = 0$, and varying reaction rate $k_{12} \in [0.1, 10]$, while the other CCW rates are set to unity. In the top row, $k_{12}$ increases to 1 from left to right, and we see the arm close to $\epsilon_2 = \epsilon_3$ axis "approach" the origin, reducing the gap along $\epsilon_2 = \epsilon_3$. In the bottom row, the arm close to $\epsilon_2 = \epsilon_3$ axis remains almost unchanged, while the vertical arm pulls up, the horizontal arm pulls toward more positive values of $\epsilon_2$ and an "island" where we have the Strong Mpemba effect emerges above $\epsilon_3 = 0$ line close to the origin.

other CCW rates are set to unity, one arm stays the same while another arm slides away from the center with the emergence of an island like structure close to the origin between the two remaining arms. The third arm transforms in a way such that the area within the arm for the Strong Mpemba effect in heating increases closer to the center while simultaneously the whole arm moves away from the center as shown on the lower panel of Fig. 5.7. Analogous figures can be obtained for adding a prefactor to one of the other pair of rates while specifying the rest with Eq. (5.22).

Next, we apply the insights to the case of a three-level system on a ring performing as a device in a Maxwell demon setup. We introduce the load distribution factor on one edge only. The Mpemba effect on such three-level systems on a ring with one edge subject to load distribution factor variations was already considered in connections to optimal transport in [114], where it was observed that for large eigenvalue gaps, $(\lambda_2 - \lambda_3)\tau \gg 1$, the optimal transport (minimal total dissipation) in finite time $\tau$ and the Strong Mpemba effect occur for the same load distribution factor $\delta$. Below we look at not-so-large gaps and the power output when the device is connected to a bath and an information reservoir.

## 5.7 Application of the Mpemba effect on a Maxwell demon setup

Maxwell thought of an agent that would "ingeniously" deliver useful work by rectifying random microscopic fluctuations [115]. If possible, such an agent, the so-called *Maxwell demon*, would violate the second law of thermodynamics. The paradox caused numerous discussions on the thermodynamic implications of information pro-

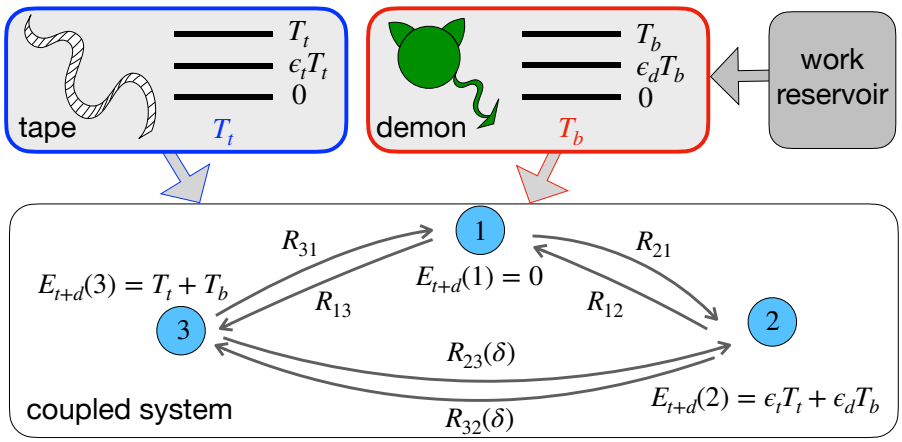


Figure 5.8: The device (demon) interacts with a heat bath reservoir with temperature $T_b$, an information-carrying tape kept at temperature $T_t$, and a work reservoir. The device and tape are three-level systems. The states of the tape are $\{0, \epsilon_t T_t, T_t\}$. The states of the device are $\{0, \epsilon_d T_b, T_b\}$. To set the units, we work with bath temperature $T_b = 1$ and rate constant $\gamma = 1$. During the interaction, the device and the tape form a composite system with levels, being the sum of the corresponding device and tape levels, $\{0, \epsilon_t T_t + \epsilon_d T_b, T_t + T_b\}$.

cessing. A consensus emerged that a mechanical demon could deliver work in rectifying fluctuations but in doing so, all of the gathered information has to be written onto a tape, see e.g. [116, 117, 118].

Statistical physics and information theory "meet" in stochastic thermodynamics; thus, we consider an application of our results to a three-level Markov jump process that, besides a thermodynamic reservoir, has access to an information reservoir (a tape). More specifically, we consider a Maxwell demon setup introduced in Hoppenau and Engel [110] and look at the thermal relaxations of the system. The authors primarily discussed a two-level system; here, we use a three-level system on a ring, as the Mpemba effect can not be realized in two-level systems.

Recently, the Mpemba effect was studied for the Mandal-Jarzynski Maxwell demon setup [109], where it was shown that the Mpemba effect could lead to faster

functionalization of the demon and tape setup [119]. Likewise, with stochastic resetting [120], the Strong Mpemba effect in a Mandal-Jarzynski setup can help minimize the time cost to enter the working state [121]. In Hoppenau and Engel's Maxwell demon, the device is already in the functional state, and we can not study the functionalization itself. Still, we can study what happens during the working state. In [33], the authors showed that a three-level system operating as a heat engine with an Otto cycle has improved performance with the Mpemba effect. The cycle length was shorter, increasing the power output for the same efficiency without sacrificing the stability of the engine. Here, we show an analogous occurrence in the operation of a Maxwell demon setup as a function of the system dynamics.

The device, or the demon in this case, is the three-level system on a ring with energies $\{E_d(y)|y \in [1,3]\} = \{0, \epsilon_d T_b, T_b\}$. The three-level device is kept in a bath with temperature $T_b$. During its operation, the device interacts with a tape. The tape is another three-level system on a ring with energies $\{E_t(y)|y \in [1,3]\} = \{0, \epsilon_t T_t, 1.1T_t\}$ which is kept at temperature $T_t$. Due to the finite temperature $T_t$, the tape is *non-ideal*, as the recordings on the tape have a finite probability of being corrupted, with thermal fluctuations, [110]. The ideal tape limit is reached by taking $T_t \to 0$. The system is illustrated on Fig. 5.8. The tape cells are populated with states drawn from the tape Boltzmann distribution, $\pi_t^{T_t}(y) \propto \exp[-\beta_t E_t(y)]$. A cell from the tape interacts with the device for some time $\tau$, called the coupling time. During the coupling, we assume that the joint system has energies that are the sum of the energies of corresponding states of the tape and the demon $\{E_{t+d}(y)|y \in [1,3]\} = \{0, \epsilon_t T_t + \epsilon_d T_b, 1.1T_t + T_b\}$. The combined system acts as an effective three-level

system with transition rates

$$R_{21} = \Gamma e^{-\frac{1}{2}\beta_b[E_{t+d}(2)-E_{t+d}(1)]}, \tag{5.34}$$

$$R_{13} = \Gamma e^{-\frac{1}{2}\beta_b[E_{t+d}(1)-E_{t+d}(3)]}, \tag{5.35}$$

$$R_{32} = \Gamma e^{-\beta_b[E_{t+d}(3)-E_{t+d}(2)]\delta}, \tag{5.36}$$

where $\Gamma^{-1} = 1$ sets the unit of time. The transition rate $R_{32}(\delta)$ has a control parameter, the load distribution factor $\delta \in [0, 1]$, with which its magnitude can be controlled. The DB condition,

$$R_{xy}\pi^{T_b}_{t+d}(y) = R_{yx}\pi^{T_b}_{t+d}(x), \tag{5.37}$$

with $\pi^{T_b}_{t+d}(x) \propto \exp[\beta_b E_{t+d}(x)]$ as the Boltzmann distribution of the joint system at $T_b$ sets the corresponding CCW transition rates. By changing the load distribution factor $\delta$, we vary the magnitude of the rates between states 2 and 3 – because of DB, this local change affects all currents of this setup. The conservation of probability sets the diagonal elements – the columns of the $R$ matrix sum to zero, i.e.,

$$R_{xx} = -\sum_{y\in\Omega; y\neq x} R_{yx}, \qquad x \neq y,\ \forall x \in \Omega. \tag{5.38}$$

The system evolves with a Master eq.,

$$\partial_t \boldsymbol{p}_{t+d} = R\,\boldsymbol{p}_{t+d}, \tag{5.39}$$

where $\boldsymbol{p}_{t+d}$ is the probability distribution of the joint system and $R$ is the rate matrix already introduced in Eqs. (5.34 - 5.38). Note that $R$ depends on $T_t$ as well because

of the scaling of the tape energies with $T_t$. The solution for $\boldsymbol{p}_{t+d}$ is

$$\boldsymbol{p}_{t+d}(t) = \boldsymbol{\pi}_{t+d}^{T_b} + a_2 \boldsymbol{v}_2 e^{\lambda_2 t} + a_3 \boldsymbol{v}_3 e^{\lambda_3 t}, \tag{5.40}$$

where $\boldsymbol{v}_\mu(\delta, T_t, T_b)$, $\boldsymbol{u}_\mu(\delta, T_t, T_b)$ are the right and left eigenvectors of $R$, $\lambda_\mu(\delta, T_t, T_b)$ are the eigenvalues of $R$, and

$$a_\mu(\delta, T_t, T_b) = \frac{\boldsymbol{u}_2 \cdot \boldsymbol{\pi}_t^{T_t}}{\boldsymbol{u}_2 \cdot \boldsymbol{v}_2}, \tag{5.41}$$

are the overlap coefficients with $\pi_t^{T_t}(y) \propto \exp[-E_t(y)/T_t]$ as the Boltzmann distribution of the tape at $T_t$. The average work provided by the work reservoir during a cycle of duration $\tau_{cyc}$

$$\langle W \rangle = \sum_{y=1}^{3} E_d(y) \left[ \pi_t^{T_t}(y) - p_{t+d}(y, \tau_{cyc}) \right]. \tag{5.42}$$

The average power output per cycle is $P = \langle W \rangle / \tau_{cyc}$. The fluctuations of power are

$$\Delta P^2 = \frac{1}{\tau_{cyc}^2} \left[ \sum_{y=1}^{3} \left( E_d(y) \right)^2 \left[ \pi_t^{T_t}(y) - p_{t+d}(y, \tau_{cyc}) \right] - \langle W \rangle^2 \right]. \tag{5.43}$$

The average heat $Q_b$ exchanged between the device and the heat bath per cycle is

$$Q_b = \sum_{y=1}^{3} E_{t+d}(y) \left[ p_{t+d}(y, \tau_{cyc}) - \pi_t^{T_t}(y) \right]. \tag{5.44}$$

While the average energy exchanged between the device and the tape is

$$Q_t = \sum_{y=1}^{3} E_t(y) \left[\pi_t^{T_t}(y) - p_t(y, \tau_{cyc})\right]. \tag{5.45}$$

The first law of thermodynamics gives the energy conservation,

$$\langle W \rangle + Q_b + Q_t = 0. \tag{5.46}$$

Finally, the change in entropy of the tape at $\tau_{cyc}$ is

$$\begin{aligned} \Delta S_t &= -\sum_{y=1}^{3} p_t(y, \tau_{cyc}) \ln p_t(y, \tau_{cyc}) + \sum_{y=1}^{3} \pi_t^{T_t}(y) \ln \pi_t^{T_t}(y) \\ &= -\frac{Q_t}{T_t} - D_{\mathrm{KL}}\left(\boldsymbol{p}_t(\tau_{cyc}) || \boldsymbol{\pi}_t^{T_t}(y)\right), \end{aligned} \tag{5.47}$$

where

$$D_{\mathrm{KL}}\left(\boldsymbol{p}_t(\tau) || \boldsymbol{\pi}_t^{T_t}\right) \equiv \sum_{y=1}^{3} p_t(y, \tau) \ln \left[\frac{p_t(y, \tau)}{\pi_t^{T_t}(y)}\right], \tag{5.48}$$

is the Kullback-Leibler (KL) divergence. The entropy of the bath is $\Delta S_b = -Q_b/T_b$, and the second law of thermodynamics is $\Delta S_b + \Delta S_t \geq 0$.

Depending on the parameters of the tape, device, and heat baths, the three-level system can perform as an information heat engine, eraser, or as a dud, see Fig. 5.9. In the heat engine phase, the device does the work; hence, the average work supplied from the work reservoir is $\langle W \rangle < 0$. In the eraser phase, the work supplied from the heat reservoir, $\langle W \rangle > 0$, is used to erase the tape, thus lowering the entropy of the tape, $\Delta S_t < 0$. While in the dud phase, the work produced, $\langle W \rangle < 0$, is used to increase the entropy of the tape $\Delta S_t > 0$. One can define different efficiencies

to quantify the device's behavior. For our examples below, it will be important to consider the eraser efficiency

$$\eta_e = -\frac{T_b \Delta S_t}{\langle W \rangle + Q_t}, \tag{5.49}$$

and the heat engine efficiency

$$\eta_h = -\frac{\langle W \rangle}{Q_b}, \tag{5.50}$$

see [110]. also other efficiencies play a role in the heat engine region

**The Strong Mpemba effect by altering dynamics** – In some cases, depending on the energies of the system and the tape, by adjusting the dynamics with the load distribution factor $\delta$, one can find a finite $0 < \delta_{\rm SM} < 1$ for which the joint system of the demon and the tape has a Strong Mpemba effect. In that case, provided that $\lambda_2 > \lambda_3$, the joint system approaches the equilibrium,

$$p^{T_b}_{t+d}(\tau) \to \pi^{T_b}_{t+d}, \tag{5.51}$$

faster, as it relaxes with dynamics that do not have the projection on the slow mode, $a_2(\delta_{\rm SM}, T_t, T_b) = 0$. This can be quantified by observing the corresponding KL divergence between the state of the system at time $t$ and the equilibrium, $D_{\rm KL}\left(\boldsymbol{p}_{t+d}(t)||\boldsymbol{\pi}^{T_b}_{t+d}\right)$, see e.g. [25] and Fig. 5.10a. At large enough times, the system will be close to equilibrium $\boldsymbol{\pi}^{T_b}_{t+d}$ and the average power goes to zero, $\lim_{\tau\to\infty} \partial_t \langle W \rangle|_{t=\tau} = 0$. By choosing a cutoff time, $D_{\rm KL,cutoff}$, we define a cycle time of the information en-

(a)

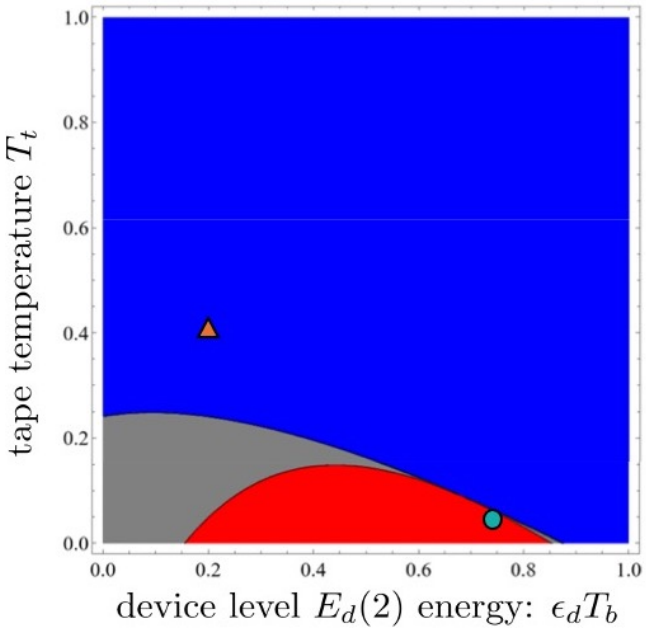


(b)

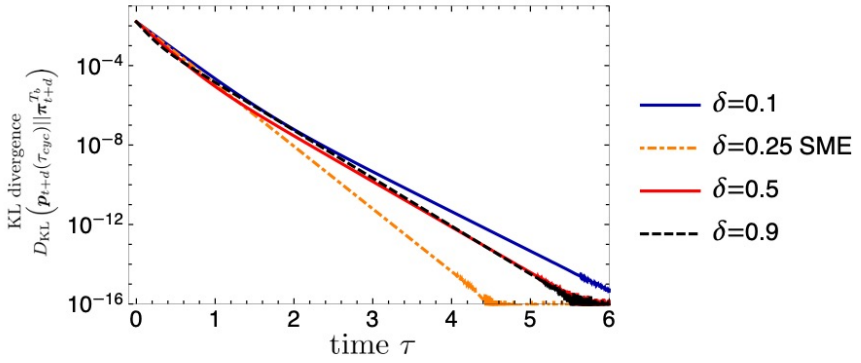


Figure 5.9: (a) Phase space of the three level system for tape energies $\{E_t(y)|y\ [1,3]\} = \{0, 0.75T_t, 1.1T_t\}$, device energies $\{E_d(y)|y\ [1,3]\} = \{0, \epsilon_d T_b, T_b\}$ and $T_b = 1$. The system acts as a heat engine in the red region, an eraser in the blue region and is a dud in the gray region. The orange triangle and blue circle is the sample we use for the stability and power plots in Fig. 5.10. Both data points have a SM effect for $\delta = 0.25$. (b) The KL divergence $D_{\mathrm{KL}}\left(\boldsymbol{p}_{t+d}(\tau)||\boldsymbol{\pi}_{t+d}^{T_b}\right)$ as a function of time $\tau$, measuring the thermal relaxation of the device for different load distribution factors, $\delta$. The KL divergence is minimal for $\delta_{\mathrm{SM}} = 0.25$. In this plot, we have chosen the orange triangle data point in the erasure regieme. The system has a Strong Mpemba effect at that value for the specified parameters: $T_t = 0.438$, $T_b = 1$, $\epsilon_t = 0.75$, and $\epsilon_d = 0.25$.

.

gine and erasure $\tau_{cyc}$ as a function of $\delta$ from

$$D_{\mathrm{KL}}\left(\boldsymbol{p}_{t+d}(\tau_{cyc})||\boldsymbol{\pi}_{t+d}^{T_b}\right) = D_{\mathrm{KL,cutoff}}. \tag{5.52}$$

Fig. 5.10a shows $\tau_{cyc}$ as a function of $\delta$ for $D_{\mathrm{KL,cutoff}} = 10^{-12}$. We notice that $\tau_{cyc}$ has a minimum for $\delta = \delta_{\mathrm{SM}}$ – i.e., the load distribution factor for which we have the Strong Mpemba effect.

We measure the average work per cycle as a function of the control parameter of the dynamics, $\delta$. The average work itself is not increased, but the derivative of work goes to zero the fastest, as the power in equilibrium is zero. Thus for a shorter cycle $\tau_{cyc}$, we can reach the same average work faster, which leads to a greater average power output per cycle, see Fig. 5.10a. So the main advantage here is from having shorter cycles. This means the same average work can be achieved in a shorter time, increasing the average power output per cycle.

Given that in a small device fluctuations can be large [63]. To gauge the stability of the device, we measure the so-called *Fano factor* [122]. The Fano factor is a measure of dispersion, defined as the ratio of the variance to the mean. Here it can be used to predict the device's stability in power output. The Fano factor for the power output, defined as $\Delta P^2/P$, is shown on Fig. 5.10c. For our parameter choice, it is always smaller than unity, indicating that running the device with this set of parameters, one has a stable power output. Note that for this reason, the gap $(\lambda_2 - \lambda_3)$ can not be too large, as we need to be able to have long cycles, $\tau_{cyc}$, to reduce the Fano factor.

To conclude, above, we give an example of a Maxwell device setup with anomalous thermal relaxations and enhanced power output. For the choice of dynamics, which given the fixed parameters of the problem, yields the Strong Mpemba effect, we have

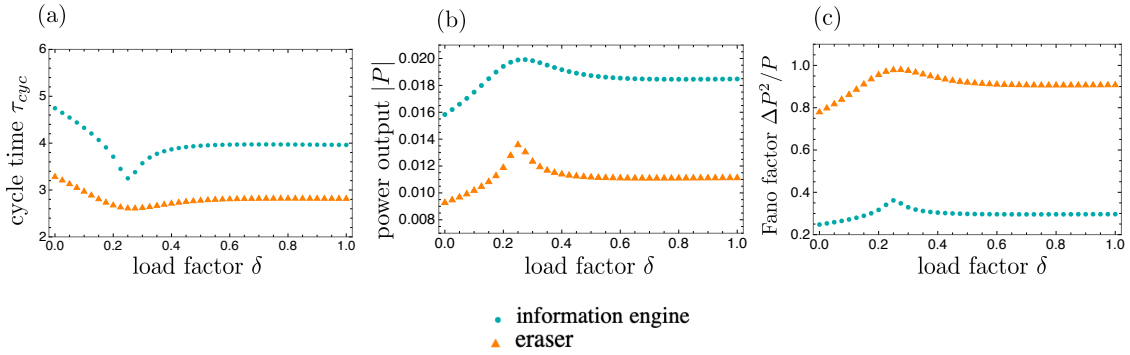


Figure 5.10: (a) Cycle time $\tau_{cyc}$ chosen so that the KL divergence is $10^{-12}$, which is an arbitrary cutoff that will determine the periodic solution that the device settles into. For small enough cutoffs and large enough times, the cycle time has a minimum at the load factor $\delta_{\text{SM}}$ where we have the Strong Mpemba effect. (b) Average power output per cycle, although the work per cycle is the same, the cycle duration depends on the load distribution factor, for $\tau_{cyc}(\delta)$ see Fig. 5.9b. Thus the average power output per cycle, $P = \langle W \rangle / \tau_{cyc}$ is maximal for $\delta_{\text{SM}}$, the load distribution factor where we have the Strong Mpemba effect. In this plot we are plotting the absolute value since the work is negative in the erasure regime. We also multiply the value of the work done for the information engine by 100 so that they both fit on the same plot. (c) The Fano factor is smaller that one, indicating that the device is stable.

a reduced cycle time. The reduced cycle time implies increased power output. It is important to note that here the increase in power output does not come at the expense of efficiency or the stability of the device.

## 5.8 Discussion

Often, one can not alter the initial condition. Here, we ask the question, if there is no anomalous thermal relaxation in the original system, can we alter the dynamics so that the overlap with the system's slow modes is zero? In other words, can we choose a new dynamic with a Strong Mpemba effect for the fixed initial temperature? We investigate such cases on linear reaction networks by controlling the dynamics with the load distribution factor.

In the first part of the chapter for a three-level linear reaction network, we explain the regions with the Strong Mpemba effect as a function of the dynamics. We derive that in a three-level system, the regions of the Strong Mpemba effect in cooling and heating are non-overlapping and that there is, at most, a single Strong Mpemba temperature. We discuss the effect of topology and the existence of gaps and islands of the energy landscape and where we see the Strong Mpemba effect.

In the second part of the paper, as an illustration of the effect of the dynamics on the thermal relaxation of the system, we study a Maxwell demon setup. Here the three-level Markov jump process interacts with a thermal and information reservoir. We show that with a suitable dynamics protocol, one can achieve the same average work with a shorter cycle. The "suitable" dynamics happens to be the one that yields the Strong Mpemba effect. As the average work output is constant, a higher average power output accompanies a shorter operation cycle. We find a regime of parameters where the device's performance is stable, and due to the Strong Mpemba effect, the power output is increased without sacrificing efficiency – the efficiency does not change considerably with load distribution factor variations.

# Chapter 6

# Conclusions and Prospects

The study of physical systems that are far from thermal equilibrium, along with transport phenomena, networks, and their relaxation dynamics, has captured significant interest within the realms of statistical physics and biophysics. In this dissertation, we have explored both the strong and weak forms of the Mpemba effect. We demonstrated that metastability is not a prerequisite for this phenomenon, linked theoretical predictions with experimental results, and developed a deeper understanding of when and why the Mpemba effect can occur. Additionally, we illustrated how the Mpemba effect can be applied to discrete systems governed by Markov jump processes through manipulated dynamics, even when the initial and final conditions remain constant.

We started our investigation by exploring the strong Mpemba effect within a system of over-damped Langevin particles moving through a piecewise constant double well potential energy landscape. By analytically solving the Fokker-Planck equation, we could examine the phase space of the system, adjusting the height and width of the barrier that separates the two wells. This allowed us to gain a thorough understanding of both the inverse and forward Strong Mpemba effects. Our findings revealed that metastability is not a necessary condition for the presence of a Mpemba effect. Interestingly, in cases where the well is perfectly symmetrical, we observed no Mpemba effect, irrespective of the barrier's height. Additionally, we identified that the areas where the Mpemba effect occurred had boundaries marked by a change in

the eigenvectors or a shift in the system's ground state.

Next, we proceeded with the same foundational concepts and utilized a continuous double well landscape model. Through meticulous approximations, we obtained an analytical solution for the Strong Mpemba effect expressed in terms of mean first passage times, which aligned well with the experimental outcomes. Additionally, we outlined the conditions necessary for observing the Weak Mpemba effect and validated our findings through Monte Carlo simulations.

In the latter part of this work, we investigated how dynamics influence anomalous thermal relaxations, optimal transport, and information transfer. By altering the dynamics, we successfully induced a Strong Mpemba effect, demonstrating its potential to identify the optimal transport plan. This capability does not hold in continuous dynamics but is achievable in a discrete context, which was quite unexpected. Finally, we examined the presence of the Mpemba effect in three and four-state networks and how dynamics impact this phenomenon. We concluded with an example illustrating how such an effect could enhance performance in a Maxwell demon setup.

Future research could explore the applications of the Mpemba effect within a double well system. This framework is fundamental across various areas in physics and chemistry, offering insights into quantum physics, chemical reactions, and even cosmology. It would be worthwhile to identify other theoretical examples or laboratory settings where the Mpemba effect can be measured or explored in these systems.

Another intriguing avenue to consider is the relationship between the Mpemba effect and optimal transport within larger networks. Many complex biophysical systems can be modeled as continuous-time Markov jump processes, and it would be fascinating to examine whether such an effect could be leveraged in biological con-

texts.

This dissertation presents some intriguing findings that significantly advance our understanding of non-equilibrium physics. It illustrates that the Strong Mpemba effect and accelerated relaxation processes align with experimental observations, revealing a fascinating aspect of our universe. Additionally, it explores applications where leveraging out-of-equilibrium relaxation pathways can enhance the efficiency of thermodynamic devices, facilitating the more effective transportation of materials. Overall, this research aims to deepen our comprehension of the intricate and often surprising mechanics of our world. Ultimately, we aspire to unify these insights into a cohesive framework, aspiring for a comprehensive description of the universe—*this remains the foundational goal of physics.*

# Bibliography

[1] Avinash Kumar, Raphaël Chétrite, and John Bechhoefer. "Anomalous heating in a colloidal system". eng. In: *Proceedings of the National Academy of Sciences of the United States of America* 119.5 (Feb. 2022), e2118484119. ISSN: 1091-6490. DOI: 10.1073/pnas.2118484119.

[2] Avinash Kumar and John Bechhoefer. "Exponentially faster cooling in a colloidal system". en. In: *Nature* 584.7819 (Aug. 2020). Number: 7819 Publisher: Nature Publishing Group, pp. 64–68. ISSN: 1476-4687. DOI: 10.1038/s41586-020-2560-x. URL: https://www.nature.com/articles/s41586-020-2560-x (visited on 03/16/2023).

[3] E. B. Mpemba and D. G. Osborne. "Cool?" en. In: *Physics Education* 4.3 (May 1969), p. 172. ISSN: 0031-9120. DOI: 10.1088/0031-9120/4/3/312. URL: https://dx.doi.org/10.1088/0031-9120/4/3/312 (visited on 03/16/2023).

[4] Monwhea Jeng. "The Mpemba effect: When can hot water freeze faster than cold?" In: *American Journal of Physics* 74.6 (June 2006), pp. 514–522. ISSN: 0002-9505. DOI: 10.1119/1.2186331. URL: https://doi.org/10.1119/1.2186331 (visited on 05/28/2023).

[5] Yun-Ho Ahn et al. "Experimental verifications of Mpemba-like behaviors of clathrate hydrates". en. In: *Korean Journal of Chemical Engineering* 33.6 (June 2016), pp. 1903–1907. ISSN: 1975-7220. DOI: 10.1007/s11814-016-0029-2. URL: https://doi.org/10.1007/s11814-016-0029-2 (visited on 05/28/2023).

[6] P. Chaddah et al. *Overtaking while approaching equilibrium*. arXiv:1011.3598 [cond-mat, physics:physics]. Nov. 2010. DOI: 10.48550/arXiv.1011.3598. URL: http://arxiv.org/abs/1011.3598 (visited on 05/28/2023).

[7] Cunliang Hu et al. "Conformation Directed Mpemba Effect on Polylactide Crystallization". In: *Crystal Growth & Design* 18.10 (Oct. 2018). Publisher: American Chemical Society, pp. 5757–5762. ISSN: 1528-7483. DOI: 10.1021/acs.cgd.8b01250. URL: https://doi.org/10.1021/acs.cgd.8b01250 (visited on 05/28/2023).

[8] Shahaf Aharony Shapira et al. "Inverse Mpemba Effect Demonstrated on a Single Trapped Ion Qubit". In: *Phys. Rev. Lett.* 133 (1 July 2024), p. 010403. DOI: 10.1103/PhysRevLett.133.010403. URL: https://link.aps.org/doi/10.1103/PhysRevLett.133.010403.

[9] Marco Baity-Jesi et al. "The Mpemba effect in spin glasses is a persistent memory effect". In: *Proceedings of the National Academy of Sciences* 116.31 (July 2019). Publisher: Proceedings of the National Academy of Sciences, pp. 15350–15355. DOI: 10.1073/pnas.1819803116. URL: https://www.pnas.org/doi/full/10.1073/pnas.1819803116 (visited on 05/28/2023).

[10] A. Gijón, A. Lasanta, and E. R. Hernández. "Paths towards equilibrium in molecular systems: The case of water". In: *Physical Review E* 100.3 (Sept. 2019). Publisher: American Physical Society, p. 032103. DOI: 10.1103/PhysRevE.100.032103. URL: https://link.aps.org/doi/10.1103/PhysRevE.100.032103 (visited on 05/28/2023).

[11] Rubén Gómez González and Vicente Garzó. "Time-dependent homogeneous states of binary granular suspensions". In: *Physics of Fluids* 33.9 (Sept. 2021),

p. 093315. ISSN: 1070-6631. DOI: 10.1063/5.0062425. URL: https://doi.org/10.1063/5.0062425 (visited on 05/28/2023).

[12] E. Mompó et al. "Memory effects in a gas of viscoelastic particles". In: *Physics of Fluids* 33.6 (June 2021), p. 062005. ISSN: 1070-6631. DOI: 10.1063/5.0050804. URL: https://doi.org/10.1063/5.0050804 (visited on 05/28/2023).

[13] Antonio Lasanta et al. "When the Hotter Cools More Quickly: Mpemba Effect in Granular Fluids". In: *Physical Review Letters* 119.14 (Oct. 2017). Publisher: American Physical Society, p. 148001. DOI: 10.1103/PhysRevLett.119.148001. URL: https://link.aps.org/doi/10.1103/PhysRevLett.119.148001 (visited on 05/28/2023).

[14] Alberto Megías and Andrés Santos. "Mpemba-like effect protocol for granular gases of inelastic and rough hard disks". In: *Frontiers in Physics* 10 (2022). ISSN: 2296-424X. URL: https://www.frontiersin.org/articles/10.3389/fphy.2022.971671 (visited on 05/28/2023).

[15] Apurba Biswas, V. V. Prasad, and R. Rajesh. "Mpemba effect in an anisotropically driven granular gas". en. In: *Europhysics Letters* 136.4 (Mar. 2022). Publisher: EDP Sciences, IOP Publishing and Società Italiana di Fisica, p. 46001. ISSN: 0295-5075. DOI: 10.1209/0295-5075/ac2d54. URL: https://dx.doi.org/10.1209/0295-5075/ac2d54 (visited on 05/28/2023).

[16] Apurba Biswas, V. V. Prasad, and R. Rajesh. "Mpemba Effect in Anisotropically Driven Inelastic Maxwell Gases". en. In: *Journal of Statistical Physics* 186.3 (Feb. 2022), p. 45. ISSN: 1572-9613. DOI: 10.1007/s10955-022-02891-w. URL: https://doi.org/10.1007/s10955-022-02891-w (visited on 05/28/2023).

[17] Aurora Torrente et al. “Large Mpemba-like effect in a gas of inelastic rough hard spheres”. In: *Physical Review E* 99.6 (June 2019). Publisher: American Physical Society, p. 060901. DOI: 10.1103/PhysRevE.99.060901. URL: https://link.aps.org/doi/10.1103/PhysRevE.99.060901 (visited on 05/28/2023).

[18] Apurba Biswas et al. “Mpemba effect in driven granular Maxwell gases”. In: *Physical Review E* 102.1 (July 2020). Publisher: American Physical Society, p. 012906. DOI: 10.1103/PhysRevE.102.012906. URL: https://link.aps.org/doi/10.1103/PhysRevE.102.012906 (visited on 05/28/2023).

[19] Tim Keller et al. “Quenches across the self-organization transition in multimode cavities”. en. In: *New Journal of Physics* 20.2 (Feb. 2018). Publisher: IOP Publishing, p. 025004. ISSN: 1367-2630. DOI: 10.1088/1367-2630/aaa161. URL: https://dx.doi.org/10.1088/1367-2630/aaa161 (visited on 05/28/2023).

[20] Andrea Nava and Michele Fabrizio. “Lindblad dissipative dynamics in the presence of phase coexistence”. In: *Physical Review B* 100.12 (Sept. 2019). Publisher: American Physical Society, p. 125102. DOI: 10.1103/PhysRevB.100.125102. URL: https://link.aps.org/doi/10.1103/PhysRevB.100.125102 (visited on 05/28/2023).

[21] Simon Kochsiek, Federico Carollo, and Igor Lesanovsky. “Accelerating the approach of dissipative quantum spin systems towards stationarity through global spin rotations”. In: *Physical Review A* 106.1 (July 2022). Publisher: American Physical Society, p. 012207. DOI: 10.1103/PhysRevA.106.012207. URL: https://link.aps.org/doi/10.1103/PhysRevA.106.012207 (visited on 05/28/2023).

[22] Federico Carollo, Antonio Lasanta, and Igor Lesanovsky. "Exponentially Accelerated Approach to Stationarity in Markovian Open Quantum Systems through the Mpemba Effect". In: *Physical Review Letters* 127.6 (Aug. 2021). Publisher: American Physical Society, p. 060401. DOI: 10.1103/PhysRevLett.127.060401. URL: https://link.aps.org/doi/10.1103/PhysRevLett.127.060401 (visited on 06/02/2023).

[23] Andrés Santos and Antonio Prados. "Mpemba effect in molecular gases under nonlinear drag". In: *Physics of Fluids* 32.7 (July 2020), p. 072010. ISSN: 1070-6631. DOI: 10.1063/5.0016243. URL: https://doi.org/10.1063/5.0016243 (visited on 08/26/2023).

[24] Alberto Megías, Andrés Santos, and Antonio Prados. "Thermal versus entropic Mpemba effect in molecular gases with nonlinear drag". In: *Physical Review E* 105.5 (May 2022). Publisher: American Physical Society, p. 054140. DOI: 10.1103/PhysRevE.105.054140. URL: https://link.aps.org/doi/10.1103/PhysRevE.105.054140 (visited on 08/26/2023).

[25] Zhiyue Lu and Oren Raz. "Nonequilibrium thermodynamics of the Markovian Mpemba effect and its inverse". en. In: *Proceedings of the National Academy of Sciences* 114.20 (May 2017), pp. 5083–5088. ISSN: 0027-8424, 1091-6490. DOI: 10.1073/pnas.1701264114. URL: https://pnas.org/doi/full/10.1073/pnas.1701264114 (visited on 03/16/2023).

[26] Israel Klich et al. "Mpemba Index and Anomalous Relaxation". In: *Physical Review X* 9.2 (June 2019). Publisher: American Physical Society, p. 021060. DOI: 10.1103/PhysRevX.9.021060. URL: https://link.aps.org/doi/10.1103/PhysRevX.9.021060 (visited on 03/16/2023).

[27] Gianluca Teza, Ran Yaacoby, and Oren Raz. *Relaxation shortcuts through boundary coupling*. arXiv:2112.10187 [cond-mat]. Dec. 2021. DOI: 10.48550/arXiv.2112.10187. URL: http://arxiv.org/abs/2112.10187 (visited on 05/28/2023).

[28] Gianluca Teza, Ran Yaacoby, and Oren Raz. *Far from equilibrium relaxation in the weak coupling limit*. arXiv:2203.11644 [cond-mat]. Mar. 2022. DOI: 10.48550/arXiv.2203.11644. URL: http://arxiv.org/abs/2203.11644 (visited on 05/28/2023).

[29] Gianluca Teza, Ran Yaacoby, and Oren Raz. "Eigenvalue Crossing as a Phase Transition in Relaxation Dynamics". In: *Physical Review Letters* 130.20 (May 2023). Publisher: American Physical Society, p. 207103. DOI: 10.1103/PhysRevLett.130.207103. URL: https://link.aps.org/doi/10.1103/PhysRevLett.130.207103 (visited on 05/28/2023).

[30] Matthew R. Walker and Marija Vucelja. "Anomalous thermal relaxation of Langevin particles in a piecewise-constant potential". en. In: *Journal of Statistical Mechanics: Theory and Experiment* 2021.11 (Nov. 2021). Publisher: IOP Publishing and SISSA, p. 113105. ISSN: 1742-5468. DOI: 10.1088/1742-5468/ac2edc. URL: https://dx.doi.org/10.1088/1742-5468/ac2edc (visited on 05/28/2023).

[31] Daniel Maria Busiello, Deepak Gupta, and Amos Maritan. "Inducing and optimizing Markovian Mpemba effect with stochastic reset". en. In: *New Journal of Physics* 23.10 (Oct. 2021). Publisher: IOP Publishing, p. 103012. ISSN: 1367-2630. DOI: 10.1088/1367-2630/ac2922. URL: https://dx.doi.org/10.1088/1367-2630/ac2922 (visited on 05/28/2023).

[32] Julius Degünther and Udo Seifert. "Anomalous relaxation from a non-equilibrium steady state: An isothermal analog of the Mpemba effect". en. In: *Europhysics Letters* 139.4 (Aug. 2022). Publisher: EDP Sciences, IOP Publishing and Società Italiana di Fisica, p. 41002. ISSN: 0295-5075. DOI: 10.1209/0295-5075/ac8573. URL: https://dx.doi.org/10.1209/0295-5075/ac8573 (visited on 05/28/2023).

[33] Jie Lin et al. "Power statistics of Otto heat engines with the Mpemba effect". In: *Physical Review E* 105.1 (Jan. 2022). Publisher: American Physical Society, p. 014104. DOI: 10.1103/PhysRevE.105.014104. URL: https://link.aps.org/doi/10.1103/PhysRevE.105.014104 (visited on 05/28/2023).

[34] Roi Holtzman and Oren Raz. "Landau theory for the Mpemba effect through phase transitions". en. In: *Communications Physics* 5.1 (Nov. 2022). Number: 1 Publisher: Nature Publishing Group, pp. 1–9. ISSN: 2399-3650. DOI: 10.1038/s42005-022-01063-2. URL: https://www.nature.com/articles/s42005-022-01063-2 (visited on 05/28/2023).

[35] Edna Ullmann-Margalit. *The Kaleidoscope of Science: The Israel Colloquium: Studies in History, Philosophy, and Sociology of Science Volume 1*. Vol. 94. Springer Science & Business Media, 2012.

[36] J. Zinn-Justin. *Quantum Field Theory and Critical Phenomena*. Oxford Science Publications, 1989.

[37] Hannes Risken. *The Fokker-Planck Equation: Methods of Solution and Applications*. en. Ed. by Hermann Haken. Vol. 18. Springer Series in Synergetics. Berlin, Heidelberg: Springer, 1996. ISBN: 978-3-540-61530-9 978-3-642-61544-3. DOI: 10.1007/978-3-642-61544-3. URL: https://link.springer.com/10.1007/978-3-642-61544-3 (visited on 05/28/2023).

[38] Crispin Gardiner. *Stochastic Methods - A Handbook for the Natural and Social Sciences*. Fourth Edition. Springer-Verlag Berlin Heidelberg, 2009.

[39] H. A. Kramers. "Brownian motion in a field of force and the diffusion model of chemical reactions". en. In: *Physica* 7.4 (Apr. 1940), pp. 284–304. ISSN: 0031-8914. DOI: 10.1016/S0031-8914(40)90098-2. URL: https://www.sciencedirect.com/science/article/pii/S0031891440900982 (visited on 05/28/2023).

[40] van Kampen N. G. *Stochastic processes in physics and chemistry*. Elsevier, 2001.

[41] A. Engel. "Asymptotics of work distributions in nonequilibrium systems". In: *PRE* 80 (2009), p. 021120.

[42] Thomas Speck, Jakob Mehl, and Udo Seifert. "Role of External Flow and Frame Invariance in Stochastic Thermodynamics". In: *Phys. Rev. Lett.* 100 (2008), p. 178302.

[43] R. B. Bird et al. *Dynamics of polymeric liquids., Fluid Mechanics Vol. 2*. New York: Willey, 1987.

[44] M. Mörsch, H. Risken, and H. D. Vollmer. "One-dimensional diffusion in soluble model potentials". In: *Zeitschrift fur Physik B Condensed Matter* 32.2 (June 1979), pp. 245–252. DOI: 10.1007/BF01320120.

[45] Avinash Kumar. "Anomalous relaxation in colloidal systems". PhD thesis. SFU, 2021.

[46] V. I. Mel'nikov. "The Kramers problem: Fifty years of development". en. In: *Physics Reports* 209.1 (Dec. 1991), pp. 1–71. ISSN: 0370-1573. DOI: 10.1016/

0370-1573(91)90108-X. URL: https://www.sciencedirect.com/science/article/pii/037015739190108X (visited on 05/28/2023).

[47] J. S. Langer. "Statistical theory of the decay of metastable states". en. In: *Annals of Physics* 54.2 (Sept. 1969), pp. 258–275. ISSN: 0003-4916. DOI: 10.1016/0003-4916(69)90153-5. URL: https://www.sciencedirect.com/science/article/pii/0003491669901535 (visited on 05/28/2023).

[48] Frank Moss and P. V. E. McClintock. *Noise in Nonlinear Dynamical Systems*. New York: Cambridge University Press, 1988.

[49] LS Pontryagin, AA Andronov, and AA Vitt. "On statistical analysis of dynamical systems". In: *Zh. Eksp. Teor. Fiz.* 3.3 (1933), pp. 165–180.

[50] Robert Zwanzig. *Nonequilibrium Statistical Mechanics*. Oxford, New York: Oxford University Press, Apr. 2001. ISBN: 978-0-19-514018-7.

[51] Benedict Leimkuhler and Charles Matthews. "Robust and efficient configurational molecular sampling via Langevin dynamics". In: *The Journal of Chemical Physics* 138.17 (May 2013), p. 174102. ISSN: 0021-9606. DOI: 10.1063/1.4802990. URL: https://doi.org/10.1063/1.4802990.

[52] Gaspard Monge. *Mémoire sur la théorie des déblais et des remblais*. De l'Imprimerie Royale, 1781.

[53] Leonid V Kantorovich. "On the translocation of masses". In: *Dokl. Akad. Nauk. USSR (NS)*. Vol. 37. 1942, pp. 199–201.

[54] Cédric Villani. *Optimal Transport*. Ed. by M. Berger et al. Vol. 338. Grundlehren der mathematischen Wissenschaften. Berlin, Heidelberg: Springer, 2009. ISBN: 978-3-540-71049-3 978-3-540-71050-9. DOI: 10.1007/978-3-540-71050-9.

URL: http://link.springer.com/10.1007/978-3-540-71050-9 (visited on 07/12/2023).

[55] Soheil Kolouri et al. "Optimal Mass Transport: Signal processing and machine-learning applications". In: *IEEE Signal Processing Magazine* 34.4 (July 2017). Conference Name: IEEE Signal Processing Magazine, pp. 43–59. ISSN: 1558-0792. DOI: 10.1109/MSP.2017.2695801.

[56] Geoffrey Schiebinger et al. "Optimal-Transport Analysis of Single-Cell Gene Expression Identifies Developmental Trajectories in Reprogramming". en. In: *Cell* 176.4 (Feb. 2019), 928–943.e22. ISSN: 0092-8674. DOI: 10.1016/j.cell.2019.01.006. URL: https://www.sciencedirect.com/science/article/pii/S009286741930039X (visited on 07/05/2023).

[57] Patrice Koehl, Marc Delarue, and Henri Orland. "Statistical Physics Approach to the Optimal Transport Problem". In: *Physical Review Letters* 123.4 (July 2019). Publisher: American Physical Society, p. 040603. DOI: 10.1103/PhysRevLett.123.040603. URL: https://link.aps.org/doi/10.1103/PhysRevLett.123.040603 (visited on 07/05/2023).

[58] Gao Huang et al. "Supervised Word Mover' s Distance". In: *Advances in Neural Information Processing Systems*. Ed. by D. Lee et al. Vol. 29. Curran Associates, Inc., 2016. URL: https://proceedings.neurips.cc/paper_files/paper/2016/file/10c66082c124f8afe3df4886f5e516e0-Paper.pdf.

[59] Steven Haker et al. "Optimal Mass Transport for Registration and Warping". en. In: *International Journal of Computer Vision* 60.3 (Dec. 2004), pp. 225–240. ISSN: 1573-1405. DOI: 10.1023/B:VISI.0000036836.66311.97. URL: https://doi.org/10.1023/B:VISI.0000036836.66311.97 (visited on 07/05/2023).

[60] Shriram Chennakesavalu and Grant M. Rotskoff. "Unified, Geometric Framework for Nonequilibrium Protocol Optimization". In: *Physical Review Letters* 130.10 (Mar. 2023). Publisher: American Physical Society, p. 107101. DOI: 10.1103/PhysRevLett.130.107101. URL: https://link.aps.org/doi/10.1103/PhysRevLett.130.107101 (visited on 06/23/2023).

[61] Tan Van Vu and Keiji Saito. "Thermodynamic Unification of Optimal Transport: Thermodynamic Uncertainty Relation, Minimum Dissipation, and Thermodynamic Speed Limits". In: *Physical Review X* 13.1 (Feb. 2023). Publisher: American Physical Society, p. 011013. DOI: 10.1103/PhysRevX.13.011013. URL: https://link.aps.org/doi/10.1103/PhysRevX.13.011013 (visited on 05/31/2023).

[62] Tan Van Vu and Keiji Saito. "Topological Speed Limit". In: *Physical Review Letters* 130.1 (Jan. 2023). Publisher: American Physical Society, p. 010402. DOI: 10.1103/PhysRevLett.130.010402. URL: https://link.aps.org/doi/10.1103/PhysRevLett.130.010402 (visited on 05/31/2023).

[63] Udo Seifert. "Stochastic thermodynamics, fluctuation theorems and molecular machines". en. In: *Reports on Progress in Physics* 75.12 (Nov. 2012). Publisher: IOP Publishing, p. 126001. ISSN: 0034-4885. DOI: 10.1088/0034-4885/75/12/126001. URL: https://dx.doi.org/10.1088/0034-4885/75/12/126001 (visited on 07/02/2023).

[64] P. Alex Greaney et al. "Mpemba-Like Behavior in Carbon Nanotube Resonators". en. In: *Metallurgical and Materials Transactions A* 42.13 (Dec. 2011), pp. 3907–3912. ISSN: 1543-1940. DOI: 10.1007/s11661-011-0843-4. URL: https://doi.org/10.1007/s11661-011-0843-4 (visited on 06/28/2023).

[65] Jaehyeok Jin and William A. III Goddard. "Mechanisms Underlying the Mpemba Effect in Water from Molecular Dynamics Simulations". In: *The Journal of Physical Chemistry C* 119.5 (Feb. 2015). Publisher: American Chemical Society, pp. 2622–2629. ISSN: 1932-7447. DOI: 10.1021/jp511752n. URL: https://doi.org/10.1021/jp511752n (visited on 06/28/2023).

[66] A. Gal and O. Raz. "Precooling Strategy Allows Exponentially Faster Heating". In: *Physical Review Letters* 124.6 (Feb. 2020). Publisher: American Physical Society, p. 060602. DOI: 10.1103/PhysRevLett.124.060602. URL: https://link.aps.org/doi/10.1103/PhysRevLett.124.060602 (visited on 06/28/2023).

[67] Matthew R. Walker and Marija Vucelja. *Mpemba effect in terms of mean first passage time*. arXiv:2212.07496 [cond-mat]. May 2023. DOI: 10.48550/arXiv.2212.07496. URL: http://arxiv.org/abs/2212.07496 (visited on 07/05/2023).

[68] Raphaël Chétrite, Avinash Kumar, and John Bechhoefer. "The Metastable Mpemba Effect Corresponds to a Non-monotonic Temperature Dependence of Extractable Work". In: *Frontiers in Physics* 9 (2021). ISSN: 2296-424X. URL: https://www.frontiersin.org/articles/10.3389/fphy.2021.654271 (visited on 06/18/2023).

[69] Apurba Biswas, R. Rajesh, and Arnab Pal. "Mpemba effect in a Langevin system: Population statistics, metastability, and other exact results". In: *The Journal of Chemical Physics* 159.4 (July 2023), p. 044120. ISSN: 0021-9606. DOI: 10.1063/5.0155855. URL: https://doi.org/10.1063/5.0155855 (visited on 08/03/2023).

[70] Amit Kumar Chatterjee, Satoshi Takada, and Hisao Hayakawa. *Quantum Mpemba effect in a quantum dot with reservoirs*. arXiv:2304.02411 [cond-mat, physics:quant-ph]. Apr. 2023. DOI: 10.48550/arXiv.2304.02411. URL: http://arxiv.org/abs/2304.02411 (visited on 06/02/2023).

[71] Filiberto Ares, Sara Murciano, and Pasquale Calabrese. "Entanglement asymmetry as a probe of symmetry breaking". en. In: *Nature Communications* 14.1 (Apr. 2023). Number: 1 Publisher: Nature Publishing Group, p. 2036. ISSN: 2041-1723. DOI: 10.1038/s41467-023-37747-8. URL: https://www.nature.com/articles/s41467-023-37747-8 (visited on 07/27/2023).

[72] Saikat Bera, Matthew R. Walker, and Marija Vucelja. *Effect of dynamics on anomalous thermal relaxations and information exchange*. 2023. arXiv: 2308.04557 [cond-mat.stat-mech]. URL: https://arxiv.org/abs/2308.04557.

[73] Jason W. Rocks, Andrea J. Liu, and Eleni Katifori. "Hidden Topological Structure of Flow Network Functionality". In: *Physical Review Letters* 126.2 (Jan. 2021). Publisher: American Physical Society, p. 028102. DOI: 10.1103/PhysRevLett.126.028102. URL: https://link.aps.org/doi/10.1103/PhysRevLett.126.028102 (visited on 07/28/2023).

[74] Georgios Gounaris and Eleni Katifori. "Braess's Paradox Analog in Physical Networks of Optimal Exploration". In: *Phys. Rev. Lett.* 133 (6 Aug. 2024), p. 067401. DOI: 10.1103/PhysRevLett.133.067401. URL: https://link.aps.org/doi/10.1103/PhysRevLett.133.067401.

[75] Jean-David Benamou and Yann Brenier. "A computational fluid mechanics solution to the Monge-Kantorovich mass transfer problem". en. In: *Numerische Mathematik* 84.3 (Jan. 2000), pp. 375–393. ISSN: 0945-3245. DOI: 10.1007/

s002110050002. URL: https://doi.org/10.1007/s002110050002 (visited on 07/04/2023).

[76] Erik Aurell, Carlos Mejía-Monasterio, and Paolo Muratore-Ginanneschi. "Optimal Protocols and Optimal Transport in Stochastic Thermodynamics". In: *Physical Review Letters* 106.25 (June 2011). Publisher: American Physical Society, p. 250601. DOI: 10.1103/PhysRevLett.106.250601. URL: https://link.aps.org/doi/10.1103/PhysRevLett.106.250601 (visited on 07/12/2023).

[77] Erik Aurell et al. "Refined Second Law of Thermodynamics for Fast Random Processes". en. In: *Journal of Statistical Physics* 147.3 (May 2012), pp. 487–505. ISSN: 1572-9613. DOI: 10.1007/s10955-012-0478-x. URL: https://doi.org/10.1007/s10955-012-0478-x (visited on 07/05/2023).

[78] Jordan M Horowitz and Todd R Gingrich. "Thermodynamic uncertainty relations constrain non-equilibrium fluctuations". In: *Nature Physics* 16.1 (2020), pp. 15–20.

[79] S. Kullback and R. A. Leibler. "On Information and Sufficiency". In: *The Annals of Mathematical Statistics* 22.1 (Mar. 1951). Publisher: Institute of Mathematical Statistics, pp. 79–86. ISSN: 0003-4851, 2168-8990. DOI: 10.1214/aoms/1177729694. URL: https://projecteuclid.org/journals/annals-of-mathematical-statistics/volume-22/issue-1/On-Information-and-Sufficiency/10.1214/aoms/1177729694.full (visited on 07/06/2023).

[80] N. G. Van kampen. "Chapter III - STOCHASTIC PROCESSES". en. In: *Stochastic Processes in Physics and Chemistry (Third Edition)*. Ed. by N. G. Van kampen. North-Holland Personal Library. Amsterdam: Elsevier, Jan. 2007, pp. 52–72. DOI: 10.1016/B978-044452965-7/50006-4. URL: https://www.

sciencedirect.com/science/article/pii/B9780444529657500064 (visited on 07/09/2023).

[81] Peter Hänggi and Harry Thomas. "Stochastic processes: Time evolution, symmetries and linear response". en. In: *Physics Reports* 88.4 (Aug. 1982), pp. 207–319. ISSN: 0370-1573. DOI: 10.1016/0370-1573(82)90045-X. URL: https://www.sciencedirect.com/science/article/pii/037015738290045X (visited on 07/09/2023).

[82] Anatoly B. Kolomeisky and Michael E. Fisher. "Molecular Motors: A Theorist's Perspective". In: *Annual Review of Physical Chemistry* 58.1 (2007). _eprint: https://doi.org/10.1146/annurev.physchem.58.032806.104532, pp. 675–695. DOI: 10.1146/annurev.physchem.58.032806.104532. URL: https://doi.org/10.1146/annurev.physchem.58.032806.104532 (visited on 07/03/2023).

[83] A. W. C. Lau, D. Lacoste, and K. Mallick. "Nonequilibrium Fluctuations and Mechanochemical Couplings of a Molecular Motor". In: *Physical Review Letters* 99.15 (Oct. 2007). Publisher: American Physical Society, p. 158102. DOI: 10.1103/PhysRevLett.99.158102. URL: https://link.aps.org/doi/10.1103/PhysRevLett.99.158102 (visited on 07/03/2023).

[84] Anatoly B. Kolomeisky. "Motor proteins and molecular motors: how to operate machines at the nanoscale". en. In: *Journal of Physics: Condensed Matter* 25.46 (Oct. 2013). Publisher: IOP Publishing, p. 463101. ISSN: 0953-8984. DOI: 10.1088/0953-8984/25/46/463101. URL: https://dx.doi.org/10.1088/0953-8984/25/46/463101 (visited on 07/03/2023).

[85] Gianluca Teza et al. "Rate dependence of current and fluctuations in jump models with negative differential mobility". en. In: *Physica A: Statistical Me-*

*chanics and its Applications*. Tributes of Non-equilibrium Statistical Physics 552 (Aug. 2020), p. 123176. ISSN: 0378-4371. DOI: 10.1016/j.physa.2019.123176. URL: https://www.sciencedirect.com/science/article/pii/S037843711931787X (visited on 06/29/2023).

[86] Benedikt Remlein and Udo Seifert. "Optimality of nonconservative driving for finite-time processes with discrete states". In: *Physical Review E* 103.5 (May 2021). Publisher: American Physical Society, p. L050105. DOI: 10.1103/PhysRevE.103.L050105. URL: https://link.aps.org/doi/10.1103/PhysRevE.103.L050105 (visited on 06/28/2023).

[87] Daniel T. Gillespie. "Exact stochastic simulation of coupled chemical reactions". In: *The Journal of Physical Chemistry* 81.25 (Dec. 1977). Publisher: American Chemical Society, pp. 2340–2361. ISSN: 0022-3654. DOI: 10.1021/j100540a008. URL: https://doi.org/10.1021/j100540a008.

[88] Tim Schmiedl and Udo Seifert. "Stochastic thermodynamics of chemical reaction networks". In: *The Journal of Chemical Physics* 126.4 (Jan. 2007). Publisher: American Institute of Physics, p. 044101. ISSN: 0021-9606. DOI: 10.1063/1.2428297. URL: https://aip.scitation.org/doi/10.1063/1.2428297 (visited on 01/26/2023).

[89] William J. Heuett and Hong Qian. "Grand canonical Markov model: A stochastic theory for open nonequilibrium biochemical networks". In: *The Journal of Chemical Physics* 124.4 (Jan. 2006), p. 044110. ISSN: 0021-9606. DOI: 10.1063/1.2165193. URL: https://doi.org/10.1063/1.2165193 (visited on 07/30/2023).

[90] Robert B. Griffiths, Chi-Yuan Weng, and James S. Langer. "Relaxation Times for Metastable States in the Mean-Field Model of a Ferromagnet". In: *Physical*

*Review* 149.1 (Sept. 1966). Publisher: American Physical Society, pp. 301–305. DOI: 10.1103/PhysRev.149.301. URL: https://link.aps.org/doi/10.1103/PhysRev.149.301 (visited on 08/04/2023).

[91] M. Kimura. "A simple method for estimating evolutionary rates of base substitutions through comparative studies of nucleotide sequences". In: *Journal of Molecular Evolution* 16.2 (Dec. 1980), pp. 111–120. ISSN: 0022-2844. DOI: 10.1007/BF01731581.

[92] Hong Qian and Hao Ge. *Stochastic Chemical Reaction Systems in Biology*. Lecture Notes on Mathematical Modelling in the Life Sciences. Cham: Springer International Publishing, 2021. ISBN: 978-3-030-86251-0 978-3-030-86252-7. DOI: 10.1007/978-3-030-86252-7. URL: https://link.springer.com/10.1007/978-3-030-86252-7 (visited on 07/30/2023).

[93] N.G. VAN KAMPEN. "Chapter IV - MARKOV PROCESSES". In: *Stochastic Processes in Physics and Chemistry (Third Edition)*. Ed. by N.G. VAN KAMPEN. Amsterdam: Elsevier, Jan. 2007, pp. 73–95. ISBN: 09255818. DOI: 10.1016/B978-044452965-7/50007-6. URL: https://www.sciencedirect.com/science/article/pii/B9780444529657500076.

[94] Christopher M. Turner, Richard Startz, and Charles R. Nelson. "A Markov model of heteroskedasticity, risk, and learning in the stock market". In: *Journal of Financial Economics* 25.1 (Nov. 1989), pp. 3–22. ISSN: 0304-405X. DOI: 10.1016/0304-405X(89)90094-9. URL: https://www.sciencedirect.com/science/article/pii/0304405X89900949 (visited on 08/04/2023).

[95] Henrik Madsen, Henrik Spliid, and Poul Thyregod. "Markov Models in Discrete and Continuous Time for Hourly Observations of Cloud Cover". In: *Journal of Climate and Applied Meteorology* 24.7 (1985). Publisher: American

Meteorological Society, pp. 629–639. ISSN: 07333021, 21635366. URL: http://www.jstor.org/stable/26181203 (visited on 08/04/2023).

[96] Burton Singer and Seymour Spilerman. "The Representation of Social Processes by Markov Models". In: *American Journal of Sociology* 82.1 (1976). Publisher: University of Chicago Press, pp. 1–54. ISSN: 0002-9602. URL: https://www.jstor.org/stable/2777460 (visited on 08/04/2023).

[97] Zhongmin Zhang and Zhiyue Lu. *Non-equilibrium Theoretical Framework and Universal Design Principles of Oscillation-Driven Catalysis*. arXiv:2303.14551 [cond-mat]. June 2023. DOI: 10.48550/arXiv.2303.14551. URL: http://arxiv.org/abs/2303.14551 (visited on 08/04/2023).

[98] Marieke Schor et al. "Shedding Light on the Dock–Lock Mechanism in Amyloid Fibril Growth Using Markov State Models". In: *The Journal of Physical Chemistry Letters* 6.6 (Mar. 2015). Publisher: American Chemical Society, pp. 1076–1081. DOI: 10.1021/acs.jpclett.5b00330. URL: https://doi.org/10.1021/acs.jpclett.5b00330 (visited on 08/08/2023).

[99] Roy J. Glauber. "Time-Dependent Statistics of the Ising Model". In: *Journal of Mathematical Physics* 4.2 (Feb. 1963), pp. 294–307. ISSN: 0022-2488. DOI: 10.1063/1.1703954. URL: https://doi.org/10.1063/1.1703954 (visited on 07/18/2023).

[100] L. Szilard. "über die Entropieverminderung in einem thermodynamischen System bei Eingriffen intelligenter Wesen". In: *Zeitschrift für Physik* 53.11 (Nov. 1929), pp. 840–856. ISSN: 0044-3328. DOI: 10.1007/BF01341281. URL: https://doi.org/10.1007/BF01341281 (visited on 08/08/2023).

[101] Massimiliano Esposito. "Stochastic thermodynamics under coarse graining". In: *Physical Review E* 85.4 (Apr. 2012). Publisher: American Physical Society,

p. 041125. DOI: 10.1103/PhysRevE.85.041125. URL: https://link.aps.org/doi/10.1103/PhysRevE.85.041125 (visited on 08/08/2023).

[102] F. J. Cao and M. Feito. "Thermodynamics of feedback controlled systems". In: *Physical Review E* 79.4 (Apr. 2009). Publisher: American Physical Society, p. 041118. DOI: 10.1103/PhysRevE.79.041118. URL: https://link.aps.org/doi/10.1103/PhysRevE.79.041118 (visited on 08/08/2023).

[103] Takahiro Sagawa and Masahito Ueda. "Generalized Jarzynski Equality under Nonequilibrium Feedback Control". In: *Physical Review Letters* 104.9 (Mar. 2010). Publisher: American Physical Society, p. 090602. DOI: 10.1103/PhysRevLett.104.090602. URL: https://link.aps.org/doi/10.1103/PhysRevLett.104.090602 (visited on 08/08/2023).

[104] Sebastian Deffner and Christopher Jarzynski. "Information Processing and the Second Law of Thermodynamics: An Inclusive, Hamiltonian Approach". In: *Physical Review X* 3.4 (Oct. 2013). Publisher: American Physical Society, p. 041003. DOI: 10.1103/PhysRevX.3.041003. URL: https://link.aps.org/doi/10.1103/PhysRevX.3.041003 (visited on 08/08/2023).

[105] Jordan M. Horowitz and Juan M. R. Parrondo. "Thermodynamic reversibility in feedback processes". In: *Europhysics Letters* 95.1 (June 2011), p. 10005. ISSN: 0295-5075. DOI: 10.1209/0295-5075/95/10005. URL: https://dx.doi.org/10.1209/0295-5075/95/10005 (visited on 08/08/2023).

[106] David Andrieux and Pierre Gaspard. "Nonequilibrium generation of information in copolymerization processes". In: *Proceedings of the National Academy of Sciences* 105.28 (July 2008). Publisher: Proceedings of the National Academy of Sciences, pp. 9516–9521. DOI: 10.1073/pnas.0802049105. URL: https://www.pnas.org/doi/10.1073/pnas.0802049105 (visited on 08/08/2023).

[107] Massimo Bilancioni, Massimiliano Esposito, and Nahuel Freitas. *A chemical reaction network implementation of a Maxwell demon*. arXiv:2307.14994 [cond-mat]. Aug. 2023. DOI: 10.48550/arXiv.2307.14994. URL: http://arxiv.org/abs/2307.14994 (visited on 08/04/2023).

[108] A. C. Barato and U. Seifert. "An autonomous and reversible Maxwell's demon". In: *Europhysics Letters* 101.6 (Mar. 2013). Publisher: EDP Sciences, IOP Publishing and Società Italiana di Fisica, p. 60001. ISSN: 0295-5075. DOI: 10.1209/0295-5075/101/60001. URL: https://dx.doi.org/10.1209/0295-5075/101/60001 (visited on 08/08/2023).

[109] Dibyendu Mandal and Christopher Jarzynski. "Work and information processing in a solvable model of Maxwell's demon". In: *Proceedings of the National Academy of Sciences* 109.29 (July 2012). Publisher: Proceedings of the National Academy of Sciences, pp. 11641–11645. DOI: 10.1073/pnas.1204263109. URL: https://www.pnas.org/doi/10.1073/pnas.1204263109 (visited on 08/05/2023).

[110] J. Hoppenau and A. Engel. "On the energetics of information exchange". In: *Europhysics Letters* 105.5 (Mar. 2014). Publisher: EDP Sciences, IOP Publishing and Società Italiana di Fisica, p. 50002. ISSN: 0295-5075. DOI: 10.1209/0295-5075/105/50002. URL: https://dx.doi.org/10.1209/0295-5075/105/50002 (visited on 06/28/2023).

[111] Suriyanarayanan Vaikuntanathan and Christopher Jarzynski. "Modeling Maxwell's demon with a microcanonical Szilard engine". In: *Physical Review E* 83.6 (June 2011). Publisher: American Physical Society, p. 061120. DOI: 10.1103/PhysRevE.83.061120. URL: https://link.aps.org/doi/10.1103/PhysRevE.83.061120 (visited on 08/08/2023).

[112] Dibyendu Mandal and Christopher Jarzynski. "A proof by graphical construction of the no-pumping theorem of stochastic pumps". In: *Journal of Statistical Mechanics: Theory and Experiment* 2011.10 (Oct. 2011), P10006. ISSN: 1742-5468. DOI: 10.1088/1742-5468/2011/10/P10006. URL: https://dx.doi.org/10.1088/1742-5468/2011/10/P10006 (visited on 07/18/2023).

[113] Gianluca Teza, Ran Yaacoby, and Oren Raz. *Eigenvalue crossing as a phase transition in relaxation dynamics*. arXiv:2209.09307 [cond-mat]. Sept. 2022. DOI: 10.48550/arXiv.2209.09307. URL: http://arxiv.org/abs/2209.09307 (visited on 02/18/2023).

[114] Matthew R. Walker, Saikat Bera, and Marija Vucelja. *Optimal transport and anomalous thermal relaxations*. arXiv:2307.16103 [cond-mat]. July 2023. DOI: 10.48550/arXiv.2307.16103. URL: http://arxiv.org/abs/2307.16103 (visited on 08/02/2023).

[115] James Clerk Maxwell. *Theory of heat*. 1st ed. Longmans, London, 1871.

[116] R. Landauer. "Irreversibility and Heat Generation in the Computing Process". In: *IBM Journal of Research and Development* 5.3 (July 1961). Conference Name: IBM Journal of Research and Development, pp. 183–191. ISSN: 0018-8646. DOI: 10.1147/rd.53.0183.

[117] Charles H. Bennett. "The thermodynamics of computation—a review". In: *International Journal of Theoretical Physics* 21.12 (Dec. 1982), pp. 905–940. ISSN: 1572-9575. DOI: 10.1007/BF02084158. URL: https://doi.org/10.1007/BF02084158 (visited on 08/05/2023).

[118] Charles H. Bennett and Rolf Landauer. "The Fundamental Physical Limits of Computation". In: *Scientific American* 253.1 (1985). Publisher: Scientific

American, a division of Nature America, Inc., pp. 48–57. ISSN: 0036-8733. URL: https://www.jstor.org/stable/24967723 (visited on 08/08/2023).

[119] Zhiyu Cao et al. "Fast Functionalization with High Performance in the Autonomous Information Engine". In: *The Journal of Physical Chemistry Letters* 14.1 (2023). _eprint: https://doi.org/10.1021/acs.jpclett.2c03335, pp. 66–72. DOI: 10.1021/acs.jpclett.2c03335. URL: https://doi.org/10.1021/acs.jpclett.2c03335.

[120] Martin R. Evans and Satya N. Majumdar. "Diffusion with Stochastic Resetting". In: *Physical Review Letters* 106.16 (Apr. 2011). Publisher: American Physical Society, p. 160601. DOI: 10.1103/PhysRevLett.106.160601. URL: https://link.aps.org/doi/10.1103/PhysRevLett.106.160601 (visited on 08/05/2023).

[121] Ruicheng Bao et al. *Designing Autonomous Maxwell Demon via Stochastic Resetting*. arXiv:2209.11419 [cond-mat]. Sept. 2022. DOI: 10.48550/arXiv.2209.11419. URL: http://arxiv.org/abs/2209.11419 (visited on 05/19/2023).

[122] U. Fano. "Ionization Yield of Radiations. II. The Fluctuations of the Number of Ions". In: *Physical Review* 72.1 (July 1947). Publisher: American Physical Society, pp. 26–29. DOI: 10.1103/PhysRev.72.26. URL: https://link.aps.org/doi/10.1103/PhysRev.72.26 (visited on 08/08/2023).

[123] D. J. Griffiths and D. F. Schroeter. *Introduction to Quantum Mechanics*. Ed. by third edition. Cambridge University Press, 2018.

[124] Oren Raz. "private communication". In: (2018).

[125] J. Schnakenberg. "Network theory of microscopic and macroscopic behavior of master equation systems". In: *Reviews of Modern Physics* 48.4 (Oct.

1976). Publisher: American Physical Society, pp. 571–585. DOI: 10.1103/RevModPhys.48.571. URL: https://link.aps.org/doi/10.1103/RevModPhys.48.571 (visited on 07/02/2023).

[126] Lars Onsager. "Reciprocal Relations in Irreversible Processes. I." In: *Physical Review* 37.4 (Feb. 1931). Publisher: American Physical Society, pp. 405–426. DOI: 10.1103/PhysRev.37.405. URL: https://link.aps.org/doi/10.1103/PhysRev.37.405 (visited on 07/03/2023).

[127] Lars Onsager. "Reciprocal Relations in Irreversible Processes. II." In: *Physical Review* 38.12 (Dec. 1931). Publisher: American Physical Society, pp. 2265–2279. DOI: 10.1103/PhysRev.38.2265. URL: https://link.aps.org/doi/10.1103/PhysRev.38.2265 (visited on 07/10/2023).

# Appendices

# Appendix A

# Supporting Information for chapter 2–Anomalous thermal relaxation of Langevin particles in a piecewise constant potential

### A.0.1 Symmetric potentials

For symmetric potentials, $V(x) = V(-x)$, the reflection operator, the operator that flips $\psi_\mu(x) \to \psi_\mu(-x)$, commutes with the Schrödinger operator $\mathcal{L}$. Thus each non-degenerate eigenvector of $\mathcal{L}$ must also be an eigenvector of the reflection operator, which implies that each eigenvector must be either even or odd under the reflection, see e.g. [123]. The ground state having no nodes must be even, and the first excited state having one node must be odd. In the case that $U$ is symmetric and $V$ is symmetric and the domain is symmetric, we have that $a_2(T) = 0$ for all $T$, as an integral of an odd function over a symmetric domain. Hence there is no Mpemba effect associated with $a_2$ in this case. The effect can be present at a higher order, i.e. for $a_\mu$ with $\mu > 2$ [45].

### A.0.2 Quadratic potential

For the quadratic potential $U(x) = kx^2/2$, the eigenvectors and eigenvalues are known. The case corresponds to the Ornstein-Ühlenbeck process, see e.g. [38], which is described by the following Fokker-Planck equation

$$\partial_t p(x,t) = \partial_x \left[kxp(x,t)\right] + \frac{D_b}{2}\partial_x^2 p(x,t) \tag{A.1}$$

where $D_b = 2k_B T_b$ is the diffusion coefficient. The left eigenfunctions $\varphi_n$ and corresponding eigenvalues are

$$\varphi_n = \left(2^n n!\right)^{-1/2} H_n\left[x\sqrt{\frac{k}{2k_B T_b}}\right], \quad \lambda_n = nk, \tag{A.2}$$

where $H_n$ are the Hermite polynomials. The stationary solution of the Fokker-Planck equation is

$$\pi(x|T_b) = \sqrt{\frac{k}{2\pi k_B T_b}} \exp\left[-\frac{kx^2}{2k_B T_b}\right], \tag{A.3}$$

and the general solution for the probability distribution is

$$p(x,t) = \sum_{n=0} \sqrt{\frac{k}{2\pi k_B T_b}} e^{-\frac{kx^2}{2k_B T_b}} \varphi_n(x) e^{-nkt} A_n, \tag{A.4}$$

with overlap coefficients $A_n \equiv \int_{-\infty}^{\infty} \varphi_n p(x,0)\, dx$. In the case of $p(x,0) = \pi(x|T)$ the coefficients $A_n$ can be found explicitly as

$$A_{2n}(T) = \sqrt{\frac{(2n)!}{2^{2n}}}\frac{1}{n!}\left(\frac{T}{T_b} - 1\right)^n, \; A_{2n+1}(T) = 0. \tag{A.5}$$

Note the overlap coefficients are $k$ independent. For finite temperatures, the coefficient $A_{2n}$ is zero only for $T = T_b$. Therefore there is no strong Mpemba effect for the Ornstein-Ühlenbeck process. Moreover, $(T/T_b - 1)^n$ is a monotonic function of $T$, thus there is no weak Mpemba effect either for the Ornstein-Ühlenbeck process.

The absence of the Mpemba effect is expected. Namely, starting from a Gaussian (Boltzmann distribution at temperature $T$) and evolving with a Gaussian kernel to get another Gaussian (Boltzmann distribution at temperature $T_b$), we are allowed to vary only the width of the Gaussian, there is no other variable to vary [124]. Thus with polynomial potentials and spatially uniform diffusion coefficients, to find a Mpemba effect, we need to go beyond a quadratic potential to polynomial of higher degree or other functions.

# Appendix B

# Supporting Information for chapter 3–Optimal transport and anomalous thermal relaxations

## B.1 Definitions

It is useful to define the following quantities. The entropy change after a state change from $y$ to $x$ is

$$s_{xy} = \ln \frac{R_{xy}}{R_{yx}} = \beta_b(E_y - E_x). \tag{B.1}$$

The frequency of jumps from $y$ to $x$ at $t$ is

$$a_{xy}(t) = R_{xy}p_y(t), \tag{B.2}$$

and the probability current from state $y$ to $x$ at $t$ is

$$j_{xy}(t) = R_{xy}p_y(t) - R_{yx}p_x(t). \tag{B.3}$$

The *dynamical activity* is the amplitude of the transitions between the states

$$a(t) = \sum_{\substack{x \neq y \\ x,y \in \Omega}} a_{xy}(t). \tag{B.4}$$

The average number of jumps during time $\tau$ is

$$\mathcal{A}(\tau) = \int_0^\tau a(t) dt. \tag{B.5}$$

The entropy of the system is the Shannon entropy

$$S(p) = -\sum_x p_x \ln p_x, \tag{B.6}$$

thus the change in the entropy of the system is

$$\Delta S_{\text{sys}} = S(p(\tau)) - S(p(0)). \tag{B.7}$$

The entropy change of the environment is

$$\Delta S_{\text{env}} = \int_0^\tau \sum_{\substack{x \neq y \\ x,y \in \Omega}} a_{xy}(t) s_{xy} \, dt. \tag{B.8}$$

By using Eqs. (B.1) and (B.2), it can be written in an explicit form as

$$\Delta S_{\text{env}} = \sum_{x \in \Omega} \beta_b E_x \left[ \pi_x^T - p_x(\tau) \right]. \tag{B.9}$$

The total entropy production is the sum of the change in the entropy of the environ-

ment and the change in the entropy of the system,

$$\Sigma(\tau) = \Delta S_{\text{env}} + \Delta S_{\text{sys}}. \tag{B.10}$$

Using Eqs. (B.6 - B.9), the total entropy production is explicitly

$$\begin{aligned} \Sigma(\tau) &= \sum_{x\in\Omega} \Big\{ \beta_b E_x \left[\pi_x^T - p_x(\tau)\right] \\ &\quad + \pi_x^T \ln \pi_x^T - p_x(\tau) \ln p_x(\tau) \Big\}. \end{aligned} \tag{B.11}$$

The entropy production rate, $\sigma(t) \equiv d\Sigma(t)/dt$, is

$$\sigma(t) = \sum_{\substack{x>y \\ x,y\in\Omega}} (a_{xy}(t) - a_{yx}(t)) \ln\left[\frac{a_{xy}(t)}{a_{yx}(t)}\right], \tag{B.12}$$

[125, 63]. Note that the entropy production rate is always non-negative, as $a_{xy} - a_{yx}$ and $\ln[a_{xy}/a_{yx}]$ always have matching signs.

Close to equilibrium for macroscopic systems, the currents depend on the thermodynamic forces in a linear fashion. The coefficients of this linear dependence are the Onsager coefficients [126, 127]. For microscopic systems far from equilibrium, one can define Onsager-like coefficients. The *generalized force* between transitions is

$$f_{xy}(t) = \ln \frac{a_{xy}(t)}{a_{yx}(t)}, \tag{B.13}$$

see e.g. [61]. The thermodynamic force is the sum of the entropy changes in the system and the environment. The ratio of the currents to the forces

$$m_{xy}(t) = \frac{j_{xy}(t)}{f_{xy}(t)} = \frac{a_{xy}(t) - a_{yx}(t)}{\ln a_{xy}(t) - \ln a_{yx}(t)}, \tag{B.14}$$

identifies the "linear response" coefficients, $m_{xy}$, which play the microscopic analogs of the Onsager coefficients, as the entropy production rate can be expressed as a quadratic form of generalized forces

$$\sigma(t) = \sum_{\substack{x>y \\ x,y\in\Omega}} m_{xy}(t) \left[f_{xy}(t)\right]^2 . \tag{B.15}$$

The sum linear response coefficients

$$m(t) = \sum_{\substack{x>y \\ x,y\in\Omega}} m_{xy}(t), \tag{B.16}$$

is the *dynamical state mobility*, while the *kinetic cost* is defined as

$$\mathcal{M}(\tau) = \int_0^\tau m(t)\, dt. \tag{B.17}$$

For the overdamped-Langevin dynamics, the dynamical mobility converges to a constant proportional to the diffusion coefficient, $m \propto T_b$, and thus, the kinetic cost linearly scales with time,

$$\mathcal{M}(\tau) \propto T_b\, \tau. \tag{B.18}$$

Other introduced quantities have straightforward analogs in the continuous case. Next, we discuss the optimal transport solutions for continuous and discrete classical cases.

# Appendix C

# Supporting Information for chapter 5– Effect of dynamics on anomalous thermal relaxations and information exchange

## C.1 Multiparticle picture

$$p_{\boldsymbol{n}}(t) = \frac{N!}{n_1!n_2!...n_M!}\prod_{i=1}^{M}\left[\rho_i^{T_b} + b_2(\boldsymbol{w}_2)_i e^{\nu_2 t}\right]^{n_i}. \tag{C.1}$$

Keeping the constant term plus the first correction with temporal dependence, we have

$$\begin{aligned} p_{\boldsymbol{n}}(t) &= \frac{N!}{n_1!n_2!\ldots n_M!}\Bigg\{\prod_{i=1}^{M}\left[\rho_i^{T_b}\right]^{n_i} + \prod_{i=1}^{M}\left[\rho_i^{T_b}\right]^{n_i-1}\Big[n_1(\boldsymbol{w}_2)_1\rho_2^{T_b}\ldots\rho_M^{T_b} \\ &+ n_2\rho_1^{T_b}(\boldsymbol{w}_2)_2\rho_3^{T_b}\ldots\rho_M^{T_b} + \cdots + n_M\rho_1^{T_b}\rho_2^{T_b}\ldots\rho_{M-1}^{T_b}(\boldsymbol{w}_2)_M\Big]b_2e^{\nu_2 t}\Bigg\}. \end{aligned} \tag{C.2}$$

The above expression simplifies to

$$p_{\boldsymbol{n}}(t) \;=\; \frac{N!}{n_1!n_2!\ldots n_M!}\prod_{i=1}^{M}\left[\rho_i^{T_b}\right]^{n_i}\left[1+\sum_{j=1}^{M} n_j \frac{b_2(\boldsymbol{w}_2)_j}{\rho_j^{T_b}} e^{\nu_2 t}\right]. \tag{C.3}$$

The equilibrium distribution is multinomial, with a constraint $N = \sum_{i=1}^{M} n_i$,

$$\pi_{\boldsymbol{n}}^{T_b} \;=\; \frac{N!}{n_1!n_2!\ldots n_M!}\prod_{i=1}^{M}\left[\rho_i^{T_b}\right]^{n_i} = \frac{N!}{n_1!n_2!\ldots n_M!}\frac{e^{-\beta_b E_{\boldsymbol{n}}}}{(Z_1(T_b))^N}.$$

## C.2 Two-level system

For a system with two types of reactants, $M = 2$, the chemical reactions are

$$X_1 \underset{k_{12}}{\overset{k_{21}}{\rightleftarrows}} X_2. \tag{C.4}$$

By looking at the single-molecule system, $N = 1$,

$$\frac{d}{dt}\boldsymbol{q} = \begin{pmatrix} -k_{21} & k_{12} \\ k_{21} & -k_{12} \end{pmatrix}\boldsymbol{q}, \tag{C.5}$$

we obtain

$$b_2(T, T_b) = \frac{1}{2}\left(\tanh\left[\frac{\beta\Delta\epsilon_{12}}{2}\right] - \tanh\left[\frac{\beta_b\Delta\epsilon_{12}}{2}\right]\right), \tag{C.6}$$

where $\Delta\epsilon_{12} \equiv \epsilon_1 - \epsilon_2$.

If $\epsilon_1 = \epsilon_2$ the overlap coefficient is zero, $b_2 = 0$, for all initial temperatures $T$. Moreover the only critical point, $\partial_T b_2 = 0$, is at $\epsilon_1 = \epsilon_2$. Thus there is no

Weak Mpemba effect for $M = 2$ associated with the overlap coefficient $b_2$. The same conclusion also holds for the case of general $N$, which is expected, as we noted in Eq. (5.19). The Appendix provides a complementary derivation of the coefficient $a_2$ for general $N$. Notice that in the case of a two-level system, the load distribution factor, $\delta$, does not play a role, as $b_2$ is independent of $\delta$.

### C.2.1 Two-level system and general $N$

The reactants $X_1$ and $X_2$ are characterized by internal energies $\epsilon_1$ and $\epsilon_2$. The system starts in thermal equilibrium at $T$. The rate matrix $R$ is a $(N+1)\times(N+1)$ tridiagonal matrix. The main diagonal of $R$ is

$$\{-Nk_{12}, -k_{21} - (N-1)k_{12}, \ldots, -Nk_{21}\}\,. \tag{C.7}$$

The subdiagonal (the first diagonal below the main) is

$$\{Nk_{12}, (N-1)k_{12}, \ldots, k_{12}\}, \tag{C.8}$$

and the superdiagonal (the first diagonal above the main) is

$$\{k_{21}, 2k_{21}, \ldots, Nk_{21}\}. \tag{C.9}$$

Note that this tridiagonal matrix can be symmetrized, as the product of the corresponding off-diagonal elements is positive, see e.g. [**meurant_review_1992**]. The first three eigenvalues are

$$\{\lambda_1, \lambda_2, \lambda_3\} \quad = \{0, -k_{21} - k_{12}, -2(k_{21} + k_{12})\}\,. \tag{C.10}$$

By noticing a pattern for specific $N$, after explicitly writing the cases for $N = 1$ to $N = 4$, we conclude, via mathematical induction, that for arbitrary $N$ the overlap $a_2$ is

$$a_2 = \frac{N e^{(N-1)\beta_b \epsilon_2} \left( e^{\beta_b \epsilon_1 + \beta \epsilon_2} - e^{\beta \epsilon_1 + \beta_b \epsilon_2} \right)}{\left( e^{\beta_b \epsilon_1} + e^{\beta_b \epsilon_2} \right)^N \left( e^{\beta \epsilon_1} + e^{\beta \epsilon_2} \right)}. \tag{C.11}$$

If $\epsilon_1 = \epsilon_2$ the coefficient $a_2 = 0$ for all temperatures $T$ and $T_b$. Moreover the only critical point, $\partial_T a_2 = 0$, is at $\epsilon_1 = \epsilon_2$. No weak Mpemba effect for $M = 2$ is associated with the overlap coefficient $a_2$. We notice from Eqs. (C.11) and (C.6) that

$$a_2(T, T_b) = \frac{N}{(e^{\beta_b \Delta \epsilon_{12}} + 1)^{N-1}} b_2(T, T_b). \tag{C.12}$$